# Control of Naturally Occurring Radioactive Material (NORM) in Produced Water by Inorganic Sorbents

by

**Alen V. Gusa**

Bachelor of Civil Engineering, University of Belgrade, 2013

Master of Civil Engineering, University of Belgrade, 2014

Submitted to the Graduate Faculty of the

Swanson School of Engineering in partial fulfillment

of the requirements for the degree of

Doctor of Philosophy

University of Pittsburgh

2019

UNIVERSITY OF PITTSBURGH

SWANSON SCHOOL OF ENGINEERING

This dissertation was presented

by

**Alen V. Gusa**

It was defended on

November 18, 2019

and approved by

Radisav D. Vidic, Professor, Ph.D., Department of Civil and Environmental Engineering

Leanne M. Gilbertson, Assistant Professor, Ph.D., Department of Civil and Environmental Engineering

Carla Ng, Assistant Professor, Ph.D., Department of Civil and Environmental Engineering

Joseph R.V. Flora, Associate Professor, Ph.D., Department of Civil and Environmental Engineering, University of South Carolina

Dissertation Director: Radisav D. Vidic, Professor, Ph.D., Department of Civil and Environmental Engineering

**Control of Naturally Occurring Radioactive Material (NORM) in Produced Water by Inorganic Sorbents**

Alen V. Gusa, Ph.D.

University of Pittsburgh, 2019

Produced water generated during unconventional gas extraction is characterized by high total dissolved solids (TDS) and high concentration (i.e., up to 4,000 times higher than the drinking water standard) of naturally occurring radioactive material (NORM). The goal of this study was to evaluate options for the control of major components of NORM in produced water, Ra-226 and Ra-228, and mitigate potential adverse health and environmental impacts.

Radium removal capacity of barite ($BaSO_4$), one of the most cost-effective solids for radium separation, was affected by monovalent and divalent cations in solution due to competition and impact on barite zeta potential. Molecular dynamics simulations showed a reasonable agreement with experimental results. The main discrepancy was due to dissolution-recrystallization reactions at barite surface that are not included in theoretical calculations. This dissertation research provided key fundamental insights into radium removal by barite and enabled accurate estimate of the effect of different cations on radium uptake.

In an attempt to sequester NORM underground and prevent its accumulation in surface impoundments, a novel coated hydraulic fracturing proppant was developed in this dissertation. Proppant sand impregnated with celestite ($SrSO_4$) and barite using heterogeneous precipitation showed remarkable capacity for Ra-226. These novel proppants, with fairly small amount of impregnate (i.e., 10-30 mg/g), exhibited sufficient capacity for Ra-226 even at high ionic strength

and elevated solution temperatures. It is also estimated that this method can control Ra-226 during the lifetime of the well (i.e., 20 years).

If Ra-226 is brought to the surface, co-precipitation as Ba-Ra-$SO_4$ is the best way to remove it prior to salt recovery or to prevent accumulation in surface impoundments. Produced water with high Sr/Ba concentration ratios is challenging due to the interference of Sr with this process. Optimization of the treatment process to achieve requisite effluent quality while minimizing the total amount of radioactive sludge involved adjustment of Sr/Ba ratio and addition of barite "seed".

Based on the improved understanding of radium removal by barite adsorption/co-precipitation, this study offers options for the control of NORM in produced water by either sequestering it in the subsurface or by treating produced water above ground.

## Table of Contents

## List of Tables

## List of Figures

## Preface

This study was performed with the financial support from National Science Foundation (Grant No. NSF CBET #1510764). I am very grateful for this financial support.

I would like to express my sincere gratitude to Dr. Radisav D. Vidic, who was not just a mentor and adviser on my dissertation, but also a friend who knew how to motivate me and point me in the right direction every time when it was necessary. He gave me a life-time opportunity to work on such an exciting and important research project. His energy, enthusiasm, creativity and vast knowledge were an essential foundation during my research career at Pitt. It was an unforgettable journey and a priceless experience that had an immense impact on my career and my life. I will be forever grateful.

I would also like to thank my Ph.D. committee members: Dr. Leanne M. Gilbertson, Dr. Carla Ng (Baumel) and Dr. Joseph R.V. Flora, who provided important suggestions and guidance during my Ph.D. studies. They urged me to think about a wider picture of my research and how to fit my study into a broader field of engineering and scientific disciplines. Dr. Gilbertson was always there to give me a feedback about my ideas and to offer a constructive suggestion. Dr. Ng's comments to my PhD proposal were of a great value to finalize this dissertation. Dr. Flora is experienced in molecular dynamics modeling and he provided help on radium removal simulations.

I want to give special thanks to my friends and colleagues: Dr. Vaclav Hasik, Daniel Luna, Dr. Omkar Lokare, Nathalia Aquino, Dr. Shardul Wadekar, Dr. Tieyuan Zhang, Yan Wang and Zhewei Zhang for their support and friendship during both good and bad times of my PhD studies. Special gratitude goes to Dr. Iva Jestrovic and Dr. Michael Rothfuss who helped me settle in

Pittsburgh and shared some great moments with me in the last four years. ‘Yinz’ will always be a part of my family.

Nothing would be possible without Dr. Branislav Babic, who always believed in me and provided tremendous support during my studies.

Finally, none of this would be possible without the most important people in my life. The love of my life, Johanna Gomez, whose love, tolerance, patience and support were key factors in decisive moments of my PhD career. You have never let me down and always helped me to stand up and keep fighting. Everything that I became is thanks to my parents Vanja and Nada Gusa, whose love and care go beyond the boundaries of this world. You always supported me in pursuing my dreams and I could not wish for better parents. My brother and my psychologist, Petar Gusa, whose devotion and huge heart are the support that each of us needs in our lives. My grandma, Draginja Maglov, who spent years taking care of me and whose love and kindness are unique and priceless. I would also like to thank my grandparents Petar and Dusanka Gusa for their support, as well as my grandfather Nicifor Maglov for taking care of me from above. Last, but not least, thanks to our little angel on the way, who motivated me to make the final effort and write this dissertation. This is the success of all of you! I am blessed to have you and I love you to infinity and beyond.

*To my dearest I dedicate*

*Because nothing matters more than family*

## Nomenclature

| | |
|---|---|
| $\varepsilon$ | water permittivity (F/m) |
| $\zeta$ | zeta potential (V) |
| $\psi(x)$ | electrical potential at the distance x (V) |
| $\psi_0$ | electrical potential at the particle surface (V) |
| $\sigma$ | specific surface charge ($C/m^2$) |
| $\Delta G^0$ | change in Gibbs free energy (kcal/mol) |
| A | total surface area of the adsorbent ($cm^2$) |
| Adj MS | adjusted mean squares |
| Adj SS | adjusted sum of squares |
| b | Langmuir coefficient |
| BET | Braunauer-Emmett-Teller theory |
| $C_e$ | final (equilibrium) Ra-226 activity in the liquid phase (pCi/L) |
| $C_{formed\ solids}$ | formed solids during produced water treatment (ton/$10^6$ gallons) |
| $C_0$ | initial Ra-226 activity in the liquid phase (pCi/L) |
| $C_{total\text{-}solids}$ | sum of solids added to the system and solids formed during treatment (g/L) |
| $C\infty$ | concentration of the electrolyte in the bulk (mol/L) |
| DF | degrees of freedom |
| e | elementary charge (C) |
| EDL | electrical double layer |
| EDTA | ethylenediaminetetraacetic acid |
| I | ionic strength (mol/L) |

| | |
|---|---|
| IC | ion chromatography |
| ICP-OES | inductively coupled plasma optical emission spectroscopy |
| IEP | isoelectric point |
| k | Boltzmann constant (J/K) |
| $K^{-1}$ | Debye length (m) |
| Ka | thermodynamic equilibrium constant |
| Kd | distribution coefficient |
| $K_F$ | Freundlich adsorption parameter |
| Ksp | solubility product constant |
| LSC | liquid scintillation counter |
| m | mass of the adsorbent (mg) |
| $m_c$ | mass of the coating agent that attached to the surface of the quartz sand (mg) |
| MD | molecular dynamics |
| $m_i$ | total mass of the coating agent that precipitated in the system (mg) |
| $m_r$ | mass of the coating agent that remained in the system (mg) |
| n | Freundlich adsorption parameter |
| $N_A$ | Avogadro constant ($mol^{-1}$) |
| NORM | naturally occurring radioactive material |
| NPDES | national pollutant discharge elimination system |
| $P/P_0$ | relative pressure |
| PMF | potential of mean force (kcal/mol) |
| PW | produced water |
| q | adsorption capacity for Ra-226 (pCi/mg or $pCi/cm^2$) |

| | |
|---|---|
| q | sludge radioactivity (pCi/g) |
| $q_{max}$ | maximal adsorption capacity based on 24 possible adsorption sites per $cm^2$ of barite |
| R | universal gas constant (J $K^{-1}$ mol-1) |
| R | ion removal (%) |
| $R^2$ | square of the correlation coefficient |
| SEM | scanning electron microscope |
| SI | saturation index |
| T | temperature (°C, °F or K) |
| TDS | total dissolved solid (g/L) |
| $TDS_f$ | final total dissolved solids (g/L) |
| $TDS_i$ | initial total dissolved solids (g/L) |
| TENORM | technologically enhanced naturally occurring radioactive material |
| TSS | total suspended solids (g/L) |
| UIC | underground injection control well |
| V | volume of the sample (L) |
| x | distance from the particle surface (nm) |
| Zi | charge number of an ion |

# 1.0 Introduction

Natural gas production in the US has been expanding since 1900 with the average yearly increase of 5.1% and projections made by US Energy Information Administration show that natural gas will be the major energy source in the US by the year of 2050 (U.S.E.I.A., 2019). Natural gas can be found in conventional and unconventional reservoirs. Conventional reservoirs are typically porous sandstone formations where natural gas is contained under pressure. Unconventional reservoirs are gas-rich black shale formations where gas extraction requires the utilization of horizontal drilling and hydraulic fracturing (fracking) to recover natural gas, as shown in Figure 1.1.

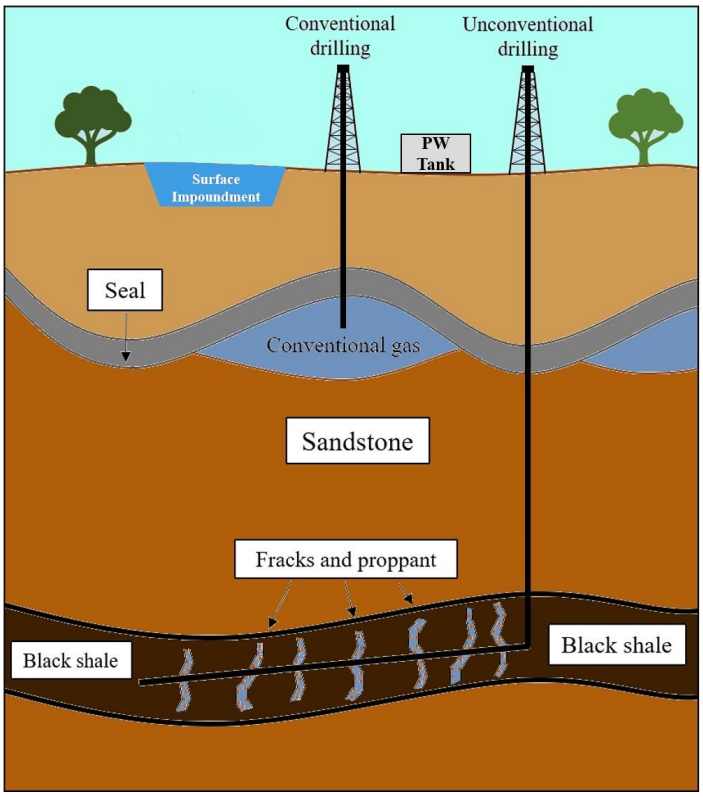


**Figure 1.1.** Schematic presentation of conventional and unconventional natural gas extraction.

According to U.S. Energy Information Administration (EIA), about 60% of total natural gas production in 2017 originated from the extraction of tight and shale gas (i.e., it is estimated at 16.76 trillion cubic feet) (U.S.E.I.A., 2018). This fraction is expected to be 90% by the year of 2050 as a result of projected increase in production of tight and shale gas due to the large area of available resources (i.e., more than 500,000 square miles) and technological advancement (U.S.E.I.A., 2019).

High expectations from unconventional natural gas extraction are the result of continuous development of hydraulic fracturing and horizontal drilling technologies. Horizontal drilling is a natural gas extraction process where the drilling pipe is placed parallel to the surface and along the shale formation (Figure 1.1). This pipe is an extension of the vertical drilling pipe and it allows recovery of natural gas from a fairly large area of a gas-rich shale. As seen in Figure 1.1, gas rich shales and low permeability reservoirs are located deep below the surface (i.e., up to 12,000 feet deep (Jackson, 2015)) and gas does not automatically flow into the well. Shale formation needs to be fractured under high pressure (i.e., up to 680 bar (Barbot, 2013)) using hydraulic fracturing fluid. It is estimated that each horizontal well can require up to 7 million gallons of fracking fluid (Hayes, 2009). Fracking fluid is used to enhance the extraction of hydrocarbons, prevent corrosion and maintain fracks opened during the lifetime of a well. It is a mixture of water (90%), hydraulic fracturing proppant (9.5%) and various chemical additives (0.5%) that are used to prevent scaling, reduce corrosion and friction, and to dissolve rocks and minerals. The exact chemical composition of the fracturing fluid depends on the geological formation and the operator, but it is certain that these chemicals pose a threat to environment and need to be treated accordingly. The primary purpose of hydraulic fracturing proppant is to keep fissures and fracks in the shale opened and allow for efficient flow and extraction of natural gas. Approximately 2,000 tons of proppant is

used per fracking well (Hayes, 2009). Fracking proppant vary in size (i.e., 105 – 2,380 μm), viscosity and type of coating (Liang, 2016). The most commonly used fracking proppants are quartz sand (high silica content; able to withstand pressure up to 410 bar), ceramic proppants (high alumina content; able to withstand pressures even up to 1,380 bar) and resin-coated sand proppant (high conductivity and prevention of proppant flowback to the well) (Liang, 2016; Palisch, 2015).

Part of the fracturing fluid flows back to the surface at a high rate for a few weeks following the hydraulic fracturing to release the underground pressure and allow the extraction of natural gas (Barbot, 2013). This fluid is known as flowback water and its chemical composition can be highly variable within first few weeks following the well stimulation (Kim, 2016; Oetjen, 2018). Additional fracking fluid is recovered at the surface during the operational lifetime of the well and this water is known as produced water. The total volume of produced water generated in both onshore and offshore hydraulic fracturing wells in the United States was approximately 882 billion gallons in 2007 (Veil, 2011), with this number likely to be much higher due to the constant expansion of unconventional oil and gas industry.

Chemical composition of produced water is highly dependent on the location of the unconventional well (Barbot, 2013). Due to the interaction with various types of rocks in the formation, produced water returns to the surface with salinity up to 10 times higher than the salinity of sea water (i.e., 35 g/L). Total dissolved solids (TDS) of produced water in Marcellus Shale, that extends through Appalachian basin in Pennsylvania and New York, is in the range between 680 – 390,000 mg/L (Barbot, 2013; Shih, 2015). Southwest region of the United States (i.e., Eagle Ford, Permian and Barnette basins) has a slightly lower TDS than Marcellus Shale, ranging from 28,900 – 213,000 mg/L (Sari, 2015; Thiel, 2014). Produced water also contains suspended solids (TSS) that can be as high as 7,600 mg/L (Barbot, 2013). There is a variety of ions found in the produced

water, but the most common are $Li^+$, $Na^+$, $K^+$, $Mg^{2+}$, $Ca^{2+}$, $Sr^{2+}$, $Ba^{2+}$, $Br^-$ and $Cl^-$ which make more than 90% of the TDS. In some regions, depending on the type of rocks and operator practice, fracking fluid is enriched with surfactants and other organics (e.g., polyethylene glycol, nonylphenol ethoxylates, 2-butoxyethanol) that are used to reduce the surface tension of the fluid and to lubricate fissures and fracks in rocks (Chen, 2017). These organics are usually found in flowback and produced water and represent environmental threat due to their toxicity (Butkovskyi, 2017). Another significant problem associated with produced water is the presence of Naturally Occurring Radioactive Material (NORM) that is usually found in the form of radioactive isotopes Ra-226 and Ra-228.

Produced water management strategies in the U.S. involve disposal via injection into Class II Underground Injection Control (UIC) wells (i.e., 94%, out of which 39% is directly disposed and 55% is reused in oil and gas industry for enhanced recovery), treatment and discharge into the surface waters (i.e., more than 4% of onshore produced water) and into the ocean (i.e., more than 91% of offshore produced water) or in agriculture for irrigation and livestock (Veil, 2011). The major problem with produced water disposal in Marcellus Shale is a very small number (only 8) of Class II wells in Pennsylvania (Figure 1.2) (Gregory, 2011) and high cost of water transportation for disposal in the surrounding states. Hence, the unconventional oil and gas industry in Pennsylvania has developed solutions to reuse the produced water for fracking purposes.

Produced water needs to undergo a purification process that will generate low salinity effluent suitable for disposal. One of the most effective ways of treating produced water is using evaporation/crystallization, but this process is not economical due to the high energy demand (Nasiri, 2017). Reverse osmosis is most commonly used method for produced water purification, but it has a high capital and operational cost due to the high hydraulic pressures required for the

process (i.e., up to 350 bar) (Thiel, 2015). Membrane distillation has been widely studied as an alternative to pressure based membrane systems and it showed significant potential for produced water desalinization (Lokare, 2017). Common method to target specific ions in produced water is using ion exchange resins and/or precipitation with sulfate or carbonate ligands.

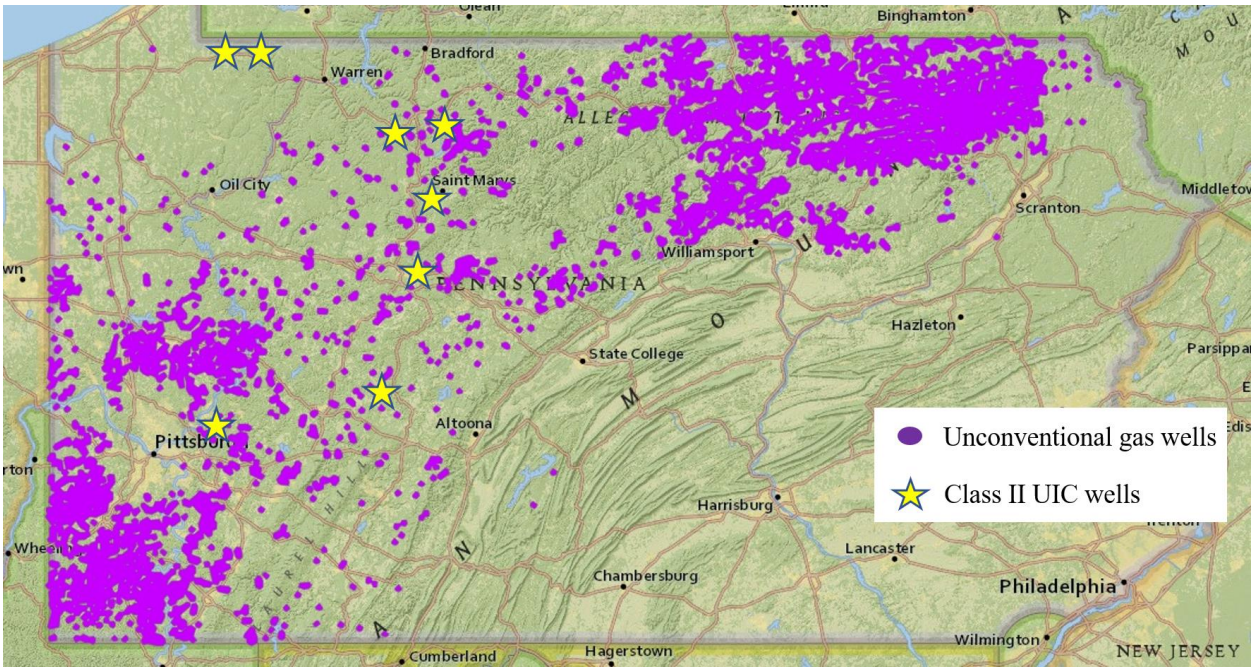


**Figure 1.2.** Unconventional natural gas wells and Class II Underground Injection Control wells in Pennsylvania – modified map (Fractracker, 2019).

There are numerous of benefits of unconventional natural gas extraction by hydraulic fracturing and horizontal drilling, such as abundance of resources (i.e., 70 shale formations around the world), lower environmental emissions compared to coal combustion for energy generation (i.e., lower emissions of sulfur oxides, nitrogen oxides), economic development (i.e., more jobs) and lower gas price (Sovacool, 2014). However, further expansion of unconventional natural gas production is limited by the lack of Class II disposal wells (i.e., only 8 disposal wells compared to

12,202 drilled shale gas wells, as shown in Figure 1.2 (Fractracker, 2019)), high methane emissions compared to conventional gas and coal, potential cause of earthquakes, social opposition and water pollution and concerns for public health.

## 1.1 NORM in Produced Water

NORM is found in produced water as a results of interaction of fracturing fluid with thorium and uranium-rich black shale (Rowan, 2011). NORM is mainly comprised of radium isotopes, Ra-226 and Ra-228, decay daughter products of U-238 and Th-232 chains, respectively (Figure 1.3). Ra-226 and Ra-228 are mostly found in produced waters generated in Northeast (i.e., Marcellus Shale, Utica Shale) and rarely in Southwest region. Ra-226 is found in produced water in concentrations up to 20,000 pCi/L with median concentrations for Marcellus Shale in the range 2,460 – 5,490 pCi/L depending on the location of the well. Although the concentration of Ra-228 generally does not exceed 20% of Ra-226 concentration, it is still 1-2 orders magnitude higher than the drinking water (i.e., 5 pCi/L) and industrial effluent (i.e., 60 pCi/L) standards (Rowan, 2011; Tasker, 2019; U.S.EPA, 1976).

After reaching the surface, produced water is typically stored in tanks and reservoirs (Figure 1.1) prior to treatment and disposal or reuse. It is shown that Ra-226 concentration is increasing over time in both liquid phase and in the sludge that is accumulated at the bottom of surface impoundments (Zhang, 2015b).

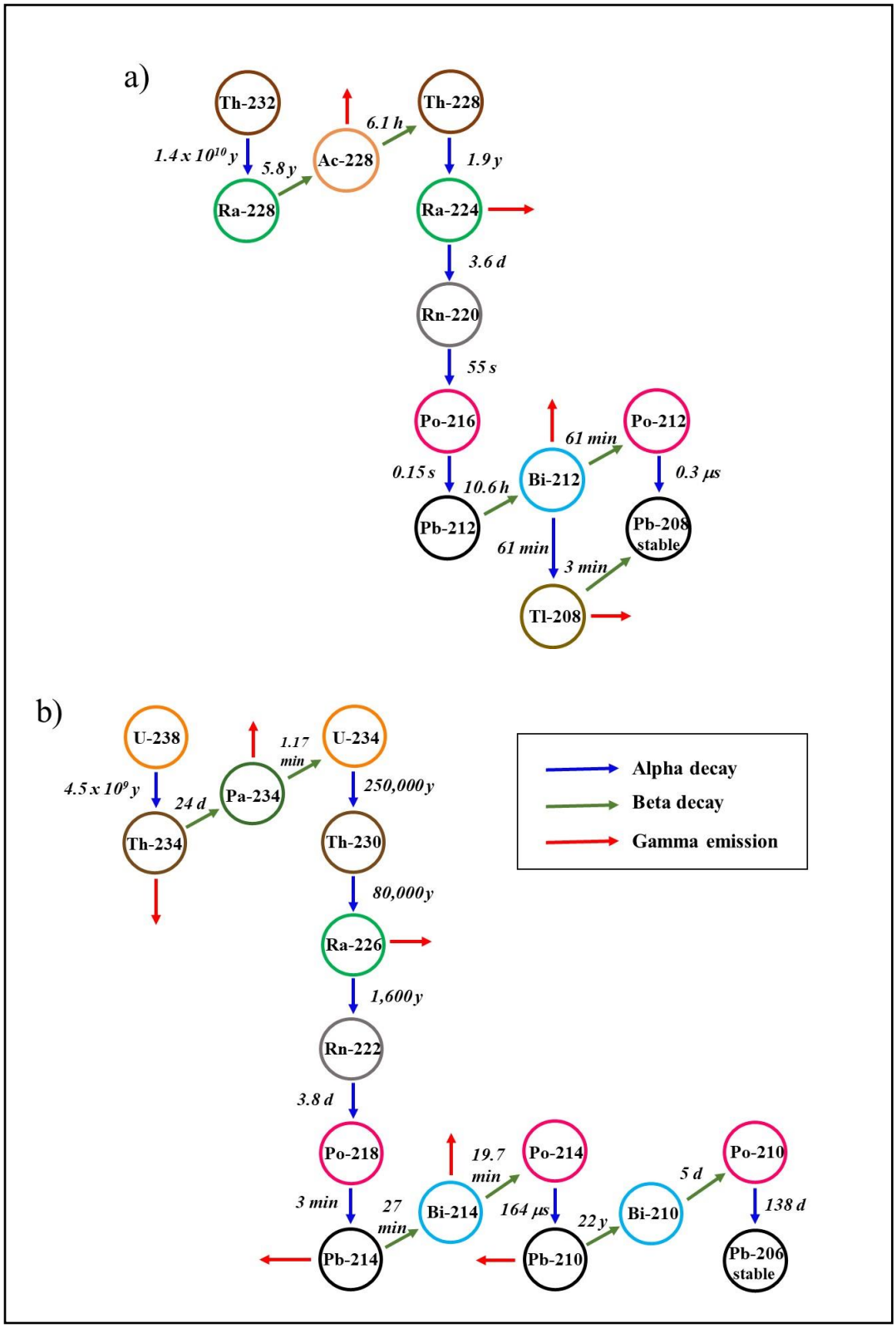


**Figure 1.3.** Decay chains for (a) Th-232 and (b) U-238 series with associated half-life and type of decay/emission.

Potential environmental and health hazards can occur if produced water spills or leaks form storage reservoirs and reaches groundwater, surface water or soil. As stated previously, produced water can have 2-4 orders of magnitude higher concentration of Ra-226 than allowed by EPA and any mixing with surface and ground water can cause serious environmental issues and adverse impacts on the ecosystem. NORM is typically accumulated in produced water sludge and radioactivity of that sludge is increasing with time (Zhang, 2015b). Considering that radioactivity of this sludge (i.e., concentration of Ra-226) can in some cases be even 30 times above the disposal limit specified for RCRA D solid waste landfills (i.e., 25 pCi/g (Silva, 2012)), daily handling of this sludge can pose a significant threat for on-site workers.

## 1.2 Mechanisms of Radium Removal Using Barite

Depending on the chemical composition of aqueous solution, radium sequestration can be achieved using various metal oxides and hydroxides, ion exchangers and minerals. However, most commonly used agent for radium removal in produced water is barium sulfate (barite). Barite can remove radium through co-precipitation or through interactions with already formed barite solids (i.e., post-precipitation).

Once the saturation index (SI) of a compound (e.g., $BaSO_4$) is higher than 0, a solid will start to form (i.e., precipitate) until the solubility equilibrium is achieved. Saturation index of a certain compound in solution can be calculated using the following equation:

$$SI = log_{10} \frac{IAP}{K_{sp}} \tag{1.1}$$

where, IAP is ion activity product and $K_{sp}$ is solubility product of a compound.

Ion activity product (IAP) is used to describe a non-equilibrium state of a compound and can be calculate using the equation 1.2:

$$IAP = (A)^a(B)^b \tag{1.2}$$

where, (A) and (B) are ionic activities for compounds A and B and $a$ and $b$ are stoichiometric coefficients. Ion activities reflect reactive concentration of a compound and can be calculated as:

$$(A) = \gamma_A[A] \tag{1.3}$$

$$(B) = \gamma_B[B] \tag{1.4}$$

where, [A] and [B] are molar concentrations of compounds A and B and $\gamma_A$ and $\gamma_B$ are activity coefficients used to describe the interaction between ions in the solution.

During precipitation of a specific salt (e.g., $BaSO_4$), a third component (e.g., $Ra^{2+}$) can be removed from the solution by inclusion in the precipitate. This process is known as co-precipitation and its mechanisms are shown in Figure 1.4.

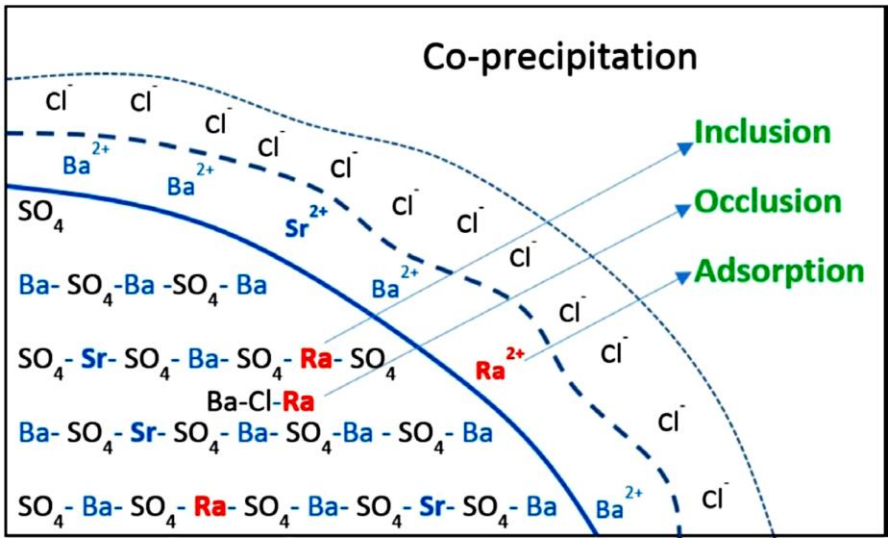


**Figure 1.4.** Mechanism of $Ra^{2+}$ co-precipitation with $BaSO_4$ and $SrSO_4$ (Zhang, 2014).

Co-precipitation can occur through a combination of three possible mechanisms: inclusion, occlusion and adsorption. Inclusion is the process of replacing the main metal (i.e., $Ba^{2+}$ or $Sr^{2+}$) with a trace metal (i.e., $Ra^{2+}$) in the crystal lattice. Occlusion happens when a trace metal is physically captured between the layers of a growing mineral (i.e., $BaSO_4$ or $SrSO_4$). Adsorption is a surface phenomenon when a trace element is physically or chemically bound to the outer layer of a mineral (Harvey, 2000). Co-precipitation is usually described using distribution (partition) coefficient, $K_d$, which is the measure of the allocation of ions between aqueous and solid phase.

Post-precipitation is a process of using preformed solids (minerals) for the sequestration of trace elements. It commonly involves two processes: adsorption and surface dissolution-recrystallization (Zhang, 2014). Both co-precipitation and post-precipitation processes will be further discussed in Chapters 2, 3 and 4.

## 1.3 Research Objectives and Dissertation Layout

This dissertation aims to evaluate the ability of different sulfate solids to remove Ra-226 from dilute and high salinity solutions by both co-precipitation and post-precipitation mechanisms. Available literature still lacks fundamental understanding of the mechanism and factors that have significant impact on Ra-226 removal by preformed barite solid. Various ions are present in produced water and each of them can affect Ra-226 sequestration process. Current literature also lacks appropriate models for Ra-226 removal and this study was designed to better understand this process through a combination of experimental studies and molecular dynamics simulations.

Most of the previous research was focused on Ra-226 control after produced water reaches the surface. However, preventing Ra-226 of reaching the surface instead of trying to remove it

from produced water could be a step in the right direction. Thus, a novel method of impregnating hydraulic fracturing proppant with a solid that has high affinity for Ra-226 could be the solution to adsorb Ra-226 and prevent it from reaching the surface.

Due to high spatial variability of produced water composition, treatment facilities often struggle with removing Ra-226 and $Ba^{2+}$ from this water. This is particularly challenging when divalent cations such as $Sr^{2+}$ and $Ca^{2+}$ are found in much higher concentrations than $Ba^{2+}$. This study also evaluated fundamental and practical aspects of a novel treatment approach that would enable selective removal of target ions (i.e, Ra-226 and $Ba^{2+}$) under these conditions while minimizing the total volume of sludge generated in the treatment process.

This dissertation contains published journal manuscript, journal manuscript under review and a manuscript in preparation to be submitted to a scientific journal. Dissertation is presented in five chapters and the objectives are accomplished through three specific tasks.

**Objective 1 (Chapter 2): Impact of solution composition and temperature on Ra-226 uptake by Barite ($BaSO_4$): Comparison of experimental and modeling results**

The main tasks in this objective are to investigate the ability of barium sulfate to sequester Ra-226 in the presence of different ions and to understand this process through a combination of experimental studies and molecular dynamics simulations. Since earth alkaline metals and sodium are the major cations in the produced water, it was important to understand competitive adsorption of Ra-226 in the presence of each of these cations. The impact of charge, size, diffusivity, zeta potential and concentration of competing ions provided insight into physical-chemical surface properties of barite that are governing the removal of Ra-226. Additional tests were done at temperatures in the range from 3-40 °C to further distinguish the mechanism of Ra-226 removal.

Molecular dynamics modeling was conducted to elucidate radium interactions with barite and develop a model for radium uptake by barite. The outcome of this work provides further insight into radium removal mechanisms, explains the impacts of major ions found in produced water and presents molecular dynamics model that can be useful in engineering practice to predict radium removal in aqueous solutions.

**Objective 2 (Chapter 3): Development of functionalized proppant for the control on NORM in Marcellus Shale produced water**

This objective is focused on finding the most suitable Ra-226 sequestrating solids and using them to impregnate hydraulic fracturing proppant. This kind of proppant would have a dual role in the fracking process: 1) maintain the stability of the fracks and allow for the efficient extraction of unconventional natural gas and 2) serve as an adsorbent for Ra-226 in the subsurface. This task evaluated the performance of major sulfates and carbonates for Ra-226 sequestration during the post-precipitation process to find the best possible functionalizing agent. Possible methods for proppant coating with selected functionalizing agents were investigated and the performance of the newly developed proppant was studied to understand the factors (i.e., pH, ionic strength) that influence the adsorption process. The efficiency of the coated proppant was evaluated both in dilute solutions and in high salinity synthetic produced water. The results of this work demonstrate a possibility of impregnating hydraulic fracturing proppant with selected sulfate solids and provide an alternative to conventional methods for Ra-226 removal from high salinity produced water.

**Objective 3 (Chapter 4): Sulfate precipitation in produced water from Marcellus Shale for the control of Naturally Occurring Radioactive Material**

This objective is aimed to evaluate Ra-226 sequestration from actual produced waters during barium sulfate co-precipitation and to find the treatment approach that will minimize residual $Ba^{2+}$ and Ra-226 concentration in the effluent to achieve water quality requirements for subsequent crystallization treatment of produced water. This is particularly important for produced waters where $Sr^{2+}$ concentration is substantial or even higher than $Ba^{2+}$ concentration and sulfate addition is not effectively utilized for barite precipitation and concomitant Ra-226 removal. Possible solutions included controlling saturation index of barite, seeding the system with barite and/or recycling of barium sulfate solids to preferentially select barite precipitation over celestite precipitation. All of these treatment approaches were evaluated in terms of the effluent $Ba^{2+}$ and Ra-226 concentrations and the amount of radioactive sludge generated during the process. An optimal method for treating produced water with high Sr/Ba ratio was found by varying the amount of barite "seed" and saturation index of barite. The outcome of this work provides guidance to achieve low $Ba^{2+}$ and Ra-226 concentrations in high Sr/Ba ratio produced water by the addition of preformed barite and sodium sulfate and minimize radioactive sludge production during the process.

## 2.0 Impact of Solution Composition and Temperature on Ra-226 Uptake by Barite ($BaSO_4$): Comparison of Experimental and Modeling Results

This chapter, written by Alen V. Gusa and coauthored by Hamid Al-Khashab, Jospeh R. V. Flora, and Radisav D. Vidic, is in preparation to be submitted to *Environmental Science & Technology*.

Mechanisms and the most relevant factors affecting radium removal by barite solids under relevant process conditions, especially at high ionic strengths, are not yet fully understood. This study evaluated radium removal by barite in DI water and in aqueous solutions in the presence of different electrolytes at concentrations ranging from 0.01-1 mol/L. Experimental studies revealed that divalent cations (i.e., $Mg^{2+}$, $Ca^{2+}$, $Sr^{2+}$ and $Ba^{2+}$) have significantly higher impact on radium removal by barite than monovalent cations ($Na^{+}$, $K^{+}$) and that ionic radii and diffusivities of these ions play an important role. Ions with higher diffusivity had more pronounced impact on electrical double layer of barite and caused lower radium uptake. Umbrella sampling and umbrella integration analysis in quantum simulations were used to delineate the impact of ionic size and charge on interaction energies between barite surface and different ions. Adsorption isotherms predicted using molecular dynamics simulations agreed reasonably well with experimental data illustrating the impact of co-ion charge and concentration on radium removal by barite. Zeta potential measurements revealed a linear relationship between the potential at the shear plane of the electric double layer and Ra-226 removal. The increase in ionic strength can reduce radium uptake by more than three-fold due to the competition between ions and double layer compression. The impact of $Ba^{2+}$ on Ra-226 uptake by barite is difficult to assess experimentally because of the additional Ra-226 removal by co-precipitation with barite solids (i.e., common ion effect). In

addition, dissolution-recrystallization of barite was found to have an impact on Ra-226 removal even within a fairly short equilibration time (i.e., 24 hours) used in this study. The results of this study offer additional insight into surface interactions during precipitation/adsorption under realistic process conditions and reveal the potential of combined experimental studies and molecular simulations for predicting radium removal from high salinity brines by preformed barite solids.

## 2.1 Introduction

Uranium mining and recent expansion of the unconventional oil and gas industry has led to increased concerns about environmental threats caused by the byproducts from these industries. Uranium ore is abundant all over the world and is used by oil and gas industry as an indicator of energy rich rock formations (Ellis, 2007). Although uranium does not have pronounced radioactivity, its isotope U-238 is the source of Ra-226, which is highly radioactive and has a half-life of 1,600 years. Whether uranium and other naturally occurring radioactive materials (NORM) come directly from mining or from black shale formations that also serve as unconventional reservoirs of natural gas and oil, it is clear that these industries need to exercise special care and treatment of their waste streams to prevent spills and environmental contamination as well as human health impacts. Unconventional gas industry uses up to 6 million gallons of water for hydraulic fracturing a single unconventional well (Gregory, 2011; Jackson, 2014; Nicot, 2012). This water comes into the contact with uranium rich rock formations and returns to the surface with total dissolved solids (TDS) of up to 345 g/L and radium activity of up to 20,000 pCi/L (Barbot, 2013; Rowan, 2011). TDS is mainly composed of alkali metal chlorides (i.e., NaCl, KCl)

and earth alkaline metal chlorides (i.e., $MgCl_2$, $CaCl_2$, $SrCl_2$ and $BaCl_2$). Produced water (i.e., water generated during the operation of a well) is usually stored in surface impoundments prior to treatment and/or reuse. Due to its high radioactive content (i.e., up to 4 orders of magnitude higher than federal standards (U.S.EPA, 1976)), any leaks or spills of this water can contaminate surface or ground waters and cause radiological and environmental problems (Ritcey, 1989; Vengosh, 2014; Zhang, 2015b).

Extraction of radium from aqueous solution can be achieved using various natural and engineered materials. Most commonly used adsorbents are iron, manganese and ferric oxides and hydroxides (Mott, 1993; Sajih, 2014; Valentine, 1990), synthetic ion-exchangers (Bi, 2016; Fan, 2016; Subramonian, 1990), quartz, and sulfate and carbonate minerals (Gusa, 2018; Jones, 2011; Wang, 1987). All these solids showed significant Ra-226 adsorptive capacity that varied notably as a function of pH, ionic strength and competitive ions in the solution, and the most studied mineral for the removal of Ra-226 from industrial effluents is barium sulfate (barite) (Ouyang, 2019). Because previous studies were conducted at widely varying conditions ranging from dilute (i.e., DI water) to high salinity (i.e., synthetic produced water) solutions there is still a lack of agreement regarding mechanisms involved in Ra-226 uptake by barite and potential impact of co-ions in solution on these interactions.

Affinity of barite mineral for radium ions was first evaluated by Germann in 1921 who used existing adsorption isotherms models (i.e., Kroeker and Freundlich (Freundlich, 1906) isotherms) (Germann, 1921) to describe radium uptake by barite in dilute solution. In 1925, Doerner and Hoskins introduced the model of "co-precipitation" and "replacement" to explain the mechanisms for radium uptake by barite (Doerner, 1925). They showed that radium sulfate ($K_{sp(RaSO4)} = 10^{-10.38}$) (Langmuir, 1985) will not form as a separate solid mineral due to very low

concentration of radium in solution, but it is likely to co-precipitate with a few orders of magnitude higher concentration of barium and sulfate. Thermodynamic properties and Pitzer activity coefficients to estimate the speciation of radium in solid solution were first calculated by Rosenberg et al. (Rosenberg, 2011a; b). They also demonstrated the impact of ionic strength and kinetics of precipitation on distribution coefficient of radium in liquid and solid phase in the case of a large pilot scale evaporitic system (Rosenberg, 2013). Possible mechanisms of co-precipitation of radium in binary and ternary systems and the impact of sodium, strontium and barium ions on the kinetics and equilibrium of radium removal were discussed by Zhang et al. (Zhang, 2014) and Rosenberg et al. (Rosenberg, 2014). The adverse impact of strontium and temperature on radium removal in ternary $(Sr,Ba,Ra)SO_4$ systems was observed in long-term studies by Klinkenberg et al. (Klinkenberg, 2018) and Vinograd et al. (Vinograd, 2018). Recent studies have demonstrated the potential of mixing sulfate rich solution with hydraulic fracturing produced water to achieve barium and radium free effluents using co-precipitation reactions (He, 2016; Ouyang, 2019).

Removal of radium by preformed barite solids (i.e., post precipitation) has been a subject of various studies, but the mechanisms and factors governing this process are not yet fully understood. Bosbach et al. pointed that radium removal by barite is not only due to the surface adsorption, but also due to the replacement of a significant fraction of barium with radium in the barite crystal (Bosbach, 2010). Measurements of Ba-133 isotope activity showed that complete dissolution-recrystallization of barite will occur in 100-600 days, while the kinetics of Ra-226 removal is even slower and it takes approximately 435 days to reach equilibrium in the presence of 0.1 mol/L NaCl. Thermodynamic analysis of Margules interaction parameter indicated that complete barite recrystallization is possible within 100 days, thereby supporting the hypothesis

that Ra-226 is fully incorporated into the bulk crystal (Vinograd, 2013). Curti et al. demonstrated that dissolution-recrystallization of barite can take up to 1 year, with Ra-226 being incorporated into the crystal structure as a non-ideal solid solution (Curti, 2010). Time of flight-secondary ion mass spectrometry revealed that incorporation of Ra-226 does not only occur on the crystal surface, but that the bulk of barite mineral is involved and that complete recrystallization of barite is responsible for Ra-226 removal during 443 days (Klinkenberg, 2014). Brandt et al. showed that more than 2 years are necessary to achieve thermodynamic equilibrium of $(Ba,Ra)SO_4$ with high initial Ra-226 concentration of 1.13 mCi/L (Brandt, 2015). Discovery of nano-size and macro-size surface oriented pores in barite crystal offered another mechanism for Ra-226 uptake by barite (Weber, 2016). Weber et al. analyzed Ra-226 removal during the recrystallization of barite and suggested that internal micro and nano pores play important role in radium uptake (Weber, 2017). Brandt et al. suggested that $Sr^{2+}$ competes with $Ba^{2+}$ and Ra-226 during barite recrystallization and inhibits Ra-226 removal (Brandt, 2018).

Adsorption on mineral surfaces is an essential process for the control of contaminants in natural environments and molecular dynamics models have been used previously to understand these processes. Katz et al. investigated the impact of temperature on magnesium, strontium and barium adsorption on gibbsite surface (Katz, 2013). They compared experimental and modeling data and pointed out differences that can occur due to the surface complexation, when the model considers only ion adsorption or when it predicts simultaneous adsorption and precipitation reactions. Bracco et al. investigated Strontium removal from aqueous solution by barite (001 surface) experimentally and computationally and demonstrated both adsorption and lattice replacement reactions (Bracco, 2018). Ho et al. demonstrated the importance of basal (i.e., 001)

surface for the adsorption of sodium, barium, calcium and chloride ions onto gibbsite mineral using molecular dynamics simulation (Ho, 2018).

Although study by Brandt et al. (Brandt, 2018) addressed the impact of sodium and strontium concentration on Ra-226 removal by preformed barite mineral, there are still gaps in understanding competitive effects of monovalent and divalent cations. Surface and/or bulk mineral dissolution-recrystallization appears to be the main mechanism of Ra-226 removal by barite over the long period of time (i.e., 1-2 years), but the key mechanisms for Ra-226 uptake by barite surface under realistic process conditions (i.e., short reaction time) remain unclear. The impact of six different cations (i.e., $Na^+$, $K^+$, $Mg^{2+}$, $Ca^{2+}$, $Sr^{2+}$ and $Ba^{2+}$) on adsorption of Ra-226 by barite was studied experimentally and compared to molecular dynamics simulations to elucidate key short-term mechanisms for Ra-226 sequestration that would be relevant in engineered systems. Concentrations of these competing ions were varied from 0.01 – 1 mol/L and temperature was adjusted in the range 3-40 $^oC$ to expand these findings to applications ranging from drinking water treatment to treatment of highly contaminated produced waters generated during oil and gas extraction from unconventional (shale) reservoirs.

## 2.2 Materials and Methods

Synthetic solutions for this study were prepared using concentrated $RaCl_2$ stock solution with radioactivity of 3.7 mCi/L that was determined using Gamma spectroscopy (Canberra BE 202). Stock solution was diluted using deionized (DI) water (Synergy, Millipore, Billerica, MA) to a desired initial Ra-226 concentration. Barium sulfate, sodium chloride, potassium chloride, magnesium chloride hexahydrate, calcium chloride dihydrate and barium chloride dihydrate were

purchased from Fischer Scientific (Pittsburgh, PA), while strontium chloride hexahydrate was purchased from Sigma Aldrich (St. Louis, MO).

### 2.2.1 Adsorption Experiments

Adsorption experiments were conducted to evaluate the ability of barite to sequester Ra-226 from solutions containing alkali metal chlorides (i.e., NaCl and KCl) and alkaline earth metal chlorides (i.e., $MgCl_2$, $CaCl_2$, $SrCl_2$ and $BaCl_2$). Each of the metal chloride salts was dissolved in separate 1 L flasks containing $RaCl_2$ solution to achieve initial concentrations of 0.01, 0.1 and 1 mol/L. Solutions were then transferred to 50 mL Falcon polypropylene conical centrifuge tubes (Fisher Scientific, Pittsburgh, PA) and pH was adjusted to 7 by adding diluted HCl or NaOH. Barite solids at concentrations ranging from 100 – 2,000 mg/L were added to polypropylene tubes, dispersed for 30 min using the sonicator (Aquasonic, West Chester, PA) and mixed for 24 hours in the horizontal benchtop shaker (Fisher Scientific, Pittsburgh, PA) at 300 rpm. Adsorption experiments at low temperature (i.e., 3 °C) were carried out in the cold room, while experiments at higher temperature (i.e., 40 °C) were performed by mixing the samples in an incubator (MaxQ 4000, Thermo Fisher Scientific, Waltham, MA). Each set of samples included control samples without barite adsorbent to confirm that Ra-226 was not adsorbed to polypropylene tubes. After 24 hours of mixing, samples were filtered through 0.45 μm mixed cellulose ester membrane (Millipore, Billerica, MA) and saved in a refrigerator for further analysis. Ra-226 was analyzed by mixing 2 mL of a sample with 14 mL of liquid scintillation Ultima Gold cocktail (Perkin Elmer, Waltham, MA) in a glass vial. Ra-226 concentration was measured using Liquid Scintillation Counter (LSC, LS 6500, Beckman Coulter, Brea, CA) for 40 min at 170-230 keV energy range.

QA/QC protocol included validation of random samples using Gamma spectroscopy (Johnston, 1997). Adsorption capacity of barite was calculated as:

$$q = \frac{(C_0 - C_e)V}{A} \quad (2.1)$$

where, q (pCi/mg) represents the adsorption capacity for Ra-226, $C_0$ and $C_e$ (pCi/L) are the initial and final Ra-226 activity in the liquid phase, V (L) is the volume of the sample and A ($cm^2$) is the total surface area of the adsorbent that was determined using a 6-point Brunauer-Emmett-Teller (BET) analysis in the relative pressure range $0.06 < P/P_0 < 0.25$ (Micromeritics ASAP 2020, Micromeritics, Norcross, GA).

### 2.2.2 Zeta Potential

Zeta potential of barite was analyzed using Litesizer 500 (Anton Paar, Ashland, VA) based on electrophoretic mobility of barite particles. Barite solids were first ground using mortar and pestle and then suspended in DI water in six different 0.1 mol/L salt solutions (i.e., NaCl, KCl, $MgCl_2$, $CaCl_2$, $SrCl_2$, $BaCl_2$) at pH 7 (i.e., pH used in adsorption isotherms experiments). Solutions were then dispersed in a sonicator for 30 min and 350 μL of each solution was placed in a polycarbonate cuvette equipped with gold electrodes for zeta potential analysis.

### 2.2.3 Molecular Dynamics Modeling

All molecular dynamics (MD) simulations were performed using AMBER software (Case, 2018). Potential of mean force (PMF) calculations were conducted using umbrella sampling (Torrie, 1977) and umbrella integration (Kästner, 2009) techniques by assigning a PMF value of 0 at 10 Å. Two cases were analyzed: 1) barite surface and each of the $MeCl_2$ (i.e., Me = $Mg^{2+}$,

$Ca^{2+}$, $Sr^{2+}$, $Ba^{2+}$, $Ra^{2+}$) separately, and 2) barite surface and a single $RaCl_2$ molecule in 0.1 and 1 mol/L concentrated solutions of each of the $MeCl_{(2)}$ (i.e., Me = $Na^+$, $K^+$, $Mg^{2+}$, $Ca^{2+}$, $Sr^{2+}$, $Ba^{2+}$). In order to keep window centers in the range from 1-12 Å at 11 ns per window, a constant spring potential was applied between the metal and the first layer of $SO_4$-S atoms perpendicular to the 100, 010 and 001 barite surface. The unit cell structure of barite was obtained from Hill (Hill, 1977) and appropriate crystal structures (i.e., 100, 010 and 001) were built using Vesta system (Momma, 2008).

Adsorption isotherms were simulated using the multicomponent Langmuir isotherm model according to the following procedure:

1) The change in Gibbs free energy $\Delta G^0$ was estimated from PMF curves as the difference between bulk and minimum PMF;
2) $\Delta G^0$ was used to calculate thermodynamic equilibrium constant $K_a$ using the following equation:

$$\Delta G^0 = -RTlnK_a \tag{2.2}$$

where, R is the universal gas constant and T is the absolute temperature;

3) Langmuir coefficient b is numerically equal to thermodynamic equilibrium constant $K_a$;
4) Assuming maximal adsorption capacity $q_{max}$ based on 2 adsorption sites per $nm^2$ of barite surface;
5) Calculate adsorption capacity $q_{Ra2+}$ using the following equation:

$$q_{Ra^{2+}} = q_{max}\frac{b_{Ra^{2+}}C_{Ra^{2+}}}{1+b_{Ra^{2+}}C_{Ra^{2+}}+b_{Ba^{2+}}C_{Ba^{2+}}+b_{Me}C_{Me}} \tag{2.3}$$

where, $C_{Ra2+}$ is the equilibrium bulk concentration of $Ra^{2+}$ and $C_{Ba2+}$ is the equilibrium buk concentration of $Ba^{2+}$.

## 2.3 Results and Discussion

### 2.3.1 Impact of Different Cations on Ra-226 Uptake by Barite

Radium removal by barite was first evaluated in DI water and in 0.1 M salt solutions. Salts were selected based on their abundance in produced water and characteristics of a metal cation to elucidate the impact of the competing cations on Ra-226 removal. Adsorption isotherms for Ra-226 in DI water and in the presence of different salts are shown in Figure 2.1.

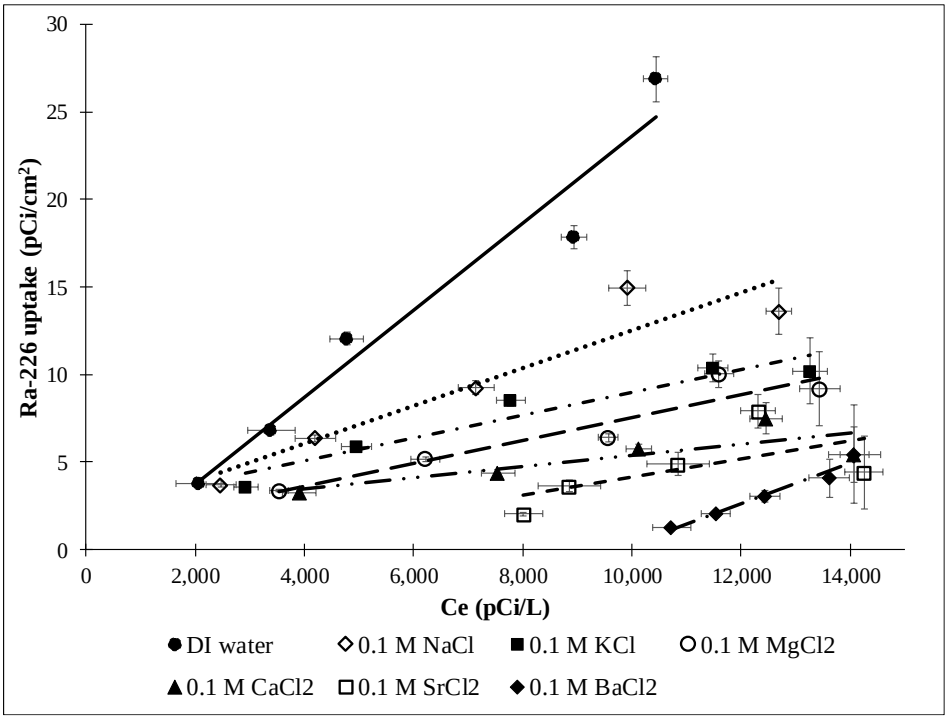


**Figure 2.1.** Adsorption isotherms for Ra-226 uptake by barite in DI water and in 0.1 mol/L salt solutions at neutral pH and with initial Ra-226 concentration of 15,000 pCi/L.

As can be seen in Figure 2.1, barite solids showed high affinity for radium ions in DI water. Ra-226 removal was in the range from 3.8 – 26.9 pCi/cm$^2$ at Ra-226 concentration in the liquid

phase from 2,060 – 10,440 pCi/L. Experimental data showed a good fit with Freundlich adsorption isotherm model where correlation coefficients for all isotherms except for $CaCl_2$ and $SrCl_2$ were at or above 0.94 (Figure A.1 in Appendix A). These results are fairly similar to adsorption trends observed in previous studies that showed that Ra-226 ions are readily removed by barite solids (Gusa, 2018; Wang, 1987). Previous studies also emphasized the importance of barite surface dissolution-recrystallization reactions for the sequestration of Ra-226 from aqueous solutions over long periods of time (i.e., 100 days – 2 years) (Bosbach, 2010; Brandt, 2015; 2018; Curti, 2010; Klinkenberg, 2014; Vinograd, 2013). However, significant Ra-226 removal was achieved in this study after just 24 hours and did not change significantly over the next 3 days (Figure A.2 in Appendix A).

Presence of monovalent or divalent cations in the solution significantly reduced radium removal by barite in the following order: $Na^+ > K^+ > Mg^{2+} > Ca^{2+} > Sr^{2+} > Ba^{2+}$. Barite surface is likely not electroneutral like the bulk of the mineral because active surface $SO_4^{2-}$ groups can form due to the incomplete coordination spheres (Bokern, 2003; Harvey, 2000). Such negatively charged surface can attract positively charged ions from the surrounding solution and form an electrical double layer (EDL) around barite particles. Thus, electrostatic interactions between negatively charged barite surface and $Ra^{2+}$ ions are hindered by 10 orders of magnitude higher concentration of other cations in the solution. Divalent cations have stronger interaction (i.e., attractive Van der Waals forces) with barite surface which results in significantly lower radium removal than in the presence of monovalent cations (Figure 2.1). However, it is somewhat surprising that different cations with the same charge do not impact the radium removal to the same extent (e.g., $K^+$ interferes more than $Na^+$, $Sr^{2+}$ interferes more than $Mg^{2+}$). This behavior can be explained by the ionic size and diffusivity of these cations listed in Table 2.1.

**Table 2.1.** Ionic radii, diffusivities and calculated Stokes radii of the ions used in Ra-226 removal experiments

| Ion | Ionic radius (Shannon, 1976) (Å) | Diffusivity (Haynes, 2014) ($10^{-5}$ $cm^2/s$) | Stokes radius (Å) |
|---|---|---|---|
| $Na^+$ | 1.16 | 1.334 | 1.75 |
| $K^+$ | 1.52 | 1.957 | 1.19 |
| $Mg^{2+}$ | 0.86 | 0.706 | 3.30 |
| $Ca^{2+}$ | 1.14 | 0.792 | 2.94 |
| $Sr^{2+}$ | 1.32 | 0.791 | 2.94 |
| $Ba^{2+}$ | 1.49 | 0.847 | 2.75 |
| $Ra^{2+}$ | 1.62 | 0.889 | 2.62 |

As can be seen in Table 2.1, $K^+$ is larger than $Na^+$ but has higher diffusivity than $Na^+$, which can explain the differences in their impact on radium removal (Figure 2.1). Potassium has greater ability to diffuse through the layer of ions (i.e., $H^+$ and $OH^-$) around barite particle and due to its bigger size (i.e., 50% bigger radius than $Na^+$) act as a physical barrier for radium adsorption. Similarly, radium removal by barite decrease with increasing ionic radii and diffusivity of divalent cations.

A set of umbrella integration analysis and potential of mean force calculations were performed to further investigate the interaction between divalent ions (i.e., $Mg^{2+}$, $Ca^{2+}$, $Sr^{2+}$. $Ba^{2+}$, $Ra^{2+}$) and barite surface to elucidate the impact of charge and size of cations on radium removal by barite. The potential of mean force calculations were performed for two cases: 1) All ions were assigned the Lennard-Jones potential of $Ba^{2+}$, while each of the ions had their own ionic mass and

2) All ions were assigned ionic mass of $Ba^{2+}$, while each of the ions had their own Lennard-Jones potential.

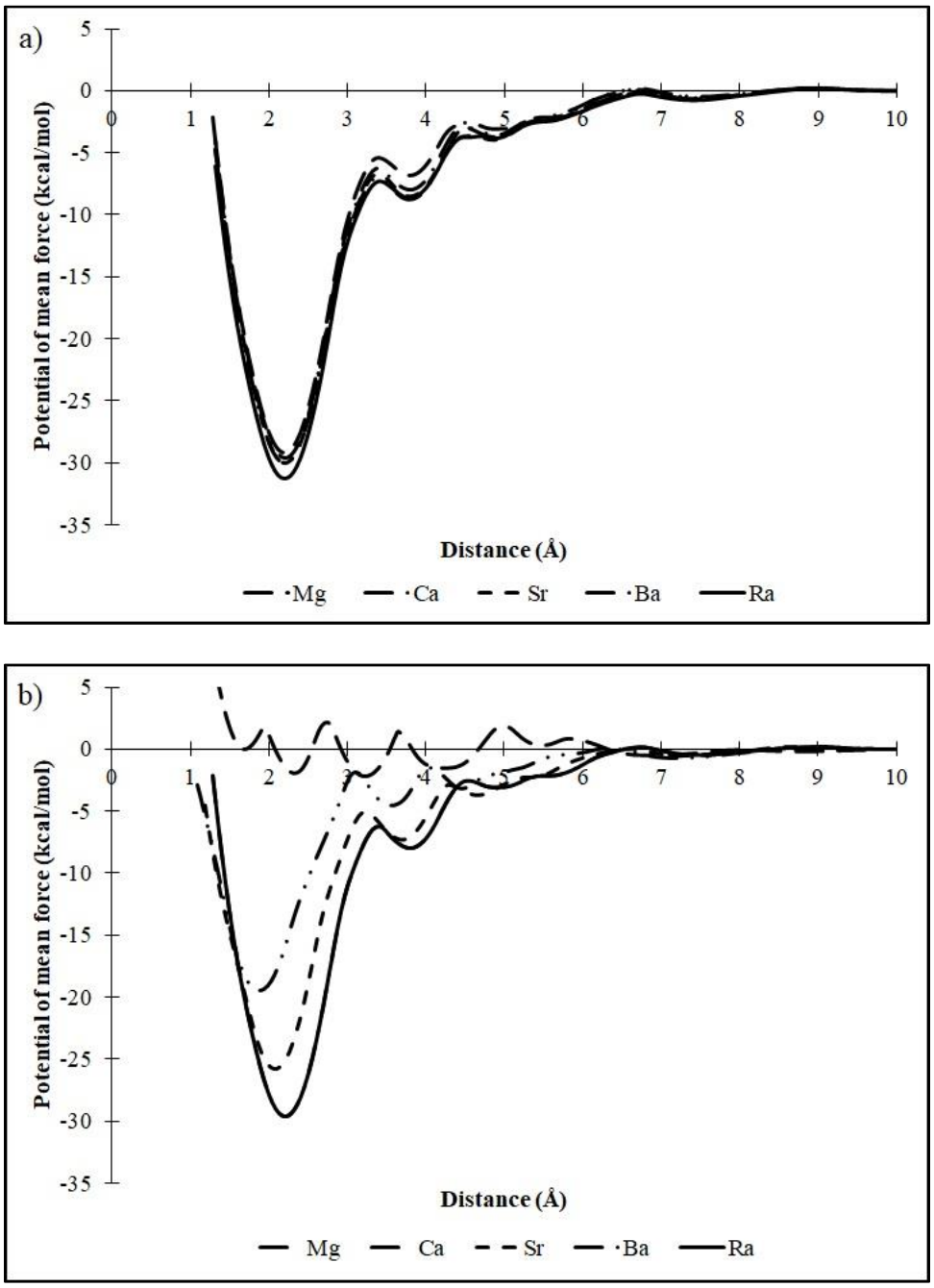


**Figure 2.2.** Potential of mean force (PMF) at constant (a) Lennard-Jones potential and (b) ionic mass for different cations onto 100 barite surface in DI water.

As can be seen in Figure 2.2a, interaction energy between ions and barite surface has the most negative value (i.e., most favorable adsorption) in the narrow range from -29 to -31 kcal/mol at approximately 2.2 Å from the mineral surface. These results suggest that ionic mass does not have significant impact on interaction energy between these ions and barite. Contrary to ionic mass, it appears that Lennard-Jones potential has significant impact on the interaction energy. As can be seen in Figure 2.2b, keeping the same mass for all ions (i.e., all ions have the mass of $Ba^{2+}$) and varying Lennard-Jones forcefield parameters resulted in different interaction energies between ions and barite surface. The lowest interaction energy of -29.61 kcal/mol was calculated for $Ra^{2+}$ and $Ba^{2+}$ at 2.2 Å from barite surface. Slightly higher (i.e., less negative) and less favorable interaction energy of -25.83 kcal/mol was calculated for $Sr^{2+}$ at 2.06 Å, followed by -19.46 kcal/mol for $Ca^{2+}$ at 1.86 Å from the surface. Interaction energy as function of distance calculated for $Mg^{2+}$ shows very unstable behavior. Figure 2.2b shows that $Ba^{2+}$ is likely to have the strongest interaction with barite surface and therefore cause the highest interference with $Ra^{2+}$ adsorption, which was confirmed by experimental results in Figure 2.1 where the lowest $Ra^{2+}$ removal was observed in the presence of $Ba^{2+}$. Interaction energies of other ions follow the same order as adsorption isotherms shown in Figure 2.1, from the smallest to the highest interaction energy: $Mg^{2+} > Ca^{2+} > Sr^{2+} > Ba^{2+}$.

To further investigate the impact of attractive forces between barite surface and each of the ions, zeta potential analyses were performed in different 0.1 M solutions and results are shown in Figure 2.3.

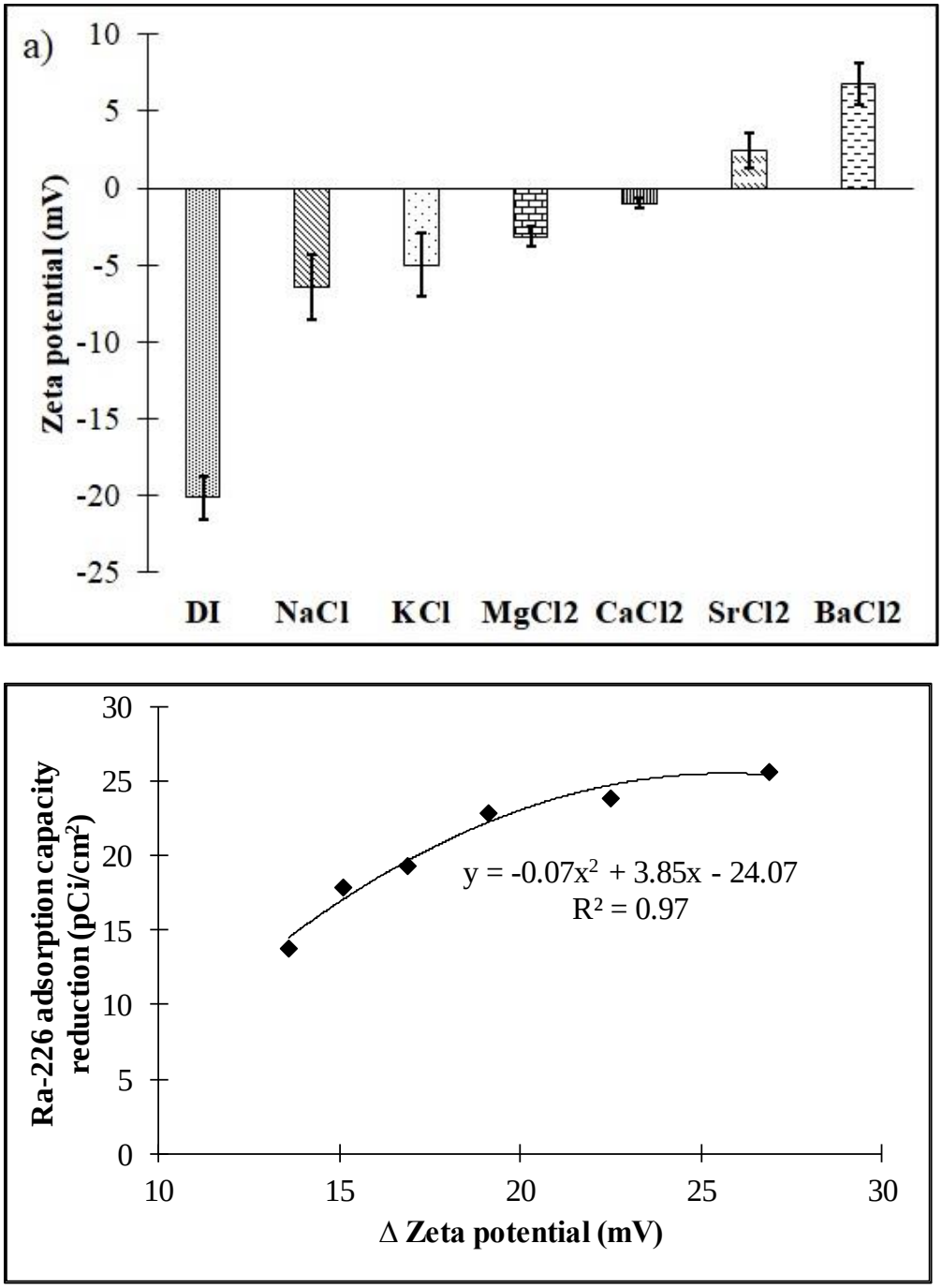


**Figure 2.3.** (a) Zeta potential of barite in DI water and in 0.1 mol/L electrolyte solution at neutral pH and (b) Ra-226 adsorption capacity reduction as a function of zeta potential change compared to that in DI water at Ce = 12,000 pCi/L. Experimental standard deviation calculated based on at least 5 replicates is shown using error bars.

As can be seen in Figure 2.3a, barite has the lowest (i.e., the most negative) zeta potential in DI water of -20.1 mV, which is increasing (i.e., becoming less negative) in the presence of ions due to the compression of EDL around barite particles. EDL thickness (Debye length) is a function of the concentration and charge of ions in the solution (Kohonen, 2000). Therefore, more pronounced EDL compression and less negative values of zeta potential are expected in the presence of divalent cations than in the presence of monovalent cations at identical concentrations. However, different monovalent and divalent cations exhibited different impact on zeta potential of barite surface. The increase in zeta potential is more pronounced in the presence of $BaCl_2$ than in the presence of $SrCl_2$ and less negative in $CaCl_2$ than in $MgCl_2$ solution and these differences are statistically significant with 95% confidence interval (Table A.1 in Appendix A). It also appears that zeta potential is less negative in KCl than in NaCl solution, but this difference is not statistically significant (Table A.1 in Appendix A). These findings can be explained by the differences in diffusivity of these cations (Table 2.1). Ions with higher diffusivity are able to approach closer to the barite surface and exert a greater impact on EDL potential (Wadekar, 2017). Radium removal can be directly related to the zeta potential and this behavior is depicted in Figure 2.3b where the reduction in radium adsorption capacity is logarithmically proportional to the increase in zeta potential relative to that observed in DI water.

Zeta potential is measured at the slipping (shear) plane of the EDL, but the exact location of this plane is not precisely defined. However, it is generally accepted that slipping plane is located between the Stern layer and the edge of the double layer (i.e., Debye length) (Hunter, 2013). Stern layer thickness is approximately equal to the radius of the major cation in the solution (Brown, 2016a; b; Herbowski, 2009), which is in the range from 0.86 - 1.62 Å under the conditions used in this study. Since the thickness of the EDL calculated using Equation A3 in the Supporting

information for 0.1 mol/L divalent cation electrolytes solutions is 5.58 Å, it can be concluded that the zeta potential was measured at 0.86 – 5.58 Å distance from barite surface. As can be seen in Figure 2.2b, favorable interaction energy was found in the range 1.5 – 3 Å which overlaps with the potential location of the shear plane for most of the divalent cations and further emphasizes the importance of zeta potential for the removal of radium from aqueous solutions.

### 2.3.2 Impact of Cation Concentration on Ra-226 Uptake by Barite

Uptake of radium by barite was also analyzed in 0.01 and 1 mol/L solutions of different divalent cations to evaluate the impact of competitive adsorption on radium uptake by barite and the results are compared in Figure 2.4.

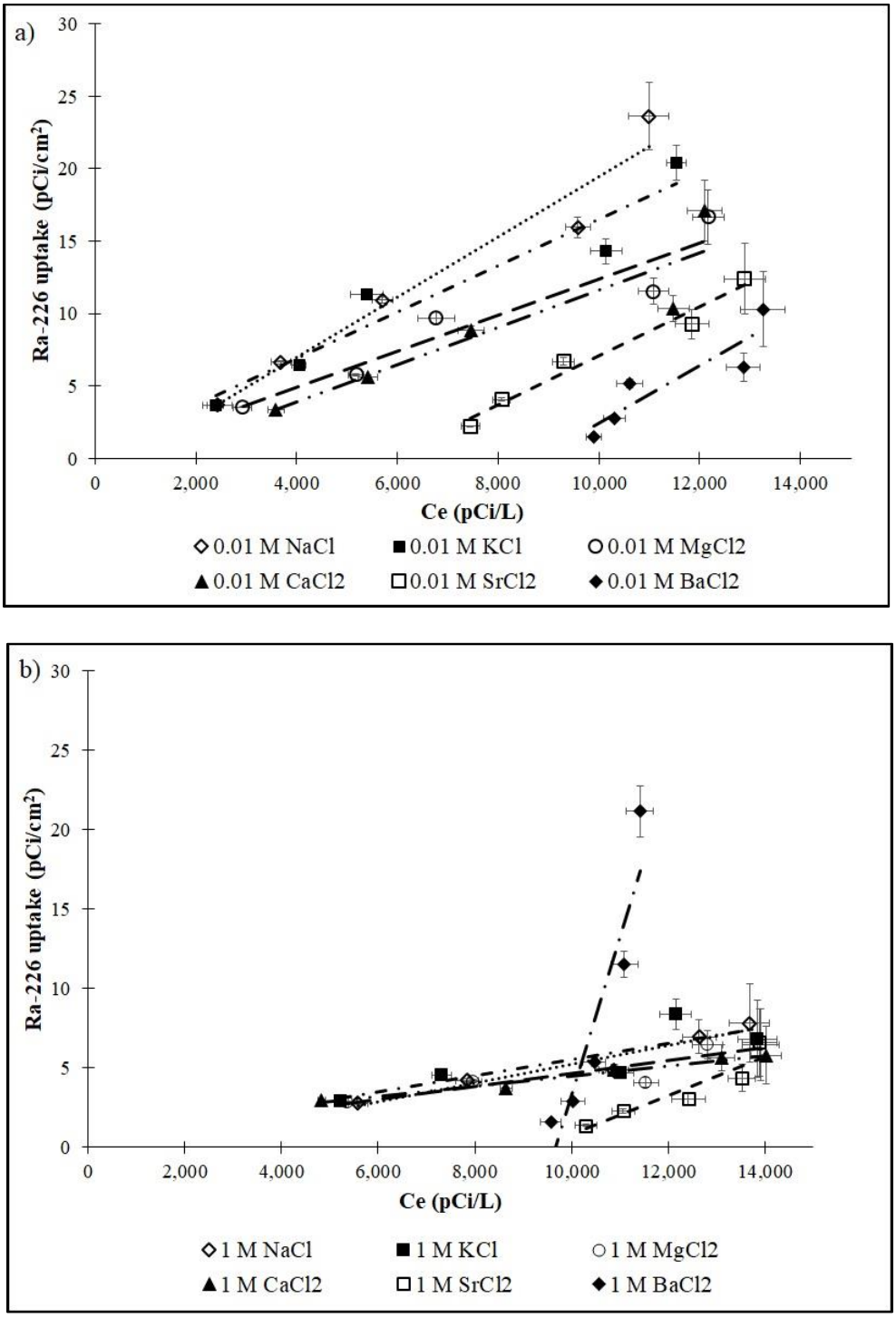


**Figure 2.4.** Adsorption isotherms for Ra-226 uptake by barite in (a) 0.01 mol/L and (b) 1 mol/L salt solutions at neutral pH with initial Ra-226 concentration of 15,000 pCi/L.

As can be seen in Figure 2.4a, previously observed adsorption isotherms trends in the presence of 0.1 mol/L solution of co-ions shown in Figure 2.1 remained the same in the presence of 0.01 mol/L solution of these ions with the highest radium uptake observed in the presence of NaCl and the lowest in the presence of $BaCl_2$. However, significantly higher radium uptake was observed at lower concentration. For example, radium removal of 17.1 pCi/cm$^2$ was observed in 0.01 mol/L $CaCl_2$ solution compared to 5.4 pCi/cm$^2$ in 0.1 mol/L $CaCl_2$ solution, which is due to less competition for sites at barite surface at lower co-ion concentrations. Similar behavior was observed by Brandt et al. (Brandt, 2018). Impact of co-ion concentration is clearly observed in Figure 2.4b, where radium removal was notably reduced when the concentration of these ions increased to 1 mol/L. As discussed previously, radium removal is higher in the presence of monovalent than divalent cations and it varied from 2.8-7.8 pCi/cm$^2$ in 1 mol/L NaCl to 1.4-6.6 pCi/cm$^2$ in 1 mol/L $SrCl_2$. However, the exception was 1 mol/L $BaCl_2$ solution where much higher radium uptake was achieved than in other solutions. Although such behavior may be considered counter intuitive, it is important to note that adding such high concentration of $BaCl_2$ to the solution with existing $BaSO_4$ can induce precipitation of fresh $BaSO_4$ solids due to the common ion effect (Monnin, 1999). Therefore, radium uptake in the presence of 1 mol/L $BaCl_2$ solution (1.6-21.1 pCi/cm$^2$) can be explained by simultaneous removal of radium through co-precipitation and post-precipitations processes (Zhang, 2014).

### 2.3.3 Comparison of Experimental and Modeling Data

Selected experimental adsorption isotherms predicted from molecular dynamics simulations are compared to experimental results in Figure 2.5.

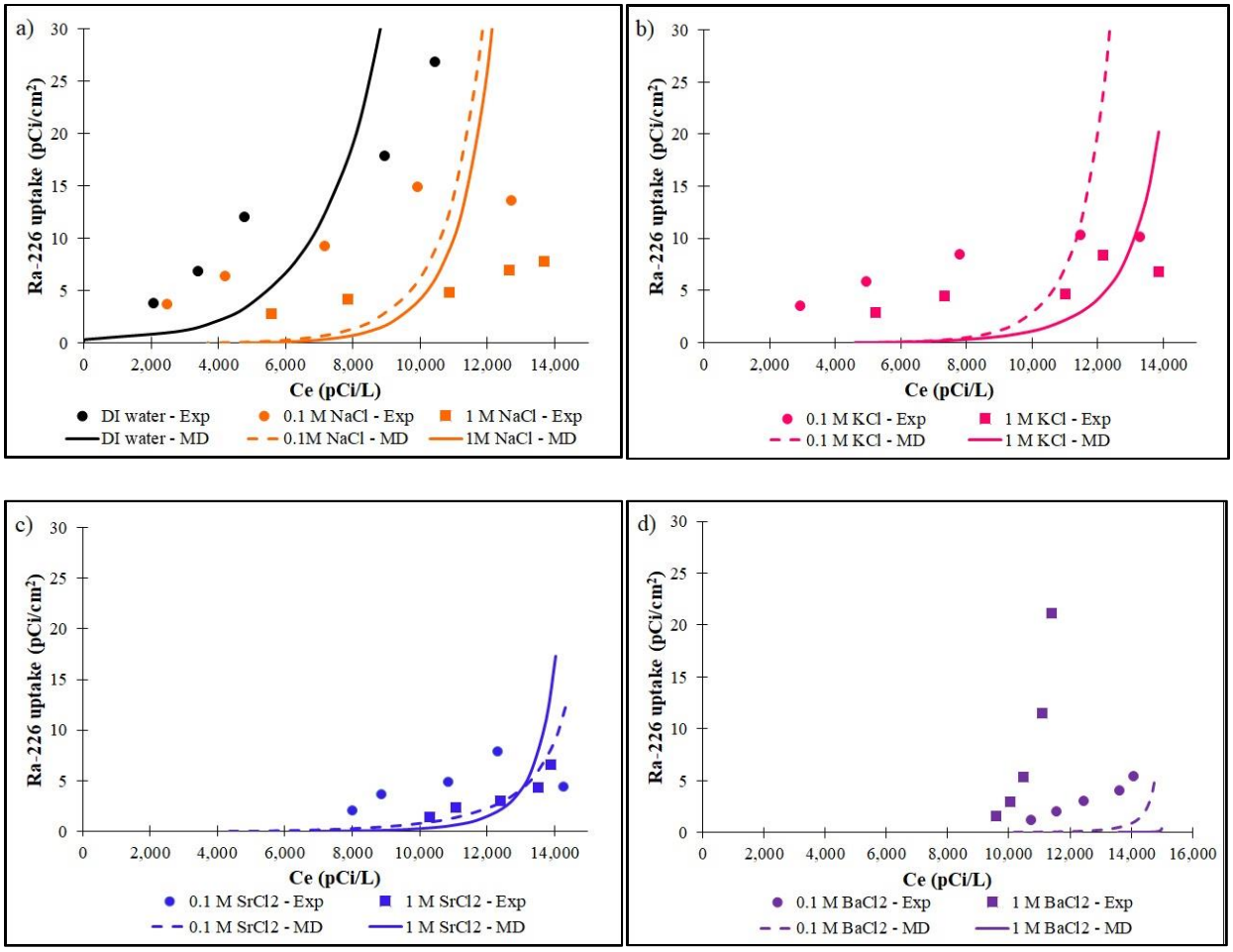


**Figure 2.5.** Experimental results and molecular dynamics predictions of Ra-226 uptake by barite (001 surface) in (a) DI water, 0.1 and 1 M NaCl, (b) 0.1 and 1 M KCl, (c) 0.1 and 1 M $SrCl_2$ and (d) 0.1 and 1 M $BaCl_2$.

As can be seen in Figure 2.5, molecular dynamics predictions obtained independently offer a reasonable match with experimental data in the order of magnitude of the removal capacity at equilibrium concentrations evaluated in this work and general trend (i.e., increase in equilibrium concentration Ce results in higher Ra-226 uptake). Similar to experimental results, the model predicts higher Ra-226 removal by barite in solutions containing 0.1 mol/L of electrolyte than in 1 mol/L solutions in all cases except for $SrCl_2$ at equilibrium concentrations above 13,000 pCi/L

(Figure 2.5c). In addition to successfully modeling the impact of co-ion concentration on radium removal, the order of magnitude of radium uptake predicted by the molecular dynamics is quite consistent with experimental results for the equilibrium concentration (i.e., Ce) range evaluated in this study. As can be seen in Figure 2.5a, experimental and modeling data match quite well in the case of radium removal by barite in DI water where even the shape of the adsorption isotherm is fairly similar between predicted and experimentally obtained results. However, other modeling results show deviation from linear trends observed in Figures 2.1 and 2.4, which could be due to inaccurate estimates of the potential of mean force. Hence, further analysis will be necessary to ascertain the exact source of these inconsistences.

The biggest discrepancy between the experimental and modeling data can be observed in Figure 2.5d where model predicts extremely low radium uptake by barite in 1 mol/L $BaCl_2$ solution. A possible reason for this and other differences between experimental and modeling results can be the fact that molecular dynamics modeling uses only surface adsorption as a mechanism for radium removal while it is very likely that radium sequestration process is governed by multiple mechanisms in the experiments conducted in this study. As previously shown, surface dissolution-recrystallization reactions have an important role in radium uptake by barite over a long period of time (Bosbach, 2010; Brandt, 2015; 2018; Curti, 2010; Klinkenberg, 2014).

A set of experiments was designed to evaluate radium removal mechanisms in experimental studies and explain the differences between measured and predicted results. Adsorption of radium is an exothermic process and is expected that radium uptake by barite should decrease with an increase in temperature (Erkey, 2011; Mor, 2007; Rouquerol, 2013). On the other hand, the extent and the rate of barite recrystallization is enhanced at higher temperature which should results in increased radium uptake from the solution (Malone, 1996). Therefore, radium

removal by barite was evaluated at three different temperatures (i.e., 3, 21 and 40 °C) to further elucidate the mechanisms involved in this process and the results are shown in Figure 2.6.

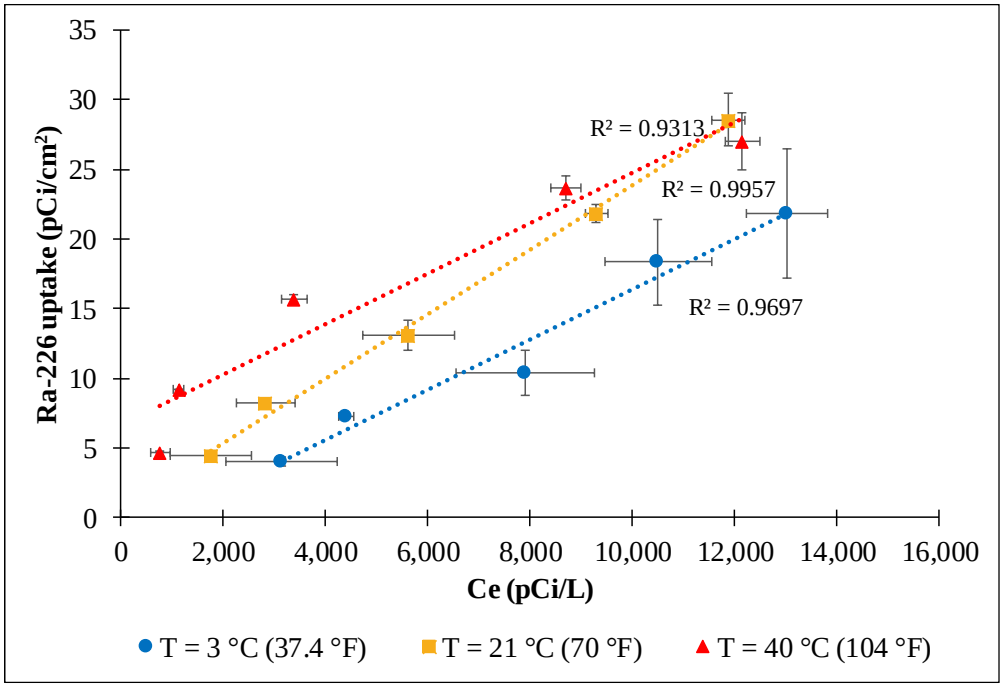


**Figure 2.6.** Ra-226 uptake by barite in DI water at different temperatures with initial Ra-226 concentration of 16,750 pCi/L. Experimental standard deviation shown with error bars was calculated based on at least 5 replicates.

The difference between the experimental data collected at 3, 21 and 40 °C shown in Figure 2.6 was statistically significant at 95% confidence interval (Table A.2 and Figure A.3 in Appendix A). As can be seen in this figure, radium uptake by barite was enhanced at 40 °C compared to the room temperature for the equilibrium conditions evaluated in this study, especially at lower equilibrium concentrations. Reducing the ambient temperature to 3 °C had an adverse impact on Ra-226 uptake ranged from 4-21.9 pCi/cm$^2$ compared to 4.4 – 28.6 pCi/cm$^2$ at room temperature. The results shown in Figure 2.6 confirm that radium uptake by barite is not the result of adsorption

alone and suggest that other mechanisms are involved in radium removal from aqueous solutions. Increased radium uptake at higher temperature suggests that dissolution-recrystallization reactions at the surface of barite with 24-hour equilibration period used in these experiments play an important role in the removal of radium from aqueous solution. Thus, deviations between experimental and modeling results can be attributed to the existence of multiple mechanism of radium removal in the experimental system and limitations of the model that is only based on pure surface adsorption.

## 2.4 Summary and Conclusions

The finding of this study suggest that Ra-226 is readily removed from aqueous solutions by barite and that this process is highly influenced by solution composition, ionic strength and temperature. Experimental studies with six different cations evaluated in this study have shown that their impact on radium removal by barite depends on the ion charge, ion size and ion diffusivity. Divalent cations reduced radium removal more than monovalent cations in 0.01 and 0.1 mol/L solutions. This trend was not as apparent in 1 mol/L solution because of very high concentration of competitive ions and inability of $Ra^{2+}$ ions to diffuse through the EDL that forms at high ionic strength. Comparison between experimental and modeling results showed that dissolution-recrystallization is an important mechanism for Ra-226 uptake by barite. However, the interaction of radium ions and barite surface is affected by the effect of zeta potential at the shear plane of EDL at approximately 2-3 Å from the surface (Figure 2.2). Because each co-ion has different impact on the behavior of zeta potential (Figure 2.3a), Ra-226 uptake strongly depends on type of ions found in a solution (Figure 2.3b). Radium removal by barite was successfully

modeled using molecular dynamics simulations and theoretical calculations showed reasonable qualitative agreement with experimental results. Temperature dependence of radium removal by barite (Figure 2.6) indicated that barite dissolution/recrystallization is an important mechanism for radium uptake. Because molecular dynamics simulations assumed only surface adsorption as the mechanism for radium removal from solution, it is not surprising to see discrepancies between experimental and modeling results. Even though the exact match of experimental and modeling data was not achieved, molecular dynamics simulations offered an insight into the existence of other mechanisms for radium removal that are not included in the model. For solids like barite that undergo dissolution/recrystallization in aqueous solution, it would be necessary to include these reactions in the theoretical model to improve its utility in practice.

## 3.0 Development of Functionalized Proppant for the Control of NORM in Marcellus Shale Produced Water

**This work has been published as:**

Gusa, A.V. and Vidic, R.D. (2018). Development of functionalized proppant for the control of NORM in Marcellus Shale produced water, Environmental science & technology 53, (1), pp. 373-382.

One of the major environmental concerns with the recovery of unconventional gas resource from Marcellus Shale is the presence of Naturally Occurring Radioactive Material (NORM) in produced water. Ra-226 is the major component of NORM with a half-life of 1,600 years that is present at concentration as high as several thousand pCi/L. Most of the studies on NORM management are focused on above-ground scenarios. The main focus of this study was on functionalizing the proppant (i.e., quartz sand) that is used in hydraulic fracturing to prevent the closure of induced fractures formed during this process and allow release of natural gas so that it can also sequester NORM from the produced water before it reaches the surface. Five different sulfates and carbonates were tested for their ability to capture Ra-226 from aqueous solution and celestite ($SrSO_4$) and barite ($BaSO_4$) were identified as the best choices because of their affinity for Ra-226 sequestration even in the presence of very high total dissolved solids that are characteristic of Marcellus Shale produced water. Among possible ways of coating the proppant with celestite or barite, precipitating mineral directly on the sand surface was found to be the best option as it provided uniform distribution of celestite and barite, and high uptake of Ra-226. Although quartz sand can adsorb some radium from the solution due to electrostatic interactions,

adding a small amount of a coating agent on the sand surface (10-30 mg/g) increased radium removal from the solution containing 5,000 pCi/L of Ra-226 to more than 80% in dilute solution and to more than 50% in high salinity solution even in the presence of very high concentrations of competing divalent cations. The results of this study indicate the potential of coated proppant to sequester NORM in the subsurface and prevent adverse environmental impacts when radiogenic produced water is brought to the surface.

## 3.1 Introduction

Natural gas can be found in both conventional and unconventional reservoirs. The extraction of natural gas from geological formations with low permeability (i.e., unconventional reservoirs) is made economical (Holditch, 2007) with the development of new technologies and advances in processes, such as horizontal well drilling and reservoir stimulation. During hydraulic fracturing, water mixed with a proppant and chemical additives is injected into the formation at high pressures (i.e., 480-680 bar (Barbot, 2013)) to enlarge existing fractures and create new ones. Stimulation of a single well requires 5-7 million gallons of water and 1,500 - 2,000 tons of proppant (Hayes, 2009). Several different proppants are used in this process with sand, resin-coated sand and ceramic proppants being the most common. The proppant makes only about 9% of the total weight of the fracturing fluid (ALLConsulting, 2009; Vidic, 2013) and is essential to prevent the collapse of microfractures that are formed during the hydraulic fracturing process and enable efficient extraction of natural gas.

One of the major environmental concerns with hydraulic fracturing is the very high salinity of flowback water generated during several weeks after the drilling process (Vidic, 2013) and

produced water generated during the life of the well. Total dissolved solids (TDS) in this water are mainly comprised of sodium and chloride as well as alkaline earth metals, such as strontium, barium, calcium and magnesium, and can range from 92-308 g/L (Lokare, 2017) depending on the location and life of the well. In the case of Marcellus Shale formation in Pennsylvania, the average TDS is 106 g/L (Barbot, 2013). However, high salinity is not the only concern with produced water as it also contains very high concentration of Naturally Occurring Radioactive Material (NORM). Marcellus Shale is the most radiogenic formation among all shale plays in the US (Rowan, 2011) and the produced water from Marcellus wells contains Ra-226 and Ra-228 as decay products of U-238 and Th-232, respectively. Due to low concentration of Th-232 in organic rich shale, Ra-228 usually represents 10-15% of the total NORM in the produced water (Rowan, 2011; Tasker, 2019; Zhang, 2015b) Ra-228 also has a shorter half-life than Ra-226 (5.75 vs 1,600 years) and most of the focus in previous studies has been on Ra-226 (Brandt, 2015; Curti, 2010; Zhang, 2015a; 2014). Radium content in produced water is a function of a local lithology and its total activity (i.e., combined Ra-226 and Ra-228 activity) can reach as high as 20,000 pCi/L, with a median value of 2,460 pCi/L for the Marcellus Shale in Pennsylvania and 5,490 pCi/L for the Marcellus Shale in New York (Rowan, 2011). The existing regulatory limit for radium activity in industrial effluents and drinking water is 60 and 5 pCi/L, respectively (U.S.EPA, 1976). Radium can cause major environmental and health problems (Vidic, 2013; Werner, 2015) and appropriate management of flowback and produced water is necessary to prevent environmental impacts and enable further development of this industry.

Current strategies for produced water management include reuse, disposal into Class II Underground Injection Control (UIC) wells, or appropriate treatment prior to disposal (Gregory, 2011; Kargbo, 2010). Reuse is the most effective option for managing this water in Pennsylvania,

but it may be of limited value depending on the drilling schedule and field maturity. The lack of disposal wells in Pennsylvania (McCurdy, 2011) and risks associated with induced seismicity motivated the development of treatment technologies for this water. One of the most cost-effective strategies for the control of radium is co-precipitation with different sulfates, most commonly with barium sulfate (barite). Zhang et al. showed that radium co-precipitation with both barium sulfate (barite) and strontium sulfate (celestite) can be utilized for NORM removal from produced water (Zhang, 2015a; 2014). Several studies evaluated radium removal by preformed barite where radium uptake occurs during barite dissolution and re-crystallization over a long period (Bosbach, 2010; Curti, 2010; Klinkenberg, 2014).

Contaminant removal from aqueous solutions based on impregnating different surfaces with inorganic materials capable of adsorbing pollutants has been investigated previously. Vaisha and Gupta evaluated arsenic(III) and arsenic(V) removal from solution by barium sulfate modified iron oxide coated sand (Vaishya, 2002; 2006). They showed that this coating complex can significantly enhance arsenic removal and analyzed the impact of process parameters (i.e., alkalinity, pH, temperature and surface area) on the kinetics and equilibrium of arsenic uptake. Arsenic removal by iron-oxide coated polymeric surface was investigated by Katsoyiannis et al (Katsoyiannis, 2002). while iron-oxide and manganese-oxide coated sand were used for arsenic removal from ground water (Bajpai, 1999; Joshi, 1996). Han et al. investigated the ability of manganese-oxide coated sand to remove heavy metals like $Cu^{2+}$ and $Pb^{2+}$ from aqueous solution (Han, 2006a; b). Goyal et al. demonstrated the potential of using existing polyurethane resin coated proppants for radium removal under various conditions (Goyal, 2017). Similar idea of NORM removal using resin coated proppant by “in-situ” approach was investigated by McDaniel et al (McDaniel, 2014).

The objective of this study was to develop a functionalized proppant that can be injected in the shale formation to sequester radium from the produced water before it reaches the surface. Although the solid solution theory (Prieto, 2009) is typically used to analyze co-precipitation equilibrium (Equations B1-B4 in Appendix B), very high theoretical distribution coefficient for radium-strontium sulfate ($K_d$=237) (Zhang, 2014) suggests that strontium sulfate may be used as an effective sequestering agent for radium even if celestite is already present in solid phase. In this study, celestite was compared with other sulfates (i.e., barium sulfate) and carbonates (i.e., strontium carbonate, barium carbonate and calcium carbonate) for its ability to sequester radium from aqueous solution when it is dispersed in solution or when it is impregnated on the surface of quartz sand that is typically used as proppant in hydraulic fracturing operations in Marcellus Shale (Liang, 2016).

## 3.2 Materials and Methods

### 3.2.1 Reagents and Materials

Concentrated $RaCl_2$ solution obtained from the Pennsylvania State University was used to prepare all solutions in this study. Gamma spectroscopy (Canberra BE 202) was used to determine the activity of Ra-226 in the stock solution of 1.44 mCi/L, which was then diluted with deionized (DI) water (Synergy, Millipore, Billerica, MA) to achieve initial Ra-226 activities ranging from 5,000-7,750 pCi/L. Strontium sulfate, barium sulfate, strontium chloride hexahydrate, sodium chloride and sodium sulfate decahydrate were purchased from Fischer Scientific (Pittsburgh, PA) and calcium carbonate, strontium carbonate, barium carbonate and quartz sand (50-70 U.S. Mesh

size with average particle size of 250 μm) were purchased from Sigma Aldrich (St. Louis, MO). All chemicals were analytical grade.

### 3.2.2 Adsorption Experiments

Adsorption experiments were first performed to evaluate the ability of five common minerals of alkaline earth metals (i.e., $SrSO_4$, $BaSO_4$, $CaCO_3$, $SrCO_3$ and $BaCO_3$) to sequester radium from dilute aqueous solutions. The solids at concentrations ranging from 100 to 2,000 mg/L were dispersed in 50 mL of 5,000 pCi/L Ra-226 solution for 1 hour using the sonicator (Aquasonic, West Chester, PA). Dispersed samples were transferred to 50 mL Falcon polypropylene conical centrifuge tubes (Fisher Scientific, Pittsburgh, PA) and mixed for 24 hours in a horizontal shaker (Darts Control Inc., Zionsville, IN) at 25 rpm to achieve adsorption equilibrium. A blank sample without solids was also mixed for 24 hours to confirm that no Ra-226 was adsorbed to centrifuge tube walls. Each sample was filtered through 0.45μm mixed cellulose ester membrane (Millipore, Billerica, MA) and analyzed using Liquid Scintillation Counter (LSC, LS 6500, Beckman Coulter, Brea, CA). Equilibrium adsorption capacity for Ra-226 was calculated as:

$$q = \frac{(C_0 - C_e)V}{m} \tag{3.1}$$

where, q (pCi/mg) represents the adsorption capacity for Ra-226, $C_0$ and $C_e$ (pCi/L) are the initial and final Ra-226 activity in the liquid phase, V (L) is the volume of the sample and m (mg) is the mass of the adsorbent. Freundlich isotherm (Kinnlburgh, 1986) was used to model the experimental results.

### 3.2.3 Kinetics of Ra-226 Adsorption

Kinetics of Ra-226 adsorption by quartz sand, commercial celestite and barite, freshly precipitated celestite and barite, (i.e., solids formed by reacting strontium chloride ($SrCl_2$) and barium chloride ($BaCl_2$) with sodium sulfate ($Na_2SO_4$)), was investigated at varying solution conditions (e.g., ionic strength, pH) and at temperature of 21 ± 2˚C unless specified otherwise. These solids were added to 50 mL of Ra-226 solution in predetermined amounts and stirred using a magnetic stirrer. Liquid samples taken from the reactor during the experiment were filtered through a 0.45 μm mixed cellulose ester membrane and stored in 15 ml Falcon polypropylene centrifuge tubes (Fisher Scientific, Pittsburgh, PA) at room temperature for Ra-226 analysis.

### 3.2.4 Zeta Potential

Zeta potential of celestite, barite and calcite particles used in this study was determined using Litesizer 500 (Anton Paar, Ashland, VA). Solids were suspended in DI water and pH was adjusted by adding HCl and NaOH. Solutions were then completely dispersed in a sonicator and a small volume of each sample (350 μL) was placed in a polycarbonate cuvette equipped with a gold electrode on each side. Zeta potential was determined based on electrophoretic mobility of solid particles. Litesizer 500 was also used to measure particle size distribution by dynamic light scattering technique.

### 3.2.5 Radium Activity

Radium activity was measured using LSC (Blackburn, 1992; Gomez Escobar, 1996; Zhang, 2014), where Ra-226 was first co-precipitated with $BaSO_4$ by adding 364 μL of 100 mM $BaCl_2$ to 2 mL of the liquid sample followed by the addition of 20 mL of 1 M $H_2SO_4$. This approach was used in order to separate Ra-226 from other ions (i.e., Na, Ca, Sr, Ba) in the solution to avoid any impact of salts on radium measurement (Akyon, 2017). Samples were heated on a hotplate at 50˚C for 1 hour to ensure equilibrium and precipitated solids were separated from the liquid phase using 0.45 μm mixed cellulose ester membrane and scraped into glass vials followed by washing the membrane with 3 mL of 0.25 M ethylenediaminetetraacetic acid (EDTA) to ensure complete transfer of solids. The samples were then heated at 60˚C for 1 hour to enhance the dissolution of Ra-Ba-$SO_4$ in EDTA and 14 mL of liquid scintillation Ultima Gold cocktail (Perkin Elmer, Waltham, MA) was added after the samples cooled for 15 min. Each sample was analyzed in LSC for 40 min at 170-230 keV energy range. QA/QC protocol included validation of random samples using Gamma spectroscopy (Johnston, 1997).

### 3.2.6 Sand Functionalization

Sand functionalization was performed by either mixing the commercial celestite ($SrSO_4$) with quartz sand or precipitating celestite on sand surface by adding supersaturated strontium sulfate solution to a reactor already containing sand particles. Both experiments were performed at pH 6 to enhance electrostatic attraction between sand and celestite particles because sand and celestite have opposite surface charges at this pH. The first procedure involved dispersing 2 g of

celestite and 5 g of sand in a sonicator followed by mixing in a tumbler for 24 hours. The second procedure involved dissolving a predetermined amount of $SrCl_2$ in DI water at pH 6 followed by the addition of 5 g of sand and sufficient concentration of $Na_2SO_4$ to precipitate 2 g of celestite. These samples were also mixed in the tumbler for 24 hours. Sand was separated from the solution by filtering through a 53-μm sieve and washed with ethanol (celestite is not soluble in ethanol) to remove loosely attached celestite particles. Sand was then dried in air until all ethanol evaporated and analyzed using scanning electron microscopy (Chapman et al.) (JEOL JSM6510, Peabody, MA). Ionic strength of the remaining aqueous sample containing celestite was adjusted to 1 mol/L using NaCl to ensure complete dissolution of celestite (celestite solubility at this ionic strength is close to 4 mmol/L) (Reardon, 1986) and analyzed for total Sr concentration to validate the mass balance. Mass of celestite coated on the sand surface by each of these procedures was calculated using the following equation:

$$m_c = m_i - m_r \tag{3.2}$$

where, $m_c$ (mg) is the mass of celestite that attached to the surface of the sand, $m_i$ (mg) is the total mass of celestite that precipitated in the system, $m_r$ (mg) is the mass of celestite that remained in the system, which included celestite in the supernatant and celestite that was washed from the sand surface. Concentration of $Sr^{2+}$ was measured using Inductively Coupled Plasma – Optical Emission Spectroscopy (ICP-OES) (5100 ICP-OES, Agilent Technologies, Santa Clara, CA).

Sand functionalization by barite was performed by direct precipitation method. Solution pH was set to 5 using HCl to enhance attraction between quartz sand and barite particles (i.e., IEP of barite in DI water is at pH 5.8 – Figure B.1 in Appendix B). $BaCl_2$ and $Na_2SO_4$ are added in sufficient concentrations to precipitate 2 g of barite. After 24 hours of mixing in a beaker using a magnetic stirrer, samples were filtered through a 53-μm sieve and washed with 50 mL of DI water

to remove loosely attached barite particles. Coated quartz sand was then dried in the air for 48 hours and weighed on the scale. Mass of barite impregnated on quartz sand was determined based on a difference between mass of coated sand and mass of clean sand mass.0

### 3.2.7 Surface Area

Surface area of quartz sand, celestite, barite, calcite, strontianite ($SrCO_3$) and witherite ($BaCO_3$) was determined using nitrogen adsorption/desorption measurements (Micromeritics ASAP 2020, Micromeritics, Norcross, GA) using a 6-point Brunauer-Emmett-Teller (BET) analysis in the relative pressure range $0.06 < P/P_0 < 0.25$.

## 3.3 Results and Discussion

### 3.3.1 Uptake of Radium by Sulfates and Carbonates

Adsorption isotherms for radium on barite, celestite, strontianite, witherite and calcite are shown in Figure 3.1. Freundlich adsorption parameters (Equation B5 in Appendix B) used to describe adsorption capacity and adsorption intensity, $K_F$ and 1/n, are shown in Table 3.1. Higher values of 1/n indicate larger change in adsorption capacity over the range of equilibrium concentrations (Ng, 2002). Celestite and barite had the lowest 1/n parameter which makes them the most reliable adsorbents (i.e., adsorption capacity is less prone to change with changes in liquid phase concentration). It is important to note that the correlation coefficients for all isotherms except for strontianite were at or above 0.9. As can be seen in Figure 3.1, all five solids showed the

potential for removing radium from solution and sulfates exhibited higher adsorption capacity than carbonates. Wang et al. (Wang, 1987) also reported that celestite and barite are more efficient radium adsorbents than strontianite.

As shown in Figure 3.1, celestite exhibited the highest radium uptake capacity among the solids tested in this study, which is in agreement with its high theoretical distribution coefficient during the co-precipitation reaction ($K_d$ = 237) (Zhang, 2014) (higher distribution coefficient indicates higher affinity of radium for the solid phase than the aqueous phase (Prieto, 2009)). Carbonates and barite have much lower distribution coefficient ranging from 0.013 to 1.54 (Gnanapragasam, 1995; Zhang, 2014) and exhibited uptake capacities that are below that of celestite.

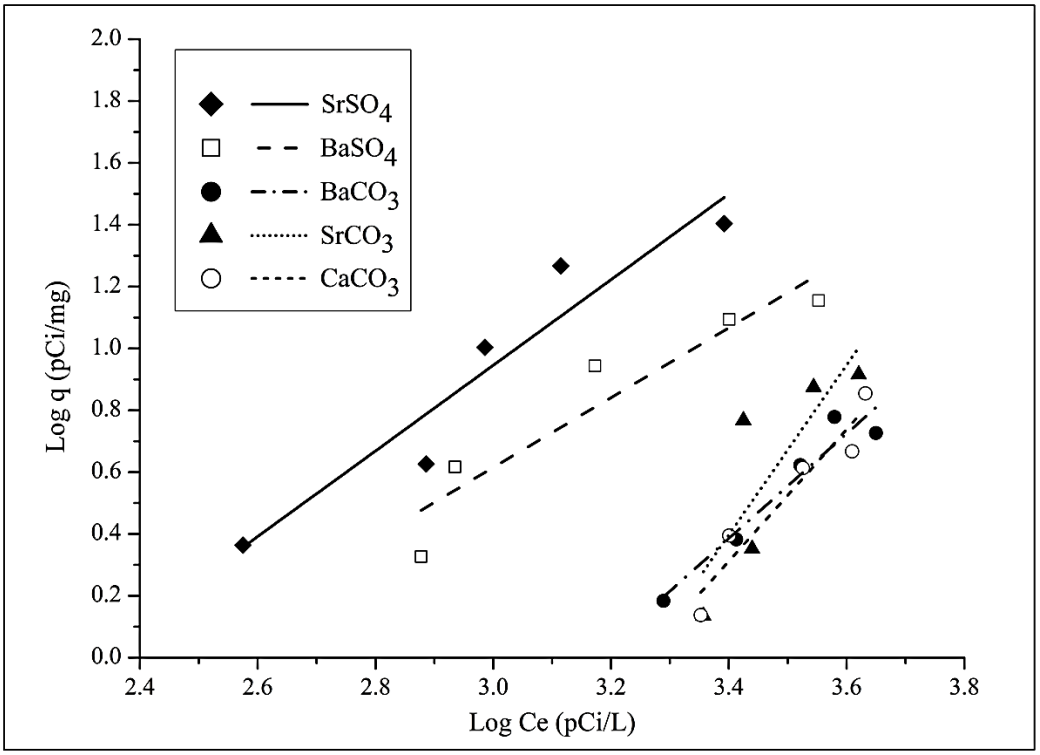


**Figure 3.1** Adsorption isotherms for Ra-226 uptake by sulfates and carbonates.

**Table 3.1.** Freundlich isotherm parameters and correlation coefficients

| Solids | $K_F$ | 1/n | $R^2$ |
|---|---|---|---|
| Barite ($BaSO_4$) | $1.68\times10^{-3}$ | 1.13 | 0.89 |
| Celestite ($SrSO_4$) | $6.19\times10^{-4}$ | 1.38 | 0.91 |
| Witherite ($BaCO_3$) | $4.08\times10^{-6}$ | 1.70 | 0.93 |
| Calcite ($CaCO_3$) | $1.17\times10^{-6}$ | 2.13 | 0.92 |
| Strontianite ($SrCO_3$) | $1.16\times10^{-9}$ | 2.74 | 0.69 |

There are many studies on zeta potential of carbonate species that reported different values as a result of complex reactions at carbonate-water interface (Alroudhan, 2016; Vdovic, 2001; 1998). Zeta potential of calcite in the pH range from 2-11 was found to be in the range of 5-10 mV (Figure B.2 in Appendix B). On the other hand, zeta potential of sulfates was close to neutral or slightly negative, which explains higher Ra-226 uptake by sulfates than carbonates.

Brandt et al. (Brandt, 2015) showed that radium uptake by dissolution-recrystallization of barite can be higher than the values observed in this study but this process is extremely slow and it can take up to one year to achieve equilibrium. Hence, it is reasonable to disregard dissolution-recrystallization as a possible mechanism for radium uptake in this study that was conducted over a period of 24 h. The concentration of surface sites is a possible reason for higher Ra-226 uptake by celestite than barite (Fan, 2016; Zhang, 2008) since BET analysis showed that the specific surface area of celestite (i.e., 0.58 $m^2/g$) is significantly higher than that of barite (i.e., 0.17 $m^2/g$). Higher measured surface area of celestite can be explained by the tendency of barite particles to agglomerate (Figure B.3d in Appendix B).

### 3.3.2 Zeta Potential of Celestite and Quartz Sand

Zeta potential previously reported for celestite (Duzyol, 2014; Lopez-Valdivieso, 2000; Martinez-Luevanos, 1999; Martinez, 1995) included a wide range of isoelectric points (IEP) from 2.4 to 5.8 because of the difference in experimental conditions. Zeta potential of commercial and freshly precipitated celestite used in this study was measured in DI water at pH range from 1.5 – 10 and is shown in Figure 3.2.

As can be seen from Figure 3.2, the IEP for celestite under experimental conditions used in this study was 6.3. Zeta potential is positive (up to +10 mV) when the solution pH is below IEP and it becomes negative (up to -20 mV) at higher pH. This behavior of celestite can be explained by the dissolution and hydrolysis processes on the mineral surface (Gonzalez-Caballero, 1989). Addition of acid will create positively charged surface through the adsorption of $H^+$, while the addition of base will make surface negatively charged through the adsorption of $OH^-$. Several studies that investigated the zeta potential of quartz sand and silica, reported that there is no significant difference between these two species and the IEP to be approximately at pH 2 (Johnson, 1999; Litton, 1993; Lorne, 1999; Rodriguez, 2006; Yukselen-Aksoy, 2011). Zeta potential of silica $SiO_2$ (i.e., particle size 1 μm) was evaluated in DI water and the results are shown in Figure 3.2. Increasing the pH of solution above 2 significantly decreases the zeta potential to -80 mV at pH 10 due to deprotonation of silanol (Si-OH) groups (Heaney, 1994; Iler, 1979) Zeta potential of celestite and sand (i.e., $SiO_2$) were measured to elucidate the role of electrostatic interactions in radium uptake and to determine the most suitable pH region for coating proppant sand with celestite. Because quartz sand and celestite have opposite surface charge in the pH range from 2.5-6.3 (Figure 3.2), impregnation of sand with celestite was performed at pH 6 to maximize the attraction between the positively charged celestite and negatively charged quartz sand.

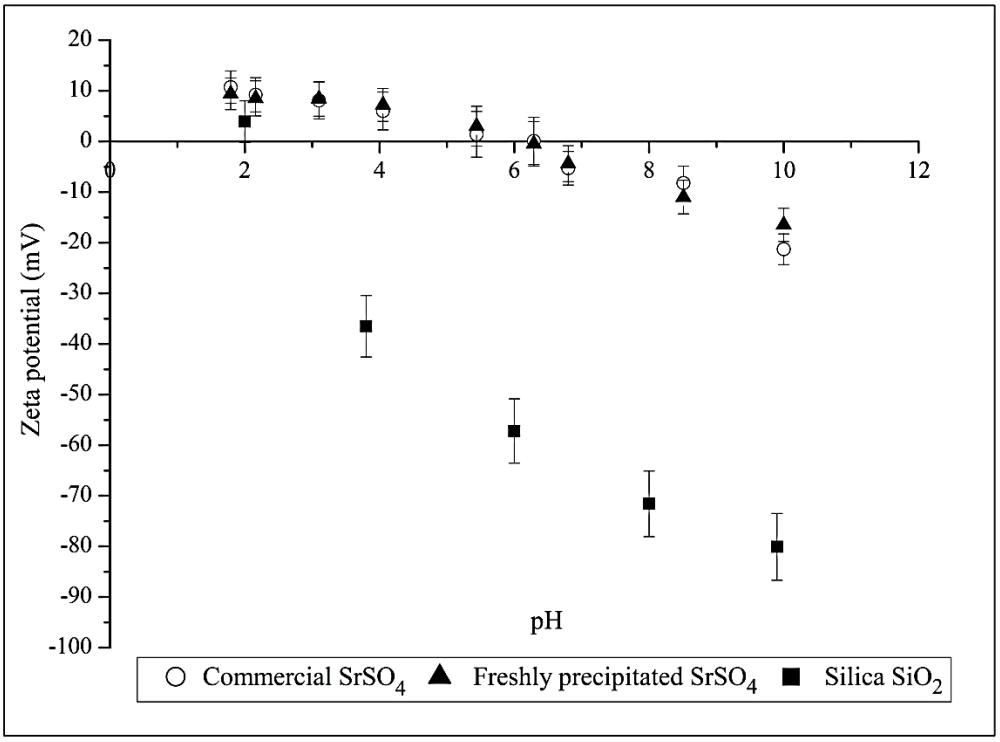


**Figure 3.2.** Zeta potential of celestite as a function of the pH of the solution; experimental standard deviation calculated based on at least 3 replicates is shown using error bars.

### 3.3.3 Radium Uptake by Quartz Sand

Because quartz sand is widely used as proppant in hydraulic fracturing (Liang, 2016), its ability to remove radium from DI water was evaluated at three different pH levels using 5 g of sand in the batch reactor and the initial Ra-226 activity of 5,000 pCi/L. Figure 3.3 shows the impact of pH and ionic strength on radium uptake by quartz sand.

As can be seen in Figure 3.3, increase in solution pH resulted in greater radium uptake by quartz sand because of the more negative surface charge (Figure 3.2) due to deprotonation of silanol groups (Iler, 1979). These results may lead to a conclusion that sand alone would serve as an excellent adsorbent for radium, especially at higher pH. However, radium uptake by sand

decreased dramatically at high ionic strength that is representative of produced water (i.e., I = 1.6 mol/L) because of the screening of electrostatic forces at high ionic strength.

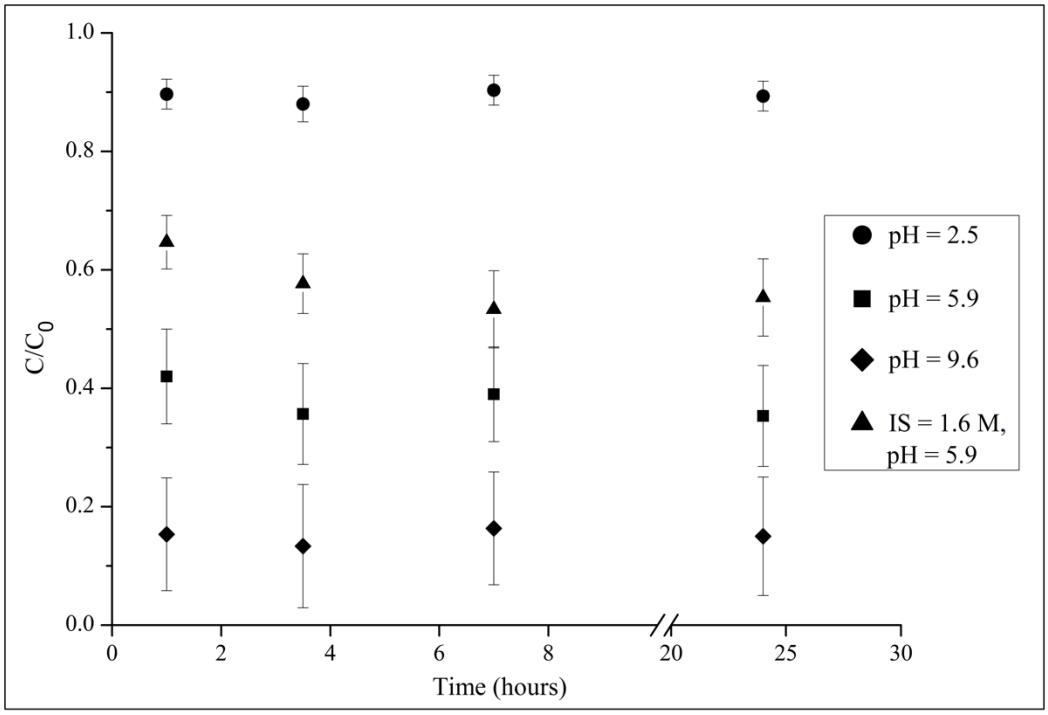


**Figure 3.3.** Radium removal by 5 g of quartz sand at initial Ra-226 concentration of 5,000 pCi/L in DI water and in 1.6 M NaCl solution; analytical procedure standard deviation is presented using error bars.

### 3.3.4 Radium Uptake by Celestite and Celestite Coated Sand

Commercially available celestite and freshly prepared celestite were used to investigate the mechanism and key parameters that influence Ra-226 uptake. As shown in Figure B.3 (Appendix B), both types of celestite had similar particle shape and morphology with an average particle diameter of 3.5 μm for freshly precipitated celestite and 4.5 μm for commercial celestite. The

analysis of particle size distribution at varying ionic strength showed no agglomeration of commercial celestite particles (Figure B.3c).

Celestite speciation in DI water evaluated using Phreeqc software (Parkhurst, 2013) showed that the solubility of celestite remained close to 120 mg/L in the pH range from 2 to 10, which was confirmed experimentally (i.e., measured $Sr^{2+}$ and $SO_4^{2-}$ concentrations were 55 mg/L and 62 mg/L, respectively). Kinetics of Ra-226 removal by celestite at three different pH values using 2,000 mg/L of celestite particles in each experiment was monitored for a period of 96 hours in a batch reactor and the results are shown in Figure 3.4.

Radium removal by celestite occurs either through lattice replacement or surface adsorption (Zhang, 2014). Lattice replacement is associated with co-precipitation of a trace contaminant during precipitation and crystal growth of the main solid (Harvey, 2000). It is reasonable to conclude that adsorption on active sites (i.e., negatively charged $SO_4^{2-}$ groups due to incomplete coordination spheres on the mineral surface (Harvey, 2000)) was the main mechanism of radium removal in these experiments because the equilibrium was achieved within two hours (Figure 3.4), which is typically not sufficient for celestite dissolution and recrystallization to affect radium uptake (Brandt, 2015).

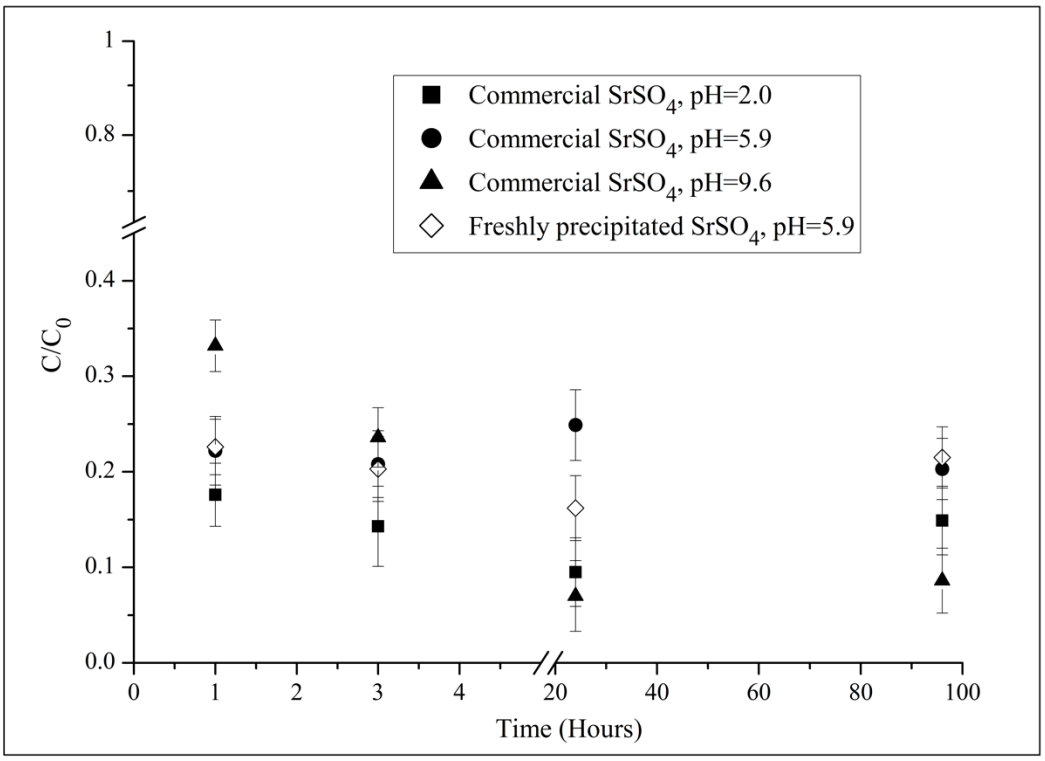


**Figure 3.4.** Radium uptake by celestite in $SrSO_4$ saturated solution (i.e., 120 mg/L) with initial Ra-226 concentration of 7,750 pCi/L; experimental standard deviation calculated based on at least 3 replicates is shown using error bars.

As expected, commercially available and freshly precipitated celestite exhibited similar trends in Ra-226 removal due to their similar size and morphology (Figure B.3). The extent of radium uptake by celestite was not influenced by the solution pH as much (Figure 3.4) because the zeta potential of celestite is much lower than that of sand (Figure 3.2). At pH 2 and 5.9, radium removal from dilute solutions was very fast and equilibrium was achieved within a few hours with no significant removal observed during the next 4 days. However, the results at pH 9.6 indicate that the kinetics of radium uptake is slower compared to that observed at lower pH. Such behavior can be explained by the reduction in double layer thickness from 6 nm at pH 9.6 to 2.6 nm at pH 2 (Chorom, 1995; Yukselen-Aksoy, 2011). At higher pH, radium ions need more time to diffuse

through the EDL resulting in slower overall adsorption kinetics. Results in Figure 3.3 indicate that the zeta potential of celestite, which can vary from +10 mV at pH 2 to -15 mV at pH 9.6 (Figure 3.2) with a corresponding surface charge varying from +0.37 mC at pH 2 to -0.39 mC at pH 9.6 (calculated using Equations B6-B9 of Appendix B), has limited impact on radium removal at equilibrium.

Because the produced water from unconventional gas wells has very high salinity, which is predominantly due to NaCl (Barbot, 2013), radium uptake by celestite was also evaluated in 1.6 M NaCl (93,500 mg/L) solution using the experimental conditions shown in Table 3.2. Figure B.4 (Appendix B) compares Ra-226 uptake by celestite in DI water and 1.6 M NaCl solution at the initial Ra-226 concentrations of 5,000 pCi/L.

**Table 3.2.** Experimental conditions and Ra-226 uptake at low and high ionic strength

| **Sample name** | **Solution** | **Ra-226 concentration (pCi/L)** | **Total $SrSO_4$ added (mg/L)** | **Dissolved $SrSO_4$ (mg/L)** | **$SrSO_4$ Solids (mg/L)** | **Ra-226 uptake ($pCi/cm^2$)** | **Ra-226 uptake (pCi/mg)** |
|---|---|---|---|---|---|---|---|
| A | DI water | 5,000 | 1,000 | 120 | 880 | 0.83 | 4.82 |
| B | 1.6 M NaCl | 5,000 | 1,000 | 800 | 200 | 1.51 | 8.78 |
| C | 1.6 M NaCl | 5,000 | 2,000 | 800 | 1,200 | 0.59 | 3.41 |

As can be seen in Table 3.2 (and Figure B.4), addition of 1,000 mg/L of celestite to solution A was sufficient to remove 85% of radium at equilibrium. Moreover, equilibrium was achieved within 1 hour of contact. However, when the ionic strength was adjusted to 1.6M with NaCl, radium removal decreased to just 35%. The increase in ionic strength increases the solubility of celestite (Reardon, 1986) from 120 mg/L to 800 mg/L as calculated by Phreeqc using Pitzer

activity corrections, which was validated experimentally by measuring the $Sr^{2+}$ concentration in NaCl solution. Increased solubility of celestite at high ionic strength lead to a decrease in the surface area of celestite available in solution by 77% and a corresponding decrease in radium removal. Higher radium uptake per unit surface area in sample B compared to sample A (Table 3.2) can be explained by the higher equilibrium concentration of radium in sample B and greater adsorption driving force. Competition for active sites on celestite surface between radium and high concentration of $Sr^{2+}$ present in solution at high ionic (i.e., eight orders of magnitude higher $Sr^{2+}$ concentration compared to radium) also contributed to reduced radium removal under these conditions. The rate of radium removal at high ionic strength decreased compared to that observed in DI water and it took 7 hours to achieve adsorption equilibrium (Figure B.4). Such behavior can be attributed to a decrease in radium diffusivity at high ionic strength (Vinograd, 1941) and reduction in the surface area of celestite (Li, 2013).

A second adsorption test was conducted under identical experimental conditions as sample B except that 2,000 mg/L of celestite was added to the batch reactor (Sample C, Table 3.2). This modification increased the surface area available for radium adsorption 6 times and the removal of radium was almost identical to the removal observed in DI water (i.e., above 80%). Although higher radium removal was achieved with the addition of more celestite solids, the rate of adsorption was still lower than in DI water and was almost identical as in the case of lower concentration of celestite solids (i.e., equilibrium was achieved after 7 hours). While the addition of 2,000 mg/L celestite increased radium removal, radium uptake per unit surface area decreased from 0.83 $pCi/cm^2$ in sample A to 0.59 $pCi/cm^2$ in sample C (Table 3.2) despite having identical equilibrium Ra-226 concentration. This decrease in capacity can be explained by the competition from $Na^+$ and $Sr^{2+}$ for active sites on celestite surface.

As the proppant itself cannot remove significant amount of Ra-226 from produced water under relevant process conditions (i.e., high salinity), in-situ sequestration of radium would require functionalization of the proppant so that radium uptake is not relying only on electrostatic interactions with quartz sand. Two different approaches for depositing celestite on the proppant surface were evaluated using identical masses of celestite (i.e., 2 g) and sand (i.e., 5 g) that were contacted using identical mixing conditions (i.e., end over end tumbling) and reaction time (i.e., 24 h). Each test was performed 5 times and the average amount of celestite deposited on sand surface is reported in Table 3.3.

**Table 3.3.** Mass balance for two celestite impregnation techniques

| **Method** | **$SrSO_4$ input (mg)** | **Filtered $SrSO_4$ (mg)** | **Washed $SrSO_4$ (mg)** | **Coated $SrSO_4$ (mg)** |
|---|---|---|---|---|
| Mixing with Preformed $SrSO_4$ | 2,000 | 1,806 ± 31 | 94.5 ± 19 | 99.5 ± 16 |
| Direct Precipitation of $SrSO_4$ | 2,000 | 1,762 ± 30 | 89 ± 14 | 149 ± 21 |

As seen from Table 3.3, direct (heterogeneous) precipitation of celestite on the surface of quartz sand as "seed" resulted in about 50% increase in celestite retention on the sand surface when compared to simple mixing of sand and preformed celestite. SEM images of sand particles with celestite coating shown in Figure 3.5 illustrate differences in morphology under different experimental protocols.

As can be seen in Figure 3.5a, the roughness of the sand surface plays a critical role in celestite deposition when mixing preformed celestite and sand with significantly more celestite deposited in crevices than on the smooth parts of the sand surface. In addition, celestite particles

were deposited in multiple layers in these crevices, which reduces the total exposed surface area available for the adsorption of Ra-226. On the other hand, coating sand surface by heterogenous celestite precipitation shows significantly better dispersion of celestite particles (Figure 3.5b) that appear to be larger than in the case of simple mixing of preformed celestite with sand. These results indicate that the sand surface served as an effective "seed" for celestite precipitation and subsequent crystal growth. It is important to note that optimization of celestite impregnation on sand surface through direct precipitation in terms of supersaturation level and kinetics of celestite precipitation could possibly yield much higher celestite loading on sand surface (Ali, 2005). However, the initial objective of this study was to demonstrate the proof of concept with follow-on work designed to optimize the impregnation protocol.

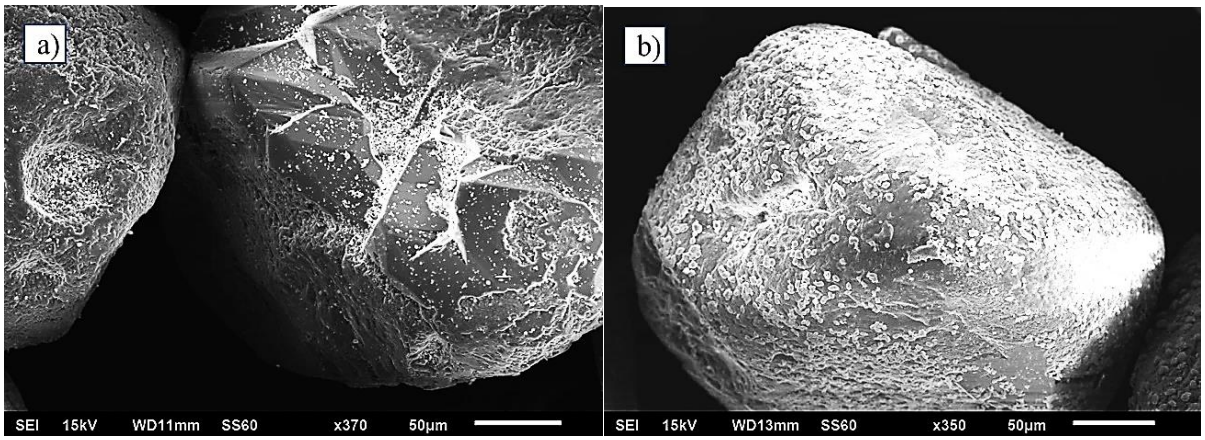


**Figure 3.5.** SEM images of quartz sand coated with celestite by (a) mixing with preformed celestite and (b) direct precipitation of celestite.

Because both quartz sand (in DI water) and celestite demonstrated significant adsorption of radium in the absence of any additional competing ions (Figures 3.3 and 3.4), it is reasonable to expect that celestite impregnated sand would show even better removal of radium due to

synergistic effects. The ability of sand and two types of celestite coated sand to remove radium from celestite saturated solution was investigated under identical conditions and it was found that sand coated with celestite by direct precipitation showed significantly better radium uptake than sand coated with celestite by mixing (Figure B.5 in Appendix B). Such behavior can be explained by greater mass of celestite that was impregnated on the sand surface through direct precipitation method (Table 3.3). Due to its higher coating efficiency and uniform distribution of celestite particles on the sand surface (Table 3.3 and Figure 3.5), sand coated through precipitation is better suited for Ra-226 removal.

It was surprising to see that Ra-226 removal by celestite coated sand was not additive for both celestite coating methods evaluated in this study. The Ra-226 uptake by sand was 0.025 pCi/mg and by celestite impregnated sand was 0.033-0.041 pCi Ra226/mg (Figure B.5) while Ra-226 uptake by celestite alone was 3.3-3.7 pCi/mg (Figure 3.4). Possible reason for such behavior could be very high affinity of celestite for Ra-226 and inability of quartz sand to contribute to Ra-226 uptake because of the celestite layer that is covering sand surface.

To investigate these hypotheses, the kinetics of Ra-226 uptake by celestite and sand alone was measured during the first 60 min using 5 g of quartz sand in DI water (K1), 5 g of quartz sand in 0.65 mmol/L of $Sr^{2+}$ (K2) and 75 mg of celestite in 0.65 mmol/L of $Sr^{2+}$ (K3). Mass of celestite in experiment K3 was 50% of the mass that was present in the experiment with sand coated by direct precipitation of celestite to test the hypothesis that only half of the celestite impregnated on the sand surface will participate in radium uptake because half of the surface area of celestite is not accessible for Ra-226 uptake (Figure 3.5). Strontium concentration in experiments K2 and K3 corresponds to the solubility equilibrium of celestite in DI water.

As can be seen in Figure 3.6, both kinetics and equilibrium of radium adsorption by sand are significantly inhibited by the presence of eight orders of magnitude higher concentration of $Sr^{2+}$ cations in solution compared to radium. It was previously shown that radium uptake by quartz sand is highly dependent on the pH (Figure 3.3). Furthermore, positively charged ions have the ability to screen negatively charged surface and significantly reduce adsorption capacity of silica (Rezwan, 2005). $Sr^{2+}$ cations with a total charge of 6.27 C would screen the surface charge of quartz sand (i.e., total charge of approximately 0.05 C) and slower diffusion of $Ra^{2+}$ through this $Sr^{2+}$ layer would hinder radium uptake kinetics (Dąbrowski, 2001). On the other hand, radium uptake by celestite is almost instantaneous and equilibrium is achieved after 1-2 minutes. Celestite capacity for radium uptake in experiment K3 is 2.86 pCi/mg, which is very close to the values calculated from Figure B.5 (i.e., 2.92-3.60 pCi/mg) under the assumption that celestite on the sand surface adsorbed all the radium removed from solution and that only half of the surface area of celestite was available for adsorption. Slower kinetics of radium uptake and significantly lower Ra-226 removal by sand in the presence of $Sr^{2+}$ observed in these tests confirm the hypothesis that most of the radium is adsorbed by the celestite impregnated on the sand surface before it has a chance to reach the sand surface. This hypothesis is further confirmed by the fact that the Debye length in celestite saturated solution (i.e., 120 mg/L) is approximately 6 nm while celestite particles that are evenly distributed on the sand surface are approximately 3.50 μm (i.e., radium cations will likely be adsorbed by celestite particles before they even have a chance to reach the sand surface). Therefore, contribution of the sand surface to radium removal is negligible and there is no synergy between sand and celestite towards radium removal when celestite is impregnated on sand surface.

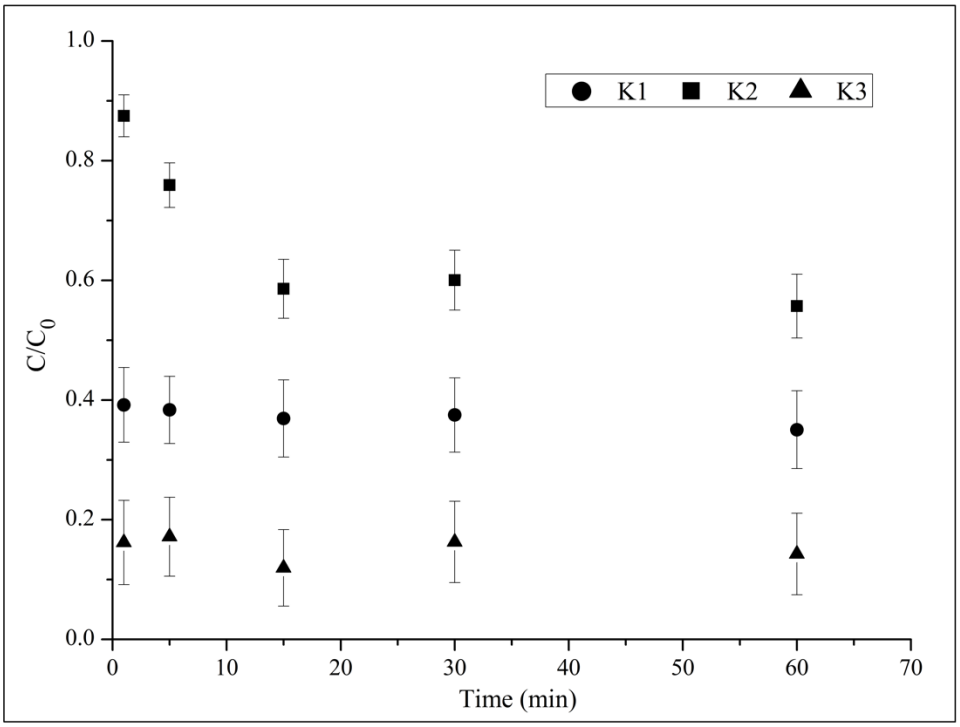


**Figure 3.6.** Kinetics of Ra-226 removal during initial 60 min at pH 5.5 and at initial Ra-226 concentration of 5,000 pCi/L (K1: 5 g of quartz sand in DI water; K2: 5 g of quartz sand in 0.65 mmol/L of $Sr^{2+}$; K3: 75 mg of celestite in 0.65 mmol/L of $Sr^{2+}$; error bars indicate standard deviation of the analytical procedure).

Produced water has a high concentration of sodium and divalent cations and temperature that can range from 35-51 °C (Halliburton, 2009; Kargbo, 2010). Radium removal by the proppant coated by direct celestite precipitation was investigated in the presence of high concentration of competing ions (i.e., $Na^{+}$ = 33,000 mg/L, $Mg^{2+}$ = 1,600 mg/L and $Ca^{2+}$ = 16,000 mg/L) at room temperature (i.e., 21 °C) and at elevated temperature (i.e., 40 °C) and the results are shown in Figure 3.7.

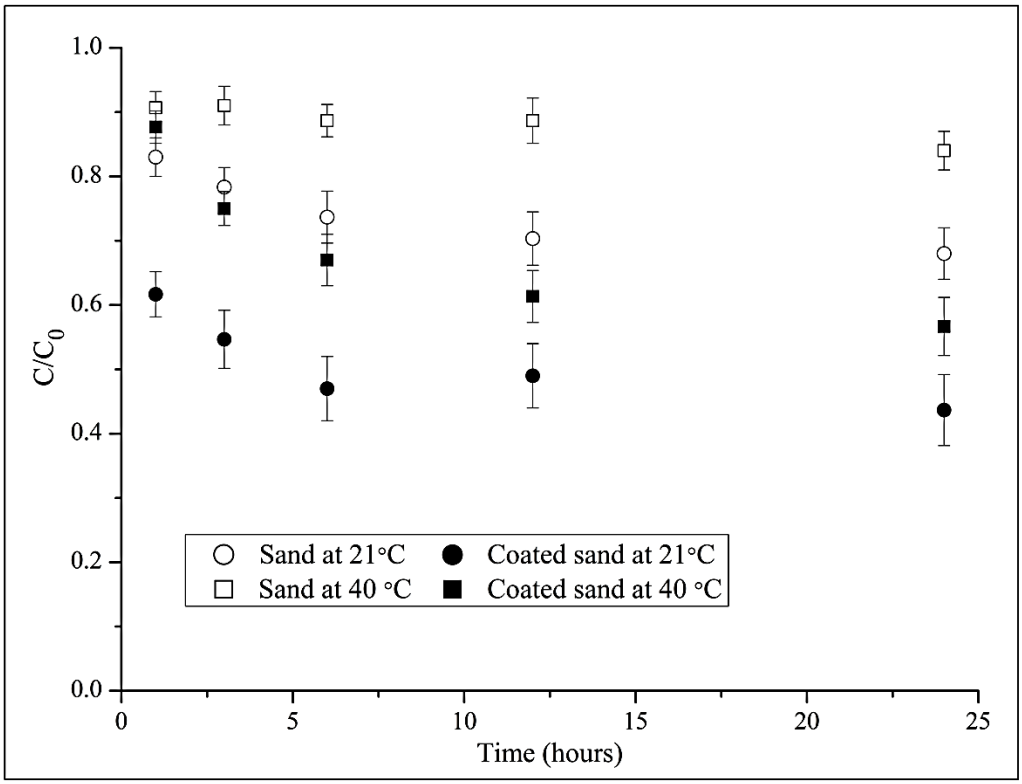


**Figure 3.7.** Ra-226 removal by celestite coated proppant in synthetic high salinity solution at pH 5.5 and at different temperatures with initial Ra-226 concentration of 5,000 pCi/L (error bars indicate standard deviation of the analytical procedure).

Uptake of Ra-226 by quartz sand decreased from 0.025 pCi/mg in celestite saturated solution (Figure B.5) to 0.016 pCi/mg in high salinity solution that contained high concentration of divalent cations (Figure 3.7). The increase in temperature to 40 $^{o}$C induced further reduction in Ra-226 removal capacity of quartz sand to 0.008 pCi/mg. It is evident from Figure 3.7 that celestite coating on sand surface significantly improved Ra-226 removal even in the presence of competing divalent cations. Radium removal by celestite impregnated sand at room temperature was 56% (adsorption capacity of 0.027 pCi/mg) and 43% (adsorption capacity of 0.021 pCi/mg) at 40 °C. Decrease in Ra-226 removal at elevated temperature points to exothermic nature of adsorption

reaction. These results are similar to the results obtained by Vinograd et al. (Vinograd, 2018) where radium uptake during co-precipitation with barite was inhibited at higher temperatures. Radium adsorption kinetics was also affected by the high ionic strength of the solution and it took 6 hours to achieve equilibrium compared to about 1 hour observed in dilute solution (Figure B.5). Such behavior can be explained by decreased diffusivity of Ra-226 ions at elevated ionic strength. Although some celestite was dissolved due to the higher solubility at elevated ionic strength (i.e., 5.8 mmol/L at I = 2.8 mol/L), it appears that most of the celestite coating remained on the sand surface throughout the experiment. This is an indication of mechanical stability of the coating (i.e., proppant was exposed to shearing in the kinetic experiments during vigorous mixing using a stir bar that was required to suspend 5 g of sand in a beaker). SEM images of the proppant after the experiment are shown in Figures B.6 and B.7. It is important to note that sulfate resulting from the solubilization of celestite would cause precipitation of barite if barium ions were present in solution, which would lead to additional Ra removal in the form of Ba-Ra-$SO_4$ (Brandt, 2018; Klinkenberg, 2018; Zhang, 2014) and it would make it difficult to assess the ability of functionalized proppant to remove radium by itself. Therefore, we excluded barium as a competing ion.

The utility of impregnated proppant to remove Ra-226 from the produced water generated during the lifetime of a single gas well can be estimated with a simplified analysis. Assuming a lifetime of 20 years, produced water flow of 1.5 $m^3$/day, and Ra-226 concentration of 2,500 pCi/L, the total radioactivity of produced water brought to the surface during this period would be 2.75 * $10^{10}$ pCi. On the other hand, assuming the uptake capacity of coated proppant of 0.021 pCi/mg at 40 °C and 2,000 tons of proppant that is typically used for each well, it can be estimated that the total Ra removal capacity of the celestite impregnated proppant under relevant process conditions

would be 4.2 * $10^{10}$ pCi (see Appendix B for additional details). These preliminary calculations suggest that the proposed solution for controlling NORM in the produced water is of significant practical relevance and it is possible that further optimization of the impregnation process could yield even more efficient radium sorbent.

### 3.3.5 Radium Uptake by Barite and Barite Coated Sand

Due to the very low solubility of barite ($K_{sp} = 10^{-9.97}$) and high affinity for Ra-226 ions (Figure 3.1), a possibility of impregnating quartz sand proppant with $BaSO_4$ was further explored. Since downhole well conditions and chemical composition of produced water can vary significantly depending on the location of a well (Barbot, 2013), Ra-226 removal was monitored over the 24 hours period, at three different pH, by using 2,000 mg/L of barite particles in each experiment and results are shown in Figure 3.8.

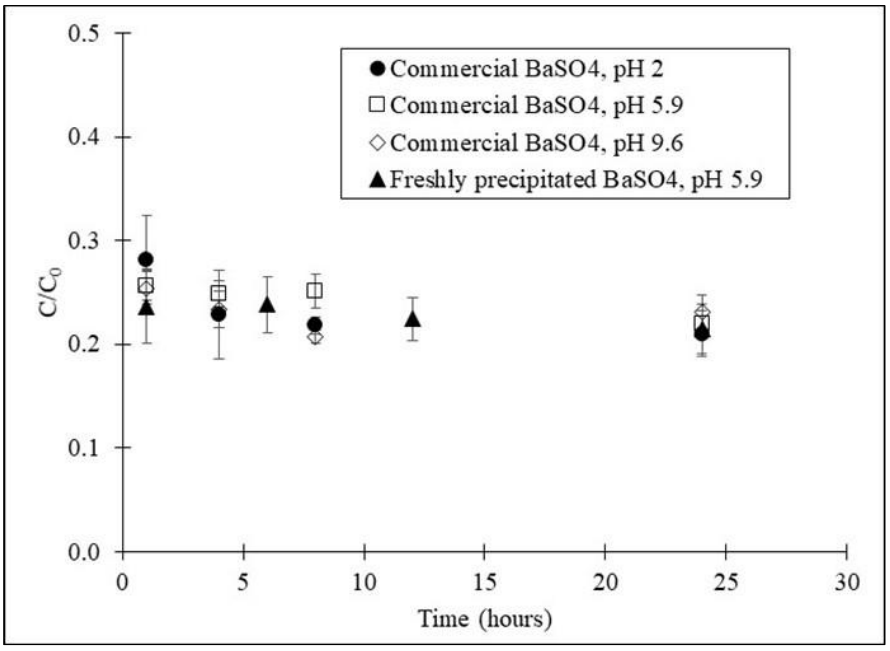


**Figure 3.8.** Radium uptake by barite in $BaSO_4$ saturated solution with initial Ra-226 concentration of 7,500 pCi/L; error bars indicate standard deviation of the analytical procedure.

As can be seen in Figure 3.8, pH of the solution and type of barite (commercially available and freshly precipitated barite) did not significantly affect Ra-226 removal kinetics and equilibrium. At all three pH levels, radium removal from dilute solutions was very fast and equilibrium was achieved within 1-5 hours with no significant removal observed after 1 day. Unlike in the case of celestite (Figure 3.4), radium removal did not exceed 80% efficiency under any of the tested conditions which agrees with adsorption isotherms results observed in Figure 3.1. The ability to remain in a solid form (i.e., only slightly dissolved) at low pH and in high ionic strength solution (Collins, 1971), as well as ability to efficiently sequester radium, makes barite a potential coating agent for quartz sand proppant.

Similar as in the case of celestite, barite coating was achieved using direct heterogeneous precipitation method and detailed results are shown in Table B.1 of Appendix B. Data analysis

showed that an average of 53 ± 61 mg of barite was deposited on the quartz sand surface. Such high standard deviation is the result of heterogeneous and highly dispersed dataset. Approximately 3 times lower efficiency of direct precipitation for barite coating compared to that of a celestite coating (Table 3.3) is likely due to much higher saturation index of barite ($SI_{BaSO4}$ = 4.91) than that of celestite ($SI_{SrSO4}$ = 1.70) under experimental conditions described in section 3.2.6 (saturation indices were calculated using PhreeQC software). Higher saturation index results in shorter induction period (i.e., time after the supersaturation is achieved and when the solids start to precipitate) (Fan, 2011; He, 2014; Lancia, 1999; Söhnel, 1988), thus allowing barite particles less time to form on the surface of the quartz sand than in the case of celestite precipitation. Heterogeneous direct precipitation of barite resulted in good dispersion of barite particles on the surface of the sand as can be seen in Figure 3.9. These results indicate that the sand surface can capture some of the barite that precipitated in the system, but further optimization is required in order to achieve higher efficiency of sand coating.

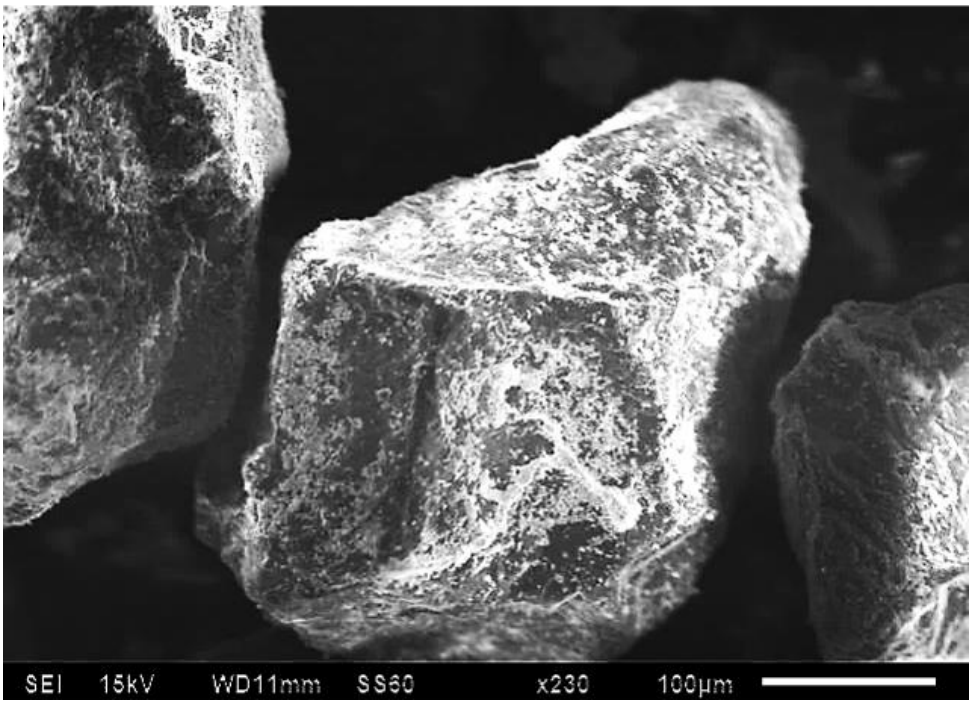


**Figure 3.9.** SEM image of quartz sand coated with barite by direct precipitation.

Radium removal by the proppant coated by direct barite precipitation was investigated in the presence of high concentration of competing ions (i.e., $Na^{+}$ = 33,000 mg/L, $Mg^{2+}$ = 1,600 mg/L and $Ca^{2+}$ = 16,000 mg/L) at room temperature (i.e., 21 °C) and at elevated temperature (i.e., 37 - 40 °C) and the results are shown in Figure 3.10.

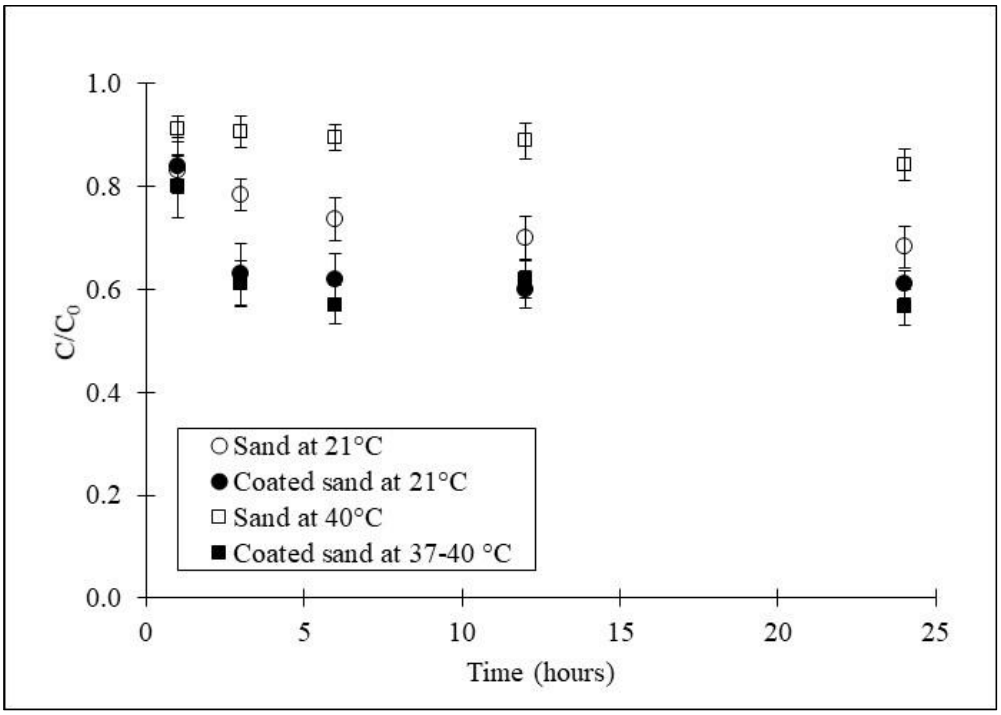


**Figure 3.10.** Ra-226 removal by barite coated proppant in synthetic high salinity solution at pH 5.5 and at different temperatures with initial Ra-226 concentration of 5,000 pCi/L (error bars indicate standard deviation of the analytical procedure).

As discussed previously, radium uptake by quartz sand in high salinity solution decreased from 0.016 pCi/mg at 21 °C to 0.008 pCi/mg at 40 °C (Figure 3.7). It is evident from Figure 3.10 that barite coating on sand surface improved Ra-226 removal even in the presence of competing divalent cations, but not as much as celestite coating (Figure 3.7). Radium removal by barite impregnated sand at room temperature was 39% (adsorption capacity of 0.019 pCi/mg) and 43.5% (adsorption capacity of 0.022 pCi/mg) at 40 °C. It is important to note that radium removal by barite coated sand slightly increased at higher temperature, which is opposite from the behavior that was observed in the case of celestite coated sand where radium removal was reduced at higher temperature. This behavior can be explained by different mechanisms involved in radium

sequestration by barite as discussed in Chapter 2. While Ra-226 is simply adsorbed onto large surface area of celestite (i.e., 0.58 $m^2/g$) and this process is exothermic (i.e., less favorable at higher temperatures), surface dissolution-recrystallization is likely the dominant driving force in Ra-226 uptake by barite and it is enhanced at higher temperatures.

## 3.4 Summary and Conclusions

The findings of this study suggest that it is possible to significantly increase the ability of proppant sand to remove NORM from the produced water by impregnating celestite or barite on its surface. Furthermore, uniform distribution of celestite and barite, achieved when the impregnation is performed by heterogenous precipitation in supersaturated solution, suggests that this method is better suited compared to simple mixing of these solids with sand. Faster adsorption kinetics, higher surface area available for adsorption and significantly higher capacity for radium uptake suggest that most of the radium will be adsorbed by celestite even when it is impregnated on sand and that quartz sand would not play a significant role in radium uptake. Radium uptake by celestite and barite impregnated proppant was investigated in synthetic high salinity water and it was shown that high TDS limit Ra-226 removal to 39 - 56% because of significantly lower (i.e., 6-9 order of magnitude) Ra-226 concentration compared to the concentration of competing ions in the solution. Impact of organics and surfactants that are typically present in produced water, as well as the impact of high temperatures and high pressures on radium uptake and coating stability will have to be further evaluated. The idea of coating sand with celestite and barite is presented as a possible alternative to other methods for Ra-226 removal from wastewater produced by the extraction of unconventional gas resource.

## 4.0 Sulfate Precipitation in Produced Water from Marcellus Shale for the Control of Naturally Occurring Radioactive Material

This chapter, written by Alen V. Gusa and coauthored by Anna Tomani, Atoosa Mashayekhi, and Radisav D. Vidic, is under review for publication in *Water Research*.

Produced water (PW) generated during unconventional oil and gas extraction is characterized by very high TDS that mainly consists of alkali and alkaline earth metals. Current dominant PW management strategy (i.e., injection in Class II disposal wells) is scrutinized by regulatory agencies and the public and PW treatment that enables high water and salt recovery (i.e., evaporation/crystallization) is being considered as an alternative. Produced water generated in the Marcellus Shale play also contains very high levels of Naturally Occurring Radioactive Material (NORM) in the form of Ra-226 and Ra-228, which is one of the key impediments for the recovery of high-quality salts. This study was designed to evaluate the efficiency of Ra-226 removal using co- and post-precipitation with barium sulfate to enable advanced PW treatment processes. High Sr/Ba ratios in PW lead to relatively low $Ba^{2+}$ and $Ra^{2+}$ removal and $Ba^{2+}$ concentration adjustment is necessary to achieve required treatment standards (i.e., $[Ba^{2+}] < 10$ mg/L and $[Ra^{2+}] < 50$ pCi/L). While seeding the reactor with barium sulfate enhanced $Ba^{2+}$ and $Ra^{2+}$ removal through induced heterogeneous precipitation of barite it was necessary to simultaneously adjust Sr/Ba ratio and barite addition to achieve treatment requirements while maintaining reasonable detention time in the reactor (i.e., < 30 min) and minimizing sludge production. Experimental and modeling results revealed that low $Ba^{2+}$ and $Ra^{2+}$ effluent concentration with minimized sludge production can be achieved only when barium sulfate

saturation index was above 4.7, Sr/Ba ratio was below 2 and there was at least 25 g/L of barite "seed" in the system. This study provides useful guidelines for centralized wastewater treatment facilities in shale plays and serves to optimize pretreatment of produced water to enable recovery of valuable resources (i.e., clean water and usable salts).

## 4.1 Introduction

Constantly increasing oil and gas demand was a major driver for technological advancement towards extraction of these resources from unconventional reservoirs. A combination of horizontal drilling and hydraulic fracturing is responsible for the projected increase in total natural gas production in the United States from 27.9 tcf in 2016 to 44.5 tcf in 2050 (i.e., 59.5% increase), with natural gas production from unconventional reservoirs contributing more than 80% of the total production in the US in 2050 (U.S.E.I.A., 2018). It is estimated that unconventional natural gas basins around the world contain 7,570 tcf of shale gas (U.S.E.I.A., 2015), which makes it a widely available fossil fuel that can be extracted economically (Sovacool, 2014). Unconventional natural gas is believed to be a good replacement for coal due to its lower environmental footprint leading to reduction in greenhouse gas emissions from the power generation sector (Burnham, 2011; Sovacool, 2014).

Extraction of unconventional shale gas is not without its own threats to human health and environment. Hydraulic fracturing of a single well requires from 2.3 – 5.7 million gallons of water, with average consumption of 3.8 million gallons (Jackson, 2014; Nicot, 2012). Portion of this water returns to the surface as flowback (i.e., during first couple of weeks) while produced water (PW) is brought to the surface during the productive life of the well.

One of the major environmental concerns related to unconventional gas extraction is high salinity of produced water with total dissolved solids (TDS) that range from 1 to 345 g/L with an average of 106.4 g/L in Marcellus Shale (Barbot, 2013). Concentration of major ions (i.e., $Na^{+}$, $Mg^{2+}$, $Ca^{2+}$, $Sr^{2+}$ and $Ba^{2+}$) in produced water normally increases with time but also depends on the geochemical characteristic of the shale formation (Barbot, 2013). For example, the ratio of Sr/Ba concentration can vary from 1 – 4 in Northeast Pennsylvania (Barbot, 2013) and from 0.7 – 12 in Southwest Pennsylvania (He, 2014; Lokare, 2017).

Black shale, the most dominant component of Marcellus Shale formation, is rich with uranium and thorium, which makes it a significant source of naturally occurring radioactive material (NORM) that is usually found in produced water (Rowan, 2011). The major components of NORM in produced water are Ra-226 (half-life of 1,600 years) and Ra-228 (half-life of 5.75 years), which are daughter isotopes of U-238 and Th-232, respectively (Akovali, 1996; Artna-Cohen, 1997). Multiple gas well analysis showed that total radium concentration (i.e., Ra-226 and Ra-228) in Marcellus Shale produced water in Pennsylvania can range from 33 to 18,045 pCi/L, while it can be as high as 16,942 pCi/L in Marcellus Shale produced water in New York (Rowan, 2011). Such high NORM concentration makes produced water treatment for the recovery of valuable resources (i.e., clean water and salts) very challenging.

Produced water management strategy depends largely on the availability of Class II underground injection control wells (UIC) wells with approximately 95% of onshore produced water being disposed (i.e., disposal and enhanced oil recovery) in these wells (Clark, 2009). The only exception is Marcellus Shale play where close to 90% of the flowback and produced water is reused in hydraulic fracturing (Jiang, 2014; Rassenfoss, 2011). However, disposal of produced water in Class II wells has been linked with induced seismicity (Ellsworth, 2013; McGarr, 2015).

Thus, thermal processes, such as evaporation and crystallization may be necessary to recover clean salts and pure water that can be reused in industrial operations. These processes, however, are energy intensive and costly (Fakhru'l-Razi, 2009). Any solids or sludge generated during produced water treatment will contain NORM and would have to be disposed in approved landfills (Zhang, 2014; 2015b). Regulations for the disposal of radioactive sludge vary by state but generally limit radioactivity in the range from 5 to 30 pCi/g (Smith, 1992; Veil, 1998). Recent study demonstrated the possibility of using a functionalized proppant as an underground filter for NORM control (Goyal, 2017; Gusa, 2018; McDaniel, 2014) to reduce the radioactivity of produced water and reduce its health and environmental risks. Salts (i.e., chlorides) that can be recovered from the produced water using evaporation/crystallization can be used for de-icing or other industrial application only if they meet standards for purity, especially concerning the NORM level (Dong, 2017).

Most common approach for NORM removal from produced water is through co-precipitation with barium sulfate (barite) where radium proportionally precipitates with barium (i.e., equal fractions of radium and barium are removed) in the form of a Ba-Ra-$SO_4$ solid (Doerner, 1925; Rosenberg, 2013; Zhang, 2014). However, this treatment step often requires adding high concentrations of sulfate (i.e., 4-5 times molar ratio of barium) to achieve more than 99% barium and radium removal. Due to high concentration of other divalent cations in PW (e.g., $Sr^{2+}$, $Ca^{2+}$), this strategy leads to precipitation of other insoluble sulfates (e.g., celestite, gypsum) that dramatically increases the volume of radioactive sludge and cost associate with its disposal.

Heterogeneous nucleation (i.e., nucleation of species in the presence of pre-existing "seed" solids) has been widely used to control precipitation of calcium sulfate (Fröhner, 1975), calcium carbonate (Mercer, 2005), barium sulfate (Kügler, 2016) and struvite (Wang, 2006). Increasing the

seed concentration and decreasing the size of seed particles typically enhances the removal of target species (Fröhner, 1975; Mercer, 2005). He et al. showed that barium sulfate precipitation can be inhibited in the presence of high concentration of sodium and other alkaline earth metals if the saturation index (SI) of barium sulfate is below 2.5 (He, 2014). Rate of barium sulfate precipitation is also affected by high concentrations of calcium and strontium due to incorporation of these ions into the crystal lattice of barium sulfate (Boon, 2016; Jones, 2004; Kelland, 2011) These side reactions reduce removal of barium and radium by sulfate precipitation when the concentration of barium is lower than that of other divalent cations in the solution. In that case, excess sulfate needs to be added to accomplish the effluent quality that is needed to achieve requisite salt purity in the crystallization process.

This study is designed to provide fundamental insight into barium and radium removal from unconventional PW when sodium, calcium, magnesium and strontium are present at concentrations that are several orders of magnitude higher than those of barium and radium. The main goal of the study is to optimize the treatment approach to achieve high barium and radium removal and enable further treatment of this water by evaporation/crystallization to recover clean water and usable byproducts (e.g., non-radioactive salts like NaCl and $CaCl_2$).

## 4.2 Materials and Methods

### 4.2.1 Reagents and Materials

Produced water (i.e., 5-gallon bucket) used in this study was received in April 2018 from northern West Virginia. Concentration of major cations in these waters was analyzed using

inductively coupled plasma – optical emission spectroscopy (5100 ICP-OES, Agilent Technologies, Santa Clara, CA), while the concentration of Ra-226 was determined using Gamma spectroscopy (Canberra BE 202, Mirion Technologies, San Ramon, CA). Composition of produced water is shown in Table 4.1. Synthetic produced water was prepared using sodium chloride, potassium chloride, magnesium chloride, calcium chloride and barium chloride salts that were purchased from Fischer Scientific (Pittsburgh, PA) and strontium chloride purchased from Sigma Aldrich (St. Louis, MO). Barium sulfate powder (Fischer Scientific, Pittsburgh, PA) with an average particle size of 4.6 μm was used in this study as seed for heterogenous precipitation.

**Table 4.1.** Major inorganic constituents of produced water

| | **Produced water PW (pH = 5.4)** | |
|---|---|---|
| **Component** | **(mg/L)** | **(mmol/L)** |
| TDS | 191,655 | - |
| TSS | 316 | - |
| $Na^+$ | 40,526 | 1,762 |
| $K^+$ | 1,061 | 27.14 |
| $Mg^{2+}$ | 1,962 | 80.71 |
| $Ca^{2+}$ | 18,078 | 451.05 |
| $Sr^{2+}$ | 3,806 | 43.44 |
| $Ba^{2+}$ | 488 | 3.55 |
| $Ra^{2+}$ (pCi/L) | 4,969 | - |
| Sr/Ba | - | 12.2 |

### 4.2.2 Co-precipitation Experiments

Produced water samples were filtered through 0.45 μm mixed cellulose ester membrane (Millipore, Billerica, MA) to separate suspended solids and stored in refrigerator prior to co-precipitation experiments. Experiments were conducted in 250 mL beakers that were mixed using

magnetic stirrer. Varying amounts of sodium sulfate decahydrate (Fischer Scientific, Pittsburgh, PA) were added to the batch reactor to precipitate barium and samples were taken at predetermined time steps (i.e., for most of the experiments after 10, 30, 60 and 120 min or as specified) to assess the kinetics of sulfate precipitation. Samples were filtered through 0.45 μm mixed cellulose ester membrane, diluted and stored in 50 mL Falcon polypropylene centrifuge tubes (Fischer Scientific, Pittsburgh, PA) at 0-4 °C to prevent any additional precipitation prior to analysis. Metals were analyzed using ICP-OES, while sulfate concentration was measured using ion chromatography (Dionex ICS 1100, Sunnywale, CA).

Ion removal was calculated as:

$$R = \frac{C_0 - C}{C_0} * 100\ (\%) \tag{4.1}$$

where, R represents removal of a specific ion and $C_0$ and C are the initial and final concentration of that ion in the liquid phase.

Solids formed during each experiment were calculated as:

$$C_{formed\ solids} = TDS_i - TDS_f \tag{4.2}$$

where, $C_{formed\ solids}$ (ton/$10^6$ gallons) represents the concentration of solids formed and $TDS_i$ and $TDS_f$ are the measured initial and final (i.e., after 30 min reaction time) total dissolved solids in produced water.

### 4.2.3 Radioactivity Measurements

Concentration of Ra-226 in the effluent was determined using liquid scintillation counting (LSC) and gamma spectroscopy with broad energy germanium detector (BE 2020). 2 mL of liquid sample (i.e., treated produced water) was mixed with 14 mL of liquid scintillation Ultima Gold

cocktail (Perkin Elmer, Waltham, MA) prior to 40 min analysis in LSC at 170-230 keV energy range. Preparation of samples for gamma spectroscopy required liquid to be evaporated at 105 °C for 24 hours and the remaining solids were ground to visually uniform powder, placed in 46 mm diameter petri-dish (Fischer Scientific, Pittsburgh, PA) and sealed with vinyl tape. Ra-226 was measured directly at 186.2 keV for 24 hours and confirmed by measuring the activities of Ra-226 daughter products (i.e., Pb-214 at 295.2 and 351.9 keV and Bi-214 at 609.3 keV) after at least 3 weeks of incubation to validate the initial results (Tasker, 2019).

Radioactivity of the solids generated during produced water treatment was calculated as:

$$q = \frac{C_0(Ra^{2+}) - C(Ra^{2+})}{C_{\text{total solids}}} \tag{4.3}$$

where, q (pCi/g) represents sludge radioactivity, $C_0(Ra^{2+})$ (pCi/L) and $C(Ra^{2+})$ (pCi/L) are initial and final $Ra^{2+}$ concentration in the liquid phase and $C_{\text{total solids}}$ (g/L) is the sum of solids added to the system (i.e., barite seed) and solids formed during produced water treatment ($C_{\text{formed solids}}$).

### 4.2.4 Chemical Equilibrium Modeling

Assessment of chemical equilibrium in the produced water after the addition of sulfate was performed using PhreeQC software (Parkhurst, 2013). This software contains a database with Pitzer activity coefficients and thermodynamic parameters that are necessary to accurately determine distribution of dissolved species at very high ionic strength of the solution that is characteristic for the unconventional onshore PW (He, 2014; 2016).

## 4.3 Results and Discussion

The overall objective of this study was to establish optimal treatment process that would achieve final $Ba^{2+}$ and $Ra^{2+}$ concentrations in the effluent below 10 mg/L and 50 pCi/L, respectively (i.e., more than 99% removal) to enable further treatment of PW in evaporation/crystallization system and recover high purity salable salts (i.e., without NORM). In addition, the proposed treatment process should minimize the amount of radioactive sludge produced to enable cost effective disposal. As can be seen in Table 4.1, concentrations of $Sr^{2+}$ and $Ca^{2+}$ in this PW are much higher than that of $Ba^{2+}$, which creates extremely challenging conditions for reducing $Ba^{2+}$ concentration by sulfate precipitation due to competition for the common ligand (i.e., sulfate). Furthermore, any celestite and gypsum that would precipitate during treatment increases the total volume of radioactive sludge for disposal, which would dramatically escalate the overall cost of PW treatment.

### 4.3.1 Impact of pH and Barite Saturation Index (SI) on Barium and Radium Removal

Radium removal is closely related to barium removal during barite precipitation (Doerner, 1925; Zhang, 2014) and it is important to understand the process parameters that affect the removal efficiency of both ions. As can be seen in Table 4.1, initial barium concentration in PW is 488 mg/L and barium removal close to 98% is necessary to achieve the required water quality (i.e., $[Ba^{2+}] < 10$ mg/L). The ability of sulfate precipitation to achieve this treatment objective was first evaluated by adding sulfate at 120% of the stoichiometric amount of barium at different pH levels and the effluent quality was evaluated after 30 min of reaction time. This sulfate dose was selected based on the findings that complete barium removal in dilute solutions can be accomplished using

the stoichiometric sulfate addition (Doerner, 1925; Zhang, 2014) while the reaction time of 30 min was selected based on a reasonable contact time that can be achieved in an actual PW treatment plant. Tests at pH of 2 and 10 were included in this study to specifically target barium removal (i.e., barite is the only sulfate salt that is virtually insoluble at pH 2) and evaluate potential contribution of hydroxide precipitation to $Ra^{2+}$ removal. In addition, $Ba^{2+}$ and $Ra^{2+}$ removal when sulfate was added to the solution at up to 5 times the stoichiometric concentration of barium was evaluated for its ability to meet treatment objective. Table 4.2 lists all experimental conditions that were evaluated in this task and Figure 4.1 shows the results of these experiments.

**Table 4.2.** Experimental conditions for $Ba^{2+}$ and $Ra^{2+}$ removal from raw produced water as a function of pH and sulfate concentration

| $SO_4$/Ba | pH | $SO_4^{2-}$ addition (mg/L) | $SI_{BaSO4}$* | Sr/Ba | Solids formation (ton/$10^6$ gallons) | Solids radioactivity (pCi/g) |
|---|---|---|---|---|---|---|
| 1.2 | 2 | 409 | 3.11 | 12.2 | 17.3 | 986 |
| 1.2 | 5.4 | 409 | 3.12 | 12.2 | 19.0 | 743 |
| 1.2 | 10 | 409 | 3.12 | 12.2 | 23.8 | 848 |
| 2 | 5.4 | 682 | 3.35 | 12.2 | 28.2 | 614 |
| 3 | 5.4 | 1,023 | 3.53 | 12.2 | 32.7 | 559 |
| 5 | 5.4 | 1,705 | 3.75 | 12.2 | 36.6 | 509 |

* Saturation index (SI) of $BaSO_4$ was calculated using PhreeQC software

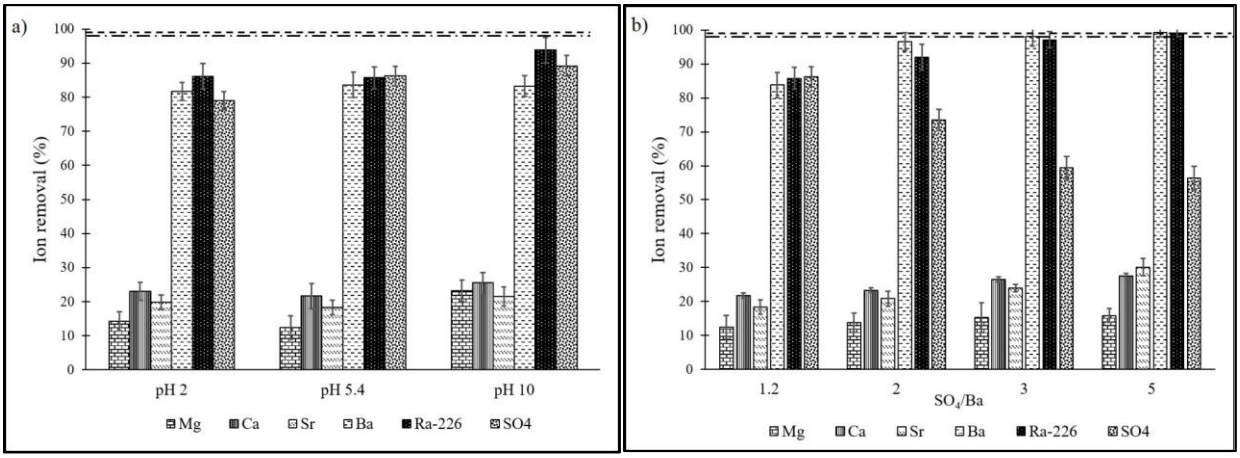


**Figure 4.1.** Removal of selected ions from raw PW after 30 min of reaction as a function of (a) pH and (b) sulfate concentration at pH 5.4; dash-dot and dashed lines represent required $Ba^{2+}$ and Ra-226 ion removal to meet efflent standards, respectively.

As can be seen in Figure 4.1a, addition of sulfate at 120% of barium concentration was not able to achieve required effluent barium concentration (i.e., $[Ba^{2+}] < 10$ mg/L or 98% removal) at any of the conditions tested. Although a reduction in $CaSO_4$ and $SrSO_4$ precipitation under acidic conditions was expected due to increased solubility (Lopez-Valdivieso, 2000; Shukla, 2008) decreasing the solution pH to 2 did not sufficiently affect $Ba^{2+}$ removal to meet the treatment standards (Figure 4.1a; Table C.1a in Appendix C). In fact, an increase in $Mg^{2+}$, $Ca^{2+}$, $Sr^{2+}$ and $Ra^{2+}$ removal was observed under acidic conditions, which is most likely due to the adsorption or co-precipitation of these ions with barite (Averyt, 2003; Ouyang, 2019; Zhang, 2014). Lower sulfate removal under acidic conditions (i.e., 79% at pH 2 compared to 86.2% at pH 5.4) and smaller amount of formed solids (Table 4.2) also suggest that barium sulfate was the only precipitate formed under these conditions.

Ion removal at pH 10 was due to the simultaneous formation of $BaSO_4$ and $Mg(OH)_2$ since the SI of $Mg(OH)_2$ of 1.38 was achieved at pH 10.0 ($Ksp_{MgSO4} = 7.1*10^{-12}$) (Harvey, 2000).

Significantly higher (i.e., 9%) $Ra^{2+}$ removal at pH 10 compared to pH 5.4 was due to co-precipitation with both barite (Zhang, 2014) and magnesium hydroxide (Clifford, 1990). As can be seen in Table 4.2, solids formation increased by 25% (i.e., from 19.0 tons/$10^6$ gallons at pH 5.4 to 23.8 tons/$10^6$ gallons at pH 10), which was due to precipitation of $Mg(OH)_{2(s)}$ and would have adverse impact on the overall cost of sludge disposal. It is important to note that $Ra^{2+}$ removal in real produced water was always higher than $Ba^{2+}$ removal regardless of the solution pH, which suggests different removal mechanism (i.e., co-precipitation and adsorption) compared to the case of dilute solutions where the removal of these ions was always proportional (Zhang, 2014). Equilibrium was calculated using PhreeQC software and results showed that barium and sulfate removal was always higher than what was observed experimentally. This discrepancy is likely due to the kinetic limitations of experimental approach and not enough time allowed for complete barite precipitation.

As can be seen in Figure 4.1b, using 3-5 times sulfate/barium molar ratio was able to achieve required barium concentration in the effluent ($Ba^{2+}$ removal above 98%). Increasing the excess sulfate in solution increases SI of all potential sulfate precipitates (i.e., $BaSO_4$, $CaSO_4$ and $SrSO_4$, Table C.1b), which results in lower induction times and faster kinetics during homogeneous precipitation (Fan, 2011; He, 1995). The SI of barite (3.12 to 3.75) was 2.6-112 times higher than the SI of gypsum (-0.19 to 0.42) and celestite (0.8 to 1.41), which leads to preferential precipitation of barite over other sulfate species. Consequently, $Ra^{2+}$ removal by co-precipitation with barite increases to more than 98% (Figure 4.1b). However, higher initial sulfate concentration leads to higher residual sulfate (i.e., 416-743 mg/L when sulfate addition was 300 - 500% of barium concentration (Table C.1b)). Such outcome is highly undesirable because high residual sulfate would most likely exceed NPDES discharge limit. Furthermore, if the facility is designed to

recover saleable salts from the produced water in a crystallization step, high concentration of sulfate in the effluent from the pretreatment step would lead to precipitation of $CaSO_4$ and $SrSO_4$ that would cause excessive scaling and/or reduce the purity of the salts recovered from the crystallizer. As can be seen in Table 4.2, increasing the sulfate dose could lead to almost doubling of the amount of precipitated radioactive solids. Hence, treatment approach that relies on excess sulfate to control $Ba^{2+}$ in the effluent is not practical.

To evaluate the impact of barite SI and Sr/Ba ratio on barium and radium removal, a set of experiments was designed where the initial $Ba^{2+}$ concentration was first increased by adding $BaCl_2$ to raw produced water, followed by sulfate addition to achieve the initial sulfate/barium molar ratio of 1.2 (i.e., 20% excess sulfate addition). Experimental conditions for these tests are shown in Table 4.3 together with the concentration of formed solids in each test and radioactivity of these solids that was calculated using Equation 4.3. All experiments were conducted for 30 min to represent reasonable detention time in a full-scale treatment plant and the results are shown in Figure 4.2.

**Table 4.3**. Experimental conditions for Ba and $Ra^{2+}$ removal from produced water with Ba concentration modification

| **Initial $Ba^{2+}$ (mg/L)** | **$SO_4^{2-}$ addition (mg/L)** | **$SO_4$/Ba** | **$SI_{BaSO4}$** | **Sr/Ba** | **Solids formation (ton/$10^6$ gallons)** | **Solids radioactivity (pCi/g)** |
|---|---|---|---|---|---|---|
| 488 | 409 | 1.2 | 3.12 | 12.2 | 19.0 | 743 |
| 1,325 | 1,112 | 1.2 | 4.00 | 4.5 | 24.4 | 680 |
| 2,710 | 2,275 | 1.2 | 4.64 | 2.2 | 30.9 | 565 |
| 5,425 | 4,553 | 1.2 | 5.27 | 1.1 | 52.6 | 352 |

As can be seen in Figure 4.2, increasing the initial barium concentration in produced water had a positive impact on the removal of all ions of interest. Increasing the initial $Ba^{2+}$ concentration from 488 to 1,325 mg/L in PW with subsequent addition of sulfate resulted in the increase in $Sr^{2+}$, $Ba^{2+}$, $Ra^{2+}$ and $SO_4^{2-}$ removal from 18.3, 83.8, 85.8 and 86.2% to 21.6, 95.6, 88.3 and 93.9%, respectively while the removal of $Mg^{2+}$ and $Ca^{2+}$ was reduced from 12.4 and 21.7% to 11.8 and 21.1%, respectively.

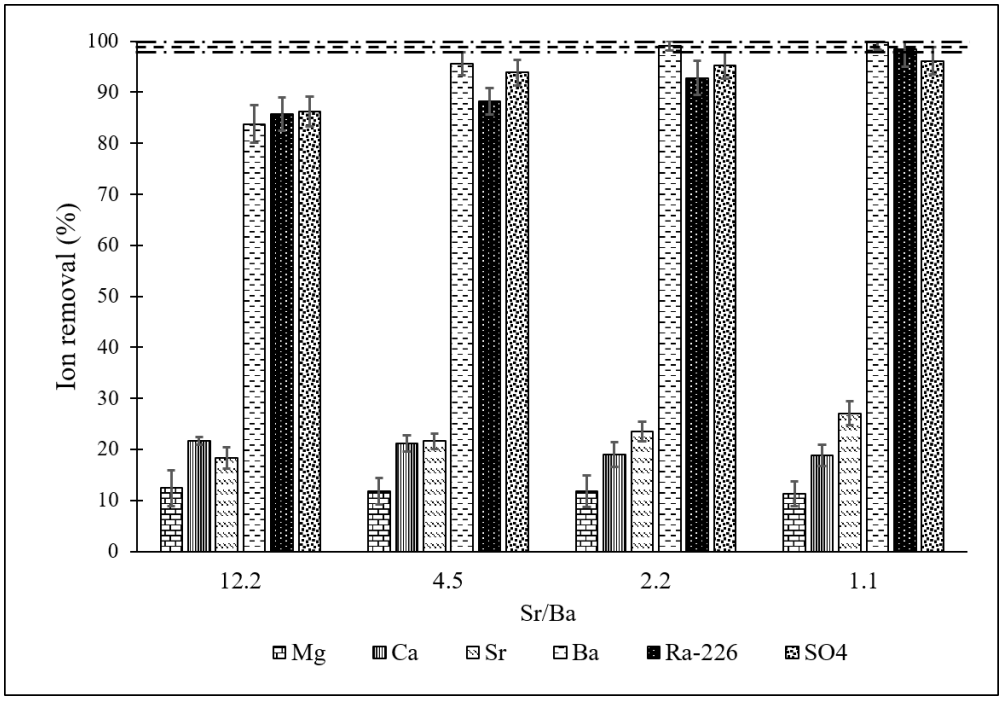


**Figure 4.2.** Impact of $Ba^{2+}$ augmentation on the removal of selected ions from raw PW after 30 min of reaction time; dash-dot range and dashed line represent required $Ba^{2+}$ and Ra-226 ion removal to meet efflent standards, respectively.

Although the solubility product of $RaSO_4$ ($K_{sp} = 10^{-10.38}$) (Langmuir, 1985) is lower than the solubility product of $BaSO_4$ ($K_{sp} = 10^{-9.97}$), none of the experimental conditions evaluated in this study resulted in direct precipitation of $RaSO_4$ because its SI was always well below 1 since

$Ra^{2+}$ concentration was 8 orders of magnitude lower than $Ba^{2+}$ concentration. Therefore, removal of different ions in produced water is governed by the changes in barite SI. Addition of $BaCl_2$ to PW increased barite SI from 3.12 to 4 (Table 4.3). Further addition of $Ba^{2+}$ to achieve initial concentration of 5,425 mg/L increased barite SI to 5.27 (Table 4.3), which resulted in higher $Ba^{2+}$ and $Ra^{2+}$ removal (Figure 4.2) and was able to achieve residual $Ba^{2+}$ concentration below 10 m/L (Table C.2 in Appendix C). Despite reducing $Ba^{2+}$ and $Ra^{2+}$ concentration to 8.9 mg/L and 80 pCi/L, respectively, this approach is not suitable for full-scale application because it generates enormous quantities of radioactive solids (i.e., 52.6 ton/$10^6$ gallons with NORM concentration of 352 pCi/g).

Generally, the induction time (i.e., time after the supersaturation is achieved and when the solids start to precipitate) is a function of the saturation index (Söhnel, 1988). Previous studies have investigated the kinetics of barite and gypsum precipitation as a function of solution composition and showed that the shorter induction periods were observed at higher saturation indices (Fan, 2011; He, 2014; Lancia, 1999). Co-precipitation is a multiphase process that includes the following main mechanisms: inclusion (i.e., lattice replacement), occlusion (i.e., ions physically captured between the layers of precipitating crystal) and adsorption (Harvey, 2000; Zhang, 2014). Due to the high salinity of the produced water and high concentration of competing divalent cations, it is reasonable to assume that the adsorption is unlikely to contribute significantly to ion removal during co-precipitation process. Precipitation of barite is most likely accompanied by the replacement of $Ba^{2+}$ in the crystal lattice with morphologically similar $Ra^{2+}$ and $Sr^{2+}$ ions. Ionic radii of $Sr^{2+}$, $Ba^{2+}$ and $Ra^{2+}$ are similar in size (i.e., ionic radii of $Sr^{2+}$, $Ba^{2+}$ and $Ra^{2+}$ are 1.32, 1.49 and 1.62 Å, respectively) (Shannon, 1976), thus allowing them to co-precipitate together in the form of solid solutions (i.e., Ba-Sr-$SO_4$, Ba-Ra-$SO_4$ and Sr-Ra-$SO_4$) (Prieto, 2009). $Mg^{2+}$ and

$Ca^{2+}$ ions are smaller ions (i.e., 0.86 and 1.14 Å, respectively) (Shannon, 1976) and unlikely to replace $Ba^{2+}$ in the crystal lattice. Therefore, concentration of $Mg^{2+}$ and $Ca^{2+}$ is controlled by the occlusion and the extent of the removal of these ions is inversely proportional to the saturation index of barite (Figure 4.2). Removal of these ions at higher $SI_{BaSO4}$ is lower due to the shorter induction time of $BaSO_4$ formation (i.e., insufficient time for these ions to be captured between barite layers).

Another important factor that influences $Ba^{2+}$ and $Ra^{2+}$ removal during sulfate precipitation in produced water is Sr/Ba ratio. Although the solubility product of strontium sulfate (i.e., celestite) of $10^{-6.63}$ is much higher than that of barite ($K_{sp} = 10^{-9.97}$), precipitation of celestite will occur if its saturation index is positive and it will affect the precipitation of barite. Adding $BaCl_2$ to the solution will decrease Sr/Ba ratio and enhance the extent of $Ba^{2+}$ and $Ra^{2+}$ removal (Table 4.3, Figure 4.2). A set of experiments was conducted in synthetic produced water (Table C.3 in Appendix C) together with PhreeQC simulations to investigate the combined impact of barite saturation index and Sr/Ba ratio in solution on $Ba^{2+}$ and $Ra^{2+}$ removal. Results of these experiments are shown together with equilibrium predictions in Figure 4.3.

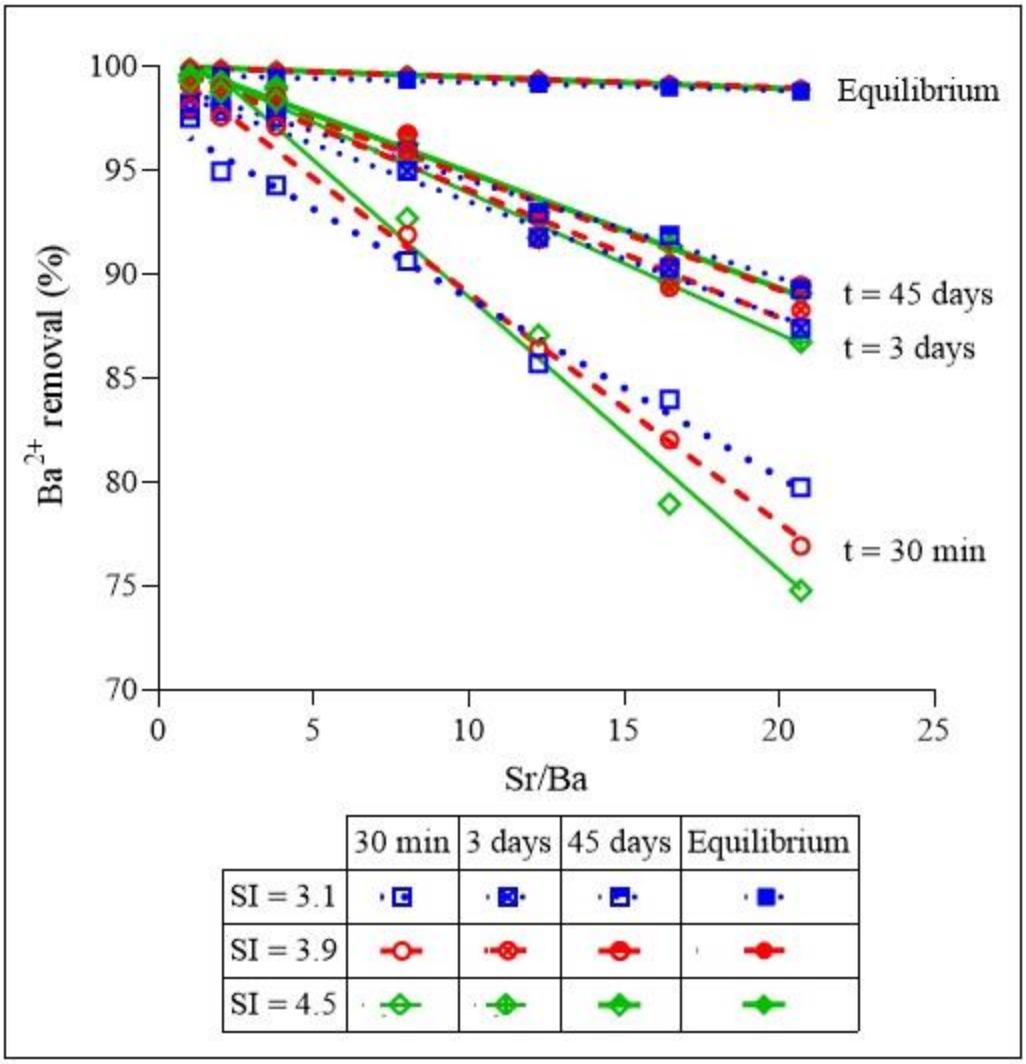


**Figure 4.3.** Barium removal from synthetic produced water as a function of $SI_{BaSO4}$ and Sr/Ba ratio.

As can be seen in Figure 4.3, barium removal by precipitation is slow and is greatly affected by both barite SI and Sr/Ba ratio while equilibrium calculations (PhreeQC) in all cases predict very high barium removal (i.e., the lowest predicted barium removal was 98.8% for $SI_{BaSO4}$ = 3.1 and Sr/Ba = 20.7). At low Sr/Ba ratios (i.e., Sr/Ba < 3), barium removal close to that predicted by thermodynamic calculations was achieved after just 30 min of reaction time for $SI_{BaSO4}$ of 3.9 and

4.5. Even when $SI_{BaSO4}$ = 3.1, barium removal after 30 min was greater than 95% if the Sr/Ba <3. Such behavior can be attributed 100 times lower $SI_{SrSO4}$ compared to $SI_{BaSO4}$ (Table C.4 in Appendix C) resulting in minimal interference of Sr with barite precipitation. Increasing Sr/Ba ratio leads to greater discrepancy between modelling and experimental results. Data in Figure 4.3 clearly indicate significant increase in equilibration time when Sr/Ba >3 so that even 45 days was not sufficient to achieve chemical equilibrium. At lower Sr/Ba ratios, barite supersaturation is the dominant driving force for barite precipitation, while the interference of high concentration of $Sr^{2+}$ becomes significant at elevated Sr/Ba ratios due to possible formation of non-miscible celestite solids (Ouyang, 2019). When $Sr^{2+}$ is present at much higher concentration than $Ba^{2+}$ (i.e., Sr/Ba > 8), celestite supersaturation becomes a significant factor in $Ba^{2+}$ removal. As can be seen in Figure 4.3, $Ba^{2+}$ removal is the highest at the lowest $SI_{BaSO4}$ (i.e., 3.1) when Sr/Ba > 8. While this outcome may not be intuitively clear, it is important to note that lower $SI_{BaSO4}$ leads to lower $SI_{SrSO4}$ due to the lower initial sulfate concentration added to the solution. For example, the range of $SI_{SrSO4}$ varies from 0.62 – 1.02 when $SI_{BaSO4}$ = 3.1 compared to $SI_{SrSO4}$ = 2.02 – 2.39 at $SI_{BaSO4}$ = 4.5.

The results presented above can be explained by the competition between $Sr^{2+}$ and $Ba^{2+}$ for sulfate as the common ligand when the reaction kinetics plays an important role in the ion removal when the reaction time is limited. Figure 4.4 shows the rate of $Ba^{2+}$ and $Sr^{2+}$ removal from the solution at $SI_{BaSO4}$ = 3.9 at different Sr/Ba ratios. Kinetics of $Ba^{2+}$ and $Sr^{2+}$ precipitation is fast when Sr/Ba = 3 and pseudo-equilibrium (i.e., initial equilibrium of homogeneous precipitation that is followed by very slow displacement of $Sr^{2+}$ with $Ba^{2+}$ in celestite formed initially) is reached within 30-60 min. At higher Sr/Ba ratio (i.e., 10 and 20), initial $Sr^{2+}$ removal is significantly faster than $Ba^{2+}$ removal and it took only 15 min to achieve pseudo-equilibrium for celestite precipitation compared to more than 2 hours that were necessary for barite precipitation.

None of these experiments reached equilibrium within 7 days since even 45 days was not sufficient to achieve equilibrium when Sr/Ba ratios are very high (Figure 4.3).

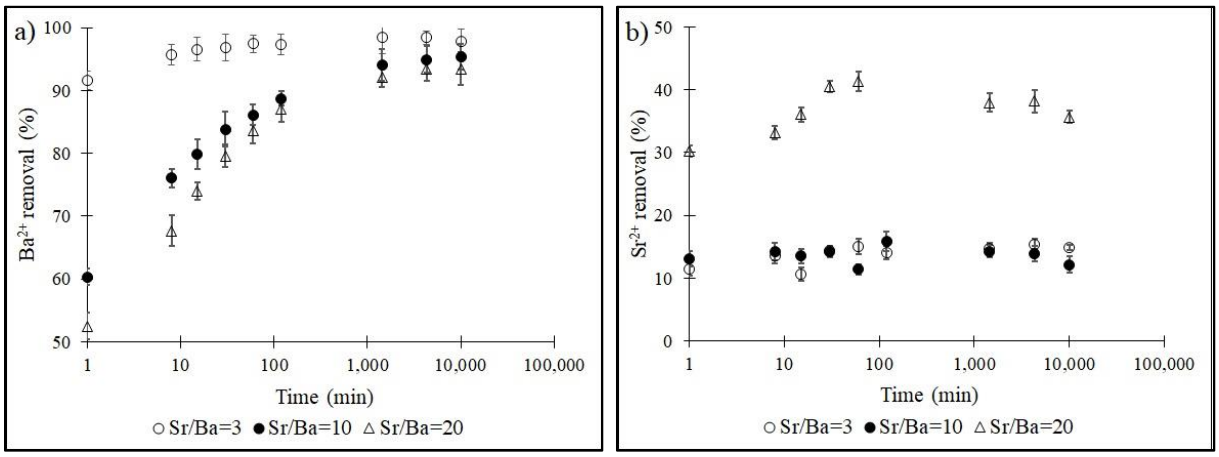


**Figure 4.4.** Kinetics of (a) $Ba^{2+}$ and (b) $Sr^{2+}$ removal from the synthetic produced water as a function of Sr/Ba ratio at $SI_{BaSO4}$ = 3.9.

The impact of Sr/Ba ratio and sulfate addition on the removal of $Ba^{2+}$ and $Ra^{2+}$ in real PW is summarized in Figure 4.5.

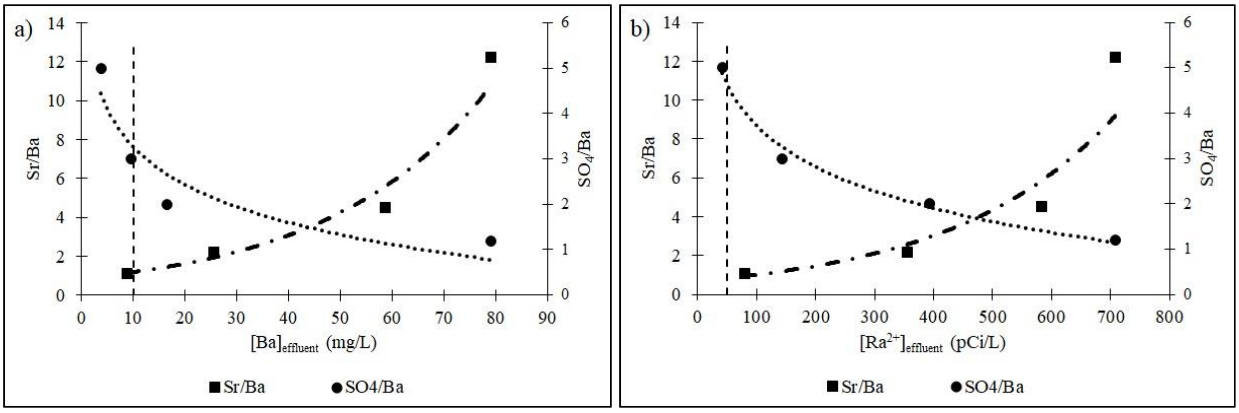


**Figure 4.5.** Impact of Sr/Ba and $SO_4$/Ba on (a) $Ba^{2+}$ effluent concentration and (b) $Ra^{2+}$ effluent concentration.

Based on the results discussed above, it can be concluded that sulfate precipitation can be used for produced water treatment to achieve required $Ba^{2+}$ and $Ra^{2+}$ concentrations and enable effective crystallization for salt recovery if appropriate $SI_{BaSO4}$ and Sr/Ba ratios are achieved in the process. As can be seen in Figure 4.5a, there are only two ways to achieve required $Ba^{2+}$ effluent concentration: 1) Decreasing Sr/Ba ratio below 1.2 or 2) adding sulfate at least 3.3 times the initial $Ba^{2+}$ concentration. The major disadvantage of this approach is the production of 30-50 tons of solids per $10^6$ gallons of treated produced water. Reducing $Ra^{2+}$ concentration below 50 pCi/L would require adding a minimum of 4.6 times more sulfate than the existing concentration of $Ba^{2+}$ (Figure 4.5b). Although EPA exempts Technologically Enhanced Naturally Occurring Radioactive Material (TENORM) generated in oil and gas industry from the hazardous materials disposal regulations, it recommends that TENORM containing between 50-2,000 pCi/g should be disposed in Resource Conservation and Recovery Act (RCRA) hazardous waste landfills (Smith, 1999). Disposal fees at these landfills and transportation distance would make this treatment approach cost prohibitive. Therefore, it is necessary to develop a different approach to achieve the required effluent concentrations for $Ba^{2+}$ and $Ra^{2+}$ without generating such large solids quantities.

### 4.3.2 Impact of the BaSO4 "Seed" on Barium and Radium Removal

As discussed previously, seed addition can enhance precipitation of the solids with structure that is similar to that of the seed material. Therefore, a set of experiments where barite "seed" particles were added to the solution was conducted in an effort to enhance $Ba^{2+}$ and $Ra^{2+}$ removal from the produced water even when Sr/Ba ratios were unfavorable for barite precipitation. These experiments were conducted using four different doses of barite particles. Solids formed during the experiment were recycled twice to compare the efficiency of fresh barite seed with

barite seed formed in the presence of impurities (i.e., $Mg^{2+}$, $Ca^{2+}$, $Sr^{2+}$, $Ra^{2+}$). Experimental conditions are listed in Table 4.4 and the removals of selected ions after 30 min of reaction are shown in Figure 4.6.

**Table 4.4.** Impact of barite seed concentration on the removal of $Ba^{2+}$ and $Ra^{2+}$ from PW with initial [$Ba^{2+}$] = 488 mg/L

| **Initial $Ba^{2+}$ (mg/L)** | **$SO_4^{2-}$ addition (mg/L)** | **$SO_4$/Ba** | **$BaSO_{4(s)}$ addition (g/L)** | **$SI_{BaSO4}$** | **Solids formation (ton/$10^6$ gallons)** | **Sludge* radioactivity (pCi/g)** |
|---|---|---|---|---|---|---|
| 488 | 409 | 1.2 | 0 | 3.12 | 19.0 | 743 |
| 488 | 409 | 1.2 | 5 | 3.12 | 19.6 | 435 |
| 488 | 409 | 1.2 | 10 | 3.12 | 19.9 | 294 |
| 488 | 409 | 1.2 | 25 | 3.12 | 19.8 | 153 |
| 488 | 409 | 1.2 | 50 | 3.12 | 20.2 | 87 |

* Sludge is the sum of added barite and solids formed in the system

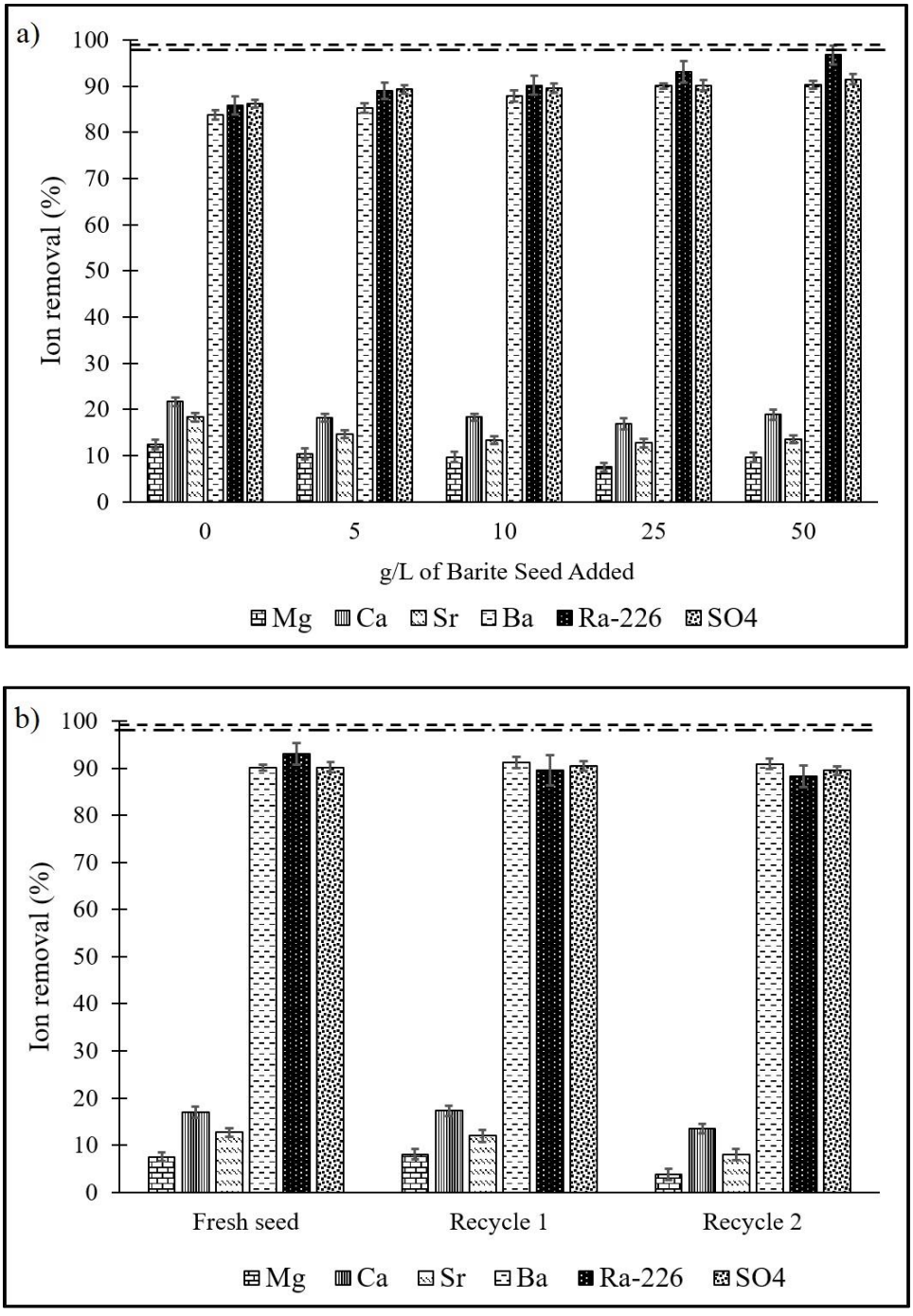


**Figure 4.6.** Impact of barite seed on the removal of $Ba^{2+}$ and $Ra^{2+}$ from PW after 30 min of contact using (a) fresh seed and (b) 25 g/L of barite seed through 3 cycles of use; dash-dot and dashed lines represent required $Ba^{2+}$ and Ra-226 ion removal to meet efflent standards, respectively; error bars indicate standard deviation of the analytical procedure.

As can be seen in Figure 4.6a, barite seed has positive impact on $Ba^{2+}$ removal from the produced water. The addition of 120% sulfate/barium to PW resulted in 83.8% removal of $Ba^{2+}$. However, simultaneous addition of 120% sulfate/barium and fresh barite seed caused an increase in $Ba^{2+}$ removal to 85.2% at 5 g/L of seed and to 90.3% at 50 g/L of seed. Similar enhancement was previously observed in the removal of gypsum (Fröhner, 1975) and calcite (Mercer, 2005). Similarly, $Ra^{2+}$ removal of 96.7% was observed with 50 g/L of seed compared to 85.8% removal without any seed. Based on the results of previous studies in dilute solutions (Brandt, 2015; Curti, 2010; Klinkenberg, 2014; Zhang, 2014), it can be concluded that $Ra^{2+}$ adsorption on fresh barite is contributing to the enhanced $Ra^{2+}$ removal in the PW. However, barite seed addition was not able to achieve $Ba^{2+}$ concentration below 10 mg/L which limits the practical use of this approach.

Interestingly, the removal of $Ca^{2+}$ and $Sr^{2+}$ decreased from 21.7 and 18.3% in the absence of seed, respectively, to 18.9 and 13.6% in the presence of 50 g/L of fresh barite seed, respectively. As discussed previously, these ions are removed by the occlusion mechanism during the co-precipitation process. The presence of barite seed lowers the activation energy of heterogeneous barite precipitation (Kügler, 2016), thus causing shorter induction times and reducing the extent of ion occlusion. The total number of moles of $Ba^{2+}$, $Sr^{2+}$ and $Ca^{2+}$ that were removed from the produced water was greater than the number of $SO_4^{2-}$ moles removed (Table C.5a in Appendix C), supporting the hypothesis that a portion of these ions is not directly precipitated with sulfate ligand but is removed by adsorption and/or occlusion. Hence, the total amount of solids removed from the PW tend to increase only slightly with an increase in the amount of barite seed (Table 4.4).

As can be seen in Figure 4.6b, recycling solids was as effective in promoting ion removal as was the introducing of fresh seed into the system. A slight decrease in $Ra^{2+}$ removal from 93.1% when fresh barite seed was added to the system to 89.5% when solids were recycled once may

suggest a slight decrease in the adsorption capacity of barite for $Ra^{2+}$ due to exposure to high concentration of other ions in the PW. However, $Ra^{2+}$ removal in the third cycle of barite use indicated no further decline in the adsorption capacity. Solids generated in each recycling stage were very close to the amount generated in the initial stage (Table C.5b in Appendix C).

### 4.3.3 Optimization of the Overall Treatment Process

Although treatment strategies evaluated above improved barium and radium removal, vast majority of the conditions evaluated in this study were not able to achieve barium concentration below 10 mg/L. One exception was the treatment approach shown in Figure 4.2 where the initial $Ba^{2+}$ concentration was increased more than 11 times requiring very high sulfate dose to achieve high barite saturation index (SI=5.27) and resulting in large volume of radioactive sludge from this process. The addition of 500% sulfate/barium to PW resulted in required barium and radium concentrations, but also in high residual sulfate in the effluent. Therefore, a treatment approach with simultaneous adjustment of Sr/Ba ratio and addition of $BaSO_4$ seed was evaluated using the experimental conditions summarized in Table 4.5 and the results are shown in Figure 4.7.

**Table 4.5.** Experimental conditions to evaluate $Ba^{2+}$ and $Ra^{2+}$ removal from PW using both adjustment of Sr/Ba ratio and $BaSO_4$ seed

| Sample ID | Initial $Ba^{2+}$ (mg/L) | $SO_4^{2-}$ addition (mg/L) | $BaSO_{4(s)}$ addition (g/L) | $SI_{BaSO4}$ | $SI_{SrSO4}$ | Sr/Ba | Solids formation (ton/$10^6$ gallons | Sludge* radioact. (pCi/g) |
|---|---|---|---|---|---|---|---|---|
| O1 | 1,325 | 1,113 | 25 | 4.00 | 1.23 | 4.5 | 25.2 | 154 |
| O2 | 1,704 | 1,430 | 25 | 4.22 | 1.34 | 3.5 | 26.3 | 155 |
| O3 | 2,983 | 2,504 | 25 | 4.72 | 1.59 | 2 | 31.8 | 148 |
| O4 | 3,977 | 3,338 | 25 | 4.98 | 1.72 | 1.5 | 44.4 | 135 |

* Sludge is the sum of added barite and solids formed in the system

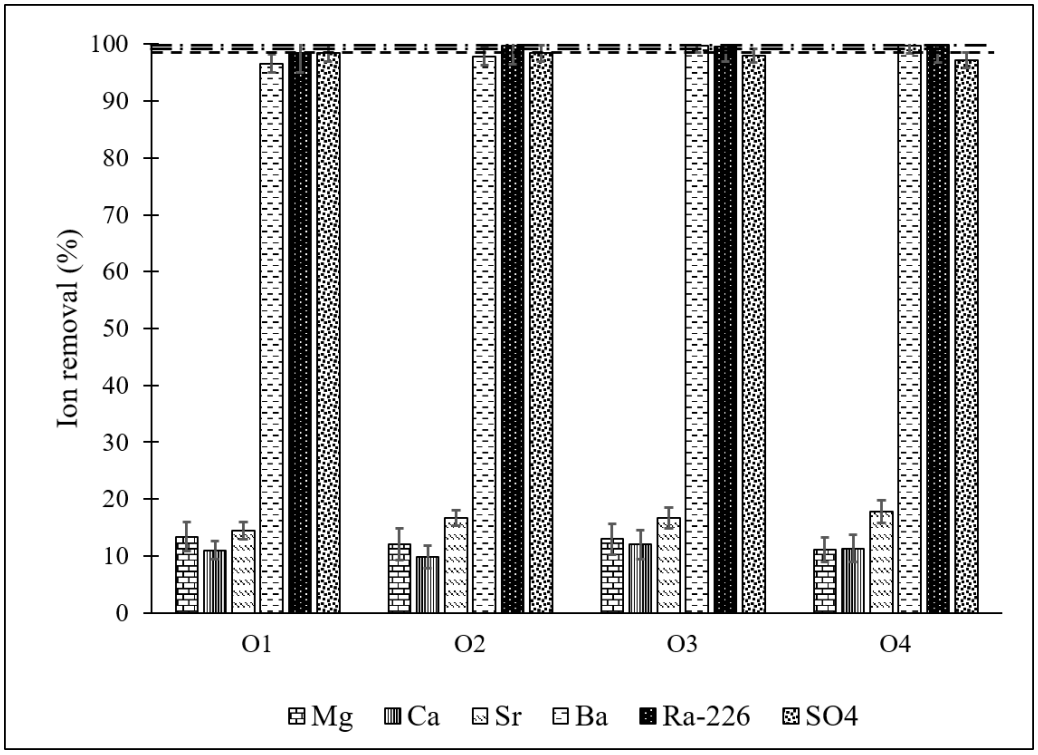


**Figure 4.7.** Ion removal in PW with simultaneous adjustment of Sr/Ba ratio and $BaSO_4$ seed addition after 30 min of reaction; dash-dot range and dashed line represent required $Ba^{2+}$ and Ra-226 ion removal to meet efflent standards, respectively.

As can be seen in Figure 4.7, simultaneous increasing initial $Ba^{2+}$ concentration and adding $BaSO_4$ seed resulted in more efficient $Ba^{2+}$ and $Ra^{2+}$ removal. Barium concentration in the effluent varied from 45 mg/L in the sample O1 to 8 mg/L in the sample O4, which can be correlated to an increase in the saturation index of barite from 4.00 to 4.98 (Table 4.5). Required $Ba^{2+}$ concentration, below 10 mg/L, was achieved in samples O3 and O4 (i.e., 9 and 8 mg/L). Chemical addition to achieve high $SI_{BaSO4}$ and low Sr/Ba ratio is important for the operation of the treatment process as it provided barium free effluent (i.e., lower than 10 mg/L) in the time frame that is typical for full-scale produced water treatment plant (i.e., detention time of 30 min).

As expected, $Ra^{2+}$ removal was also enhanced due to simultaneous co-precipitation and post-precipitation reaction with barium sulfate. $Ra^{2+}$ concentration in the O2, O3 and O4 effluents was 14, 20 and 5 pCi/L, respectively (i.e., removal above 99%). Similar to data shown in Figure 4.6a, $Ra^{2+}$ removal is higher than $Ba^{2+}$ removal due to the multiple mechanisms involved in $Ra^{2+}$ removal. Most of the $Ra^{2+}$ is co-precipitated with barite forming a Ba-Ra-$SO_4$ solid solution, while the rest is most likely removed through adsorption onto introduced and/or formed barite solids.

While $Mg^{2+}$ and $Ca^{2+}$ removal remained constant at different experimental conditions, slight increase in $Sr^{2+}$ removal with increase in the initial $Ba^{2+}$ concentration was observed in these experiments. Higher $Ba^{2+}$ concentration in the PW required higher $SO_4^{2-}$ concentration to maintain sulfate/barium ratio of 1.2. Assuming that all barium was removed through precipitation as barite, excess sulfate in experiments O1-O4 was in the range from 218 – 562 mg/L. This excess sulfate was sufficient to exceed solubility product of celestite (i.e. Ksp = $10^{-6.63}$) to achieve $SI_{SrSO4}$ in the range from 1.23 – 1.72 and contribute to a slight increase in solids formed (Table 4.5).

Combined effect of reducing Sr/Ba ratio and adding barite seed successfully reduced barium and radium concentration to required values and resulted in less sludge formed compared to previously evaluated treatment approaches (Tables 4.2 and 4.3). Furthermore, experimental results shown in Figure 4.6b show that recycling barite solids in the treatment process can achieve similar effect as the addition of fresh barite seed and control the concentration of $Ra^{2+}$ in the effluent at a desired value.

## 4.4 Summary and Conclusions

Laboratory experiments were conducted to evaluate removal of specific ions from the produced water generated during unconventional gas extraction using barium sulfate precipitation. Several methods were investigated with the focus on modifying initial Sr/Ba ratio, adding $BaSO_4$ seed, and reducing sludge production while achieving requisite $Ba^{2+}$ and $Ra^{2+}$ removal. It was found that fairly high saturation index (i.e., above 5) is necessary to achieve required $Ba^{2+}$ and $Ra^{2+}$ removal and that a large mass of radioactive sludge would be generated in that treatment process.

Barium removal was modelled using the thermodynamic database in PhreeQC software for various $SI_{BaSO4}$ and Sr/Ba ratios and compared to experimental results. It was found that both kinetics and equilibrium of $Ba^{2+}$ removal is highly dependent on Sr/Ba ratio. At Sr/Ba < 3 and $SI_{BaSO4}$ = 4.5, $Ba^{2+}$ removal was fast and pseudo equilibrium was reached within 30 min while it took approximately 3 days to reach pseudo equilibrium for $SI_{BaSO4}$ < 4.5. $Ba^{2+}$ removal was much slower for Sr/Ba > 3 (equilibrium was not achieved after 45 days) and was not dependent on $SI_{BaSO4}$.

Addition of fresh barite seeds improved $Ba^{2+}$ removal and significantly enhanced $Ra^{2+}$ uptake from the solution. Such behavior can be explained by $Ra^{2+}$ adsorption onto barite solids. Optimization of the treatment methods by simultaneously reducing the Sr/Ba ratio and addition of barite seed resulted in high $Ba^{2+}$ and $Ra^{2+}$ removal, while generating less sludge than previously evaluated approaches. It was found that the optimal treatment is achieved when dosing is somewhere between approaches O2 and O3. This study suggests that proper optimization of chemical addition can achieve low $Ba^{2+}$ and $Ra^{2+}$ in the effluent after a reasonable reaction time (i.e., 30 min) while minimizing the production of radioactive sludge in the process.

# 5.0 Summary, Conclusions and Future Work

## 5.1 Summary and Conclusions

This study was designed to investigate the control strategies for the NORM that is brought to the surface with produced water from unconventional oil and gas industry. The first part of the study was focused on understanding the mechanisms and factors that control the ability of inorganic sorbents to sequester radium from dilute and high salinity solutions. These findings were then used to develop a new strategy for creating functionalized proppant that could be used to sequester NORM in the subsurface and prevent it from reaching the surface with produced water. The last part of the study was focused on developing optimal treatment approach to remove the NORM from produced water if it is brought to the surface using sulfate coprecipitation. In summary, the specific objectives of this study were to: 1) understand the mechanisms of radium uptake by barite solids in the solution containing orders of magnitude greater concentrations of monovalent and divalent cation using experiments and computational modeling; 2) develop an functionalized hydraulic fracturing proppant for the control of radium in underground phases of unconventional natural gas extraction; and 3) investigate radium uptake during barium sulfate precipitation in produced water that has a high Sr/Ba ratio and evaluate possible modifications to standard treatment approach. The main findings of each objective are summarized in subsequent sections.

### 5.1.1 Impact of Solution Composition and Temperature on Ra-226 Removal by Barite ($BaSO_4$): Comparison of Experimental and Modeling Results

Radium removal by barite solids was evaluated in dilute and high salinity solution (i.e., up to 1 mol/L) and at different temperatures (3-40 °C). Molecular dynamics modeling was used to further expand the understanding of mechanisms responsible for radium uptake by barite. Both experimental and modeling results showed that radium removal will be highly affected by size, charge and concentration of dissolved ions in the solution. Increasing concentration of co-ions had an adverse impact on radium uptake due to the competition for active sites on barite surface and changes in the electric double layer (EDL) of barite. Radium uptake was more inhibited in the presence of divalent cations that in the presence of monovalent cations due to their higher charge and higher impact on zeta potential of barite. Zeta potential effect was observed at approximately 2-3 Å measured from the surface of barite and it was more pronounced (i.e., less negative or more positive) in the presence of ions with increasing charge and diffusivity (e.g., less negative zeta potential was observed in 0.1 mol/L of $MgCl_2$ than in 0.1 mol/L NaCl solution and more positive zeta potential was observed in 0.1 mol/L $BaCl_2$ than in 0.1 mol/L $SrCl_2$). Comparison of modeling and experimental results revealed that multiple mechanisms were involved in radium uptake in aqueous systems. These findings were supported by experimental studies on radium uptake barite at low (i.e., 3 °C) and high (i.e, 40 °C) temperature, which showed that surface dissolution-recrystallization is an important mechanism for radium uptake. Overall process of radium uptake is affected by zeta potential of barite (i.e., at 2-3 Å in EDL) and carried out by dissolution-recrystallization reactions at barite surface. This study shows that modeling Ra-226 uptake by solids that undergo dissolution/recrystallization process needs to include mechanisms other than adsorption to be relevant in practice.

### 5.1.2 Development of Functionalized Proppant for the Control of NORM in Marcellus Shale Produced Water

Most of the current treatment technologies are designed to deal with Ra-226 once produced water is stored in tanks or in surface impoundments. This study aimed to develop a hydraulic fracturing proppant that will be able to prevent Ra-226 from reaching the surface with produced water. After evaluating multiple inorganic sorbents for Ra-226 removal, $SrSO_4$ and $BaSO_4$ were selected as potential coating agents for quartz sand proppant. These solids were able to sequester most of the radium from dilute solutions at pH range from 2 – 9.5 and ionic strength up to 1.6 M. Quartz sand was able to sequester radium by itself, but this uptake was highly affected by the solution pH and the presence of competing cations. Sand was the most effective at high pH (i.e., 9.6) due to very low (i.e., highly negative) zeta potential of approximately -80 mV. Radium uptake by sand was inhibited when other ions (i.e., $Na^+$, $Sr^{2+}$) were present in solution. Two impregnation techniques for functionalizing this proppant were evaluated in this study: 1) direct mixing of sand and preformed solids and 2) heterogeneous precipitation of strontium/barium sulfate on quartz sand as a "seed". Heterogeneous precipitation resulted in higher mass of coating agent on the sand surface: 149 and 53 mg/g of celestite and barite, respectively. Coated sand was tested for radium removal in high salinity solution (i.e., $Na^+$ = 33,000 mg/L, $Mg^{2+}$ = 1,600 mg/L and $Ca^{2+}$ = 16,000 mg/L) at room temperature (i.e., 21 °C) and at elevated temperature (i.e., 37-40 °C) and it was shown that modified proppant can successfully remove up to 56 % of Ra-226 even in the presence of high concentration of competing ions. Preliminary analysis suggested that the functionalized proppant can retain keeping Ra-226 in the subsurface for the life of a well, which would significantly reduce health and environmental risks associated with produced water.

### 5.1.3 Sulfate Precipitation in Produced Water from Marcellus Shale for the Control of Naturally Occurring Radioactive Material

Barium sulfate precipitation is a commonly used method for the control of Ra-226 in produced water stored in surface impoundments. However, produced water with high concentration of $Sr^{2+}$ and high Sr/Ba ratio can be exceptionally challenging due to low solubility of strontium sulfate (i.e., Ksp = $10^{-6.63}$) and significant $Sr^{2+}$ interference with barium sulfate precipitation. It was shown that such produced water requires a high amount of excess sulfate (i.e., 3-5 times higher than $Ba^{2+}$ molar concentration) to achieve acceptable effluent concentrations of $Ba^{2+}$ (i.e., < 10 mg/L) and Ra-226 (i.e., 50 pCi/L). Adding such high sulfate concentration will generate high amount of radioactive sludge (i.e., 32.7 – 36.6 ton/$10^6$ gallons) whose disposal would add significantly to the overall treatment cost.

This study found that barium sulfate saturation index above 5 is necessary to achieve required effluent barium standard. Barium sulfate precipitation was modeled using PhreeQC software for various saturation indices of barite and Sr/Ba ratios. Chemical equilibrium predicted by PhreeQC was experimentally reached only at Sr/Ba < 3 and $SI_{BaSO4}$ = 4.5, while other conditions exhibited significantly slower kinetics. Seeding the system with preformed barite solids resulted in higher $Ba^{2+}$ and Ra-226 removal due to the simultaneous co-precipitation and post-precipitation reactions. Optimizations of the system was necessary to achieve required effluent standards and minimize radioactive sludge production. Optimal treatment solution was found to be simultaneous addition of 25 g/L of preformed barite seed, adjustment of Sr/Ba ratio to 2 and $SI_{BaSO4}$ to 1.59 by the addition of $BaCl_2$ and addition of sulfate at 1.2 times molar ratio of barium. This treatment approach generated the lowest amount of radioactive sludge (i.e., 31.8 ton/$10^6$ gallons) while achieving effluent $Ba^{2+}$ and Ra-226 concentrations of 9 mg/L and 20 pCi/L, respectively. This

study provides a guidance for treating produced water with high Sr/Ba ratio to achieve low $Ba^{2+}$ and Ra-226 concentrations in the effluent.

## 5.2 Key Contributions

The research presented in this dissertation contributed to fundamental understanding of NORM sequestration by inorganic sorbents from low and high salinity water and provided alternative solutions to ongoing environmental problems and challenges associated with management of produced water from unconventional reservoirs.

Key mechanism and factors involved in radium uptake by barite were analyzed experimentally and using molecular dynamics modeling. Presence of ions that are typically found in produced water at high concentrations inhibited radium uptake due to the change in zeta potential in the electrical double layer of barite. Temperature dependence of radium uptake indirectly supported the hypothesis that surface dissolution-recrystallization reactions at barite surface contribute to radium removal from solution. Molecular dynamics simulations matched experimental data reasonably well. In summary, this study provided further insight into barite interaction with radium in the presence of co-ions, which is essential for understanding the fate of radium in produced water.

An alternative to sometimes complicated and expensive removal of radium from produced water is keeping radium in the subsurface. Thus, the idea of coating hydraulic fracturing proppant with inorganic sorbents is presented and evaluated in this study. It is important to notice that quartz sand by itself can serve as a sorbent for radium, but its capacity is highly reduced at lower pH and in the presence of other co-ions. Among five inorganic candidates for functionalizing the

conventional proppant used in hydraulic fracturing operations (i.e., quartz sand), celestite and barite exhibited the highest radium uptake. Proppant coated using heterogeneous precipitations improved radium removal in high salinity solutions at both room temperature and 40 °C, which is a common temperature in unconventional gas wells. Development of coated proppant is one of the key contributions of this study because such proppant can keep radium underground and avoid environmental and health risks associated with radium accumulated in surface impoundments.

Chemical composition of produced water varies significantly with geologic formation and well location. Achieving required effluent standards with a respect to $Ba^{2+}$ and $Ra^{2+}$ is challenging and it requires adding high sulfate concentration and generates significant amount of highly radioactive sludge that is quite difficult and expensive to dispose. It was found that Sr/Ba ratio and saturation index of barite $SI_{BaSO4}$ play a crucial role in the kinetics and equilibrium of barium precipitation with sulfate. $Ba^{2+}$ and $Ra^{2+}$ removal was enhanced when preformed barite was added to the system, which showed the importance of heterogeneous precipitation in produced water. Finding an optimal treatment approach that would provide low concentration of $Ba^{2+}$ and $Ra^{2+}$ in the effluent and minimize sludge production was the major achievement of this study. Varying the amount of barite seed and Sr/Ba ratio lead to a novel treatment approach that serves as guide for produced water treatment plant operators.

## 5.3 Future Directions

Future research should aim to expand existing work and provide data and information that can be used for reducing environmental and health risks associated with NORM and also support efficient and safe unconventional natural gas extraction. Based on studies described in Chapters 2,

3 and 4, the following research topics could be beneficial for the control of radium in flowback and produced water generated in hydraulic fracturing:

- Discrepancies observed between experimental and molecular modeling data in Chapter 2 are due to inability of molecular dynamics to simulate all processes that are involved in radium uptake in natural aqueous systems. Improving a model to simulate surface dissolution-recrystallization would be beneficial for acquiring more accurate data and better matching with experiments. In additions, getting a better estimate of $Ra^{2+}$ forcefield relative to $Ba^{2+}$ forcefield could lead to more accurate modeling. It is clear that $Mg^{2+}$ potential of mean force needs to be recalculated to achieve accurate modeling of adsorption isotherms;
- Expanding these experimental and modeling results from Chapter 2 to analyze radium uptake by barite in the presence of multiple co-ions would have a significant impact on developing an ultimate model of radium removal in produced water. In addition, investigating the impact of temperature on radium uptake in the presence of one or more co-ions would be beneficial for understanding radium uptake in downhole conditions (i.e., high salinity and higher temperature).
- Impregnated proppant in Chapter 3 exhibited significant radium uptake even at high concentrations of co-ions and at 40 °C. However, finding a more sophisticated method for proppant coating that could achieve higher coating efficiency and better stability of a coating agent at high pressures in a wellbore, would be beneficial for implementing this technology in industry.
- Mechanical stability of the coated material under high shear stress conditions present while pumping proppant at high flowrate and at high concentration would be required to validate practical relevance of the proposed method for proppant functionalization.

- From the practical standpoint, it would be useful to analyze the impact of organics and surfactants that are typically present in produced water on radium uptake by coated proppant.
- Exploring the possibility of ferrous and manganese oxides coating on quartz sand (or other proppant) surface for radium uptake in underground phases of hydraulic fracturing. Multiple studies showed high affinity of these solids for radium ions.
- Produced water treatment methods investigated in Chapter 4 achieved high $Ba^{2+}$ and Ra-226 removal, but some potentially useful ions, $Mg^{2+}$ and $Ca^{2+}$, are also highly affected in the process. These ions, precipitated as chlorides or sulfates, can be reused in industry, agriculture or for roads deicing. Thus, decreasing precipitation of these ions during $Ba^{2+}$ and Ra-226 removal and allowing them to be recovered as pure solids in a crystallizer is another objective that needs to be addressed. This could potentially be done by further increasing saturation index of barite which would lead to lower induction period for barite precipitation and less time for other ions to be picked up by occlusion process.
- Investigating the impact of Ca/Ba ratio on barium and radium co-precipitation with sulfate would contribute to better understanding of produced water treatment processes.
- As seen in Chapter 2, carbonate sorbents ($CaCO_3$, $SrCO_3$ and $BaCO_3$) were able to sequester radium in DI water. Thus, investigating the impact of factors such as ionic strength, presence of co-ions, temperature and pH on radium uptake during post-precipitation and co-precipitation of these carbonate solids would be a significant contribution to NORM fate and control.

## Appendix A Supporting Information for Chapter 2

**Freundlich Adsorption Isotherm (Kinnlburgh, 1986) Model** was used to analyze experimental results:

$$q_e = K_F C_e^{\frac{1}{n}} \quad \text{(A1)}$$

$$\log q_e = \frac{1}{n} \log C_e + \log K_F \quad \text{(A2)}$$

where, $q_e$ (pCi/cm$^2$) is adsorption capacity for Ra-226, $C_e$ (pCi/L) is the final (equilibrium) concentration of Ra-226 in the liquid phase and $K_F$ and n are Freundlich constants that are used to describe the observed adsorption trends.

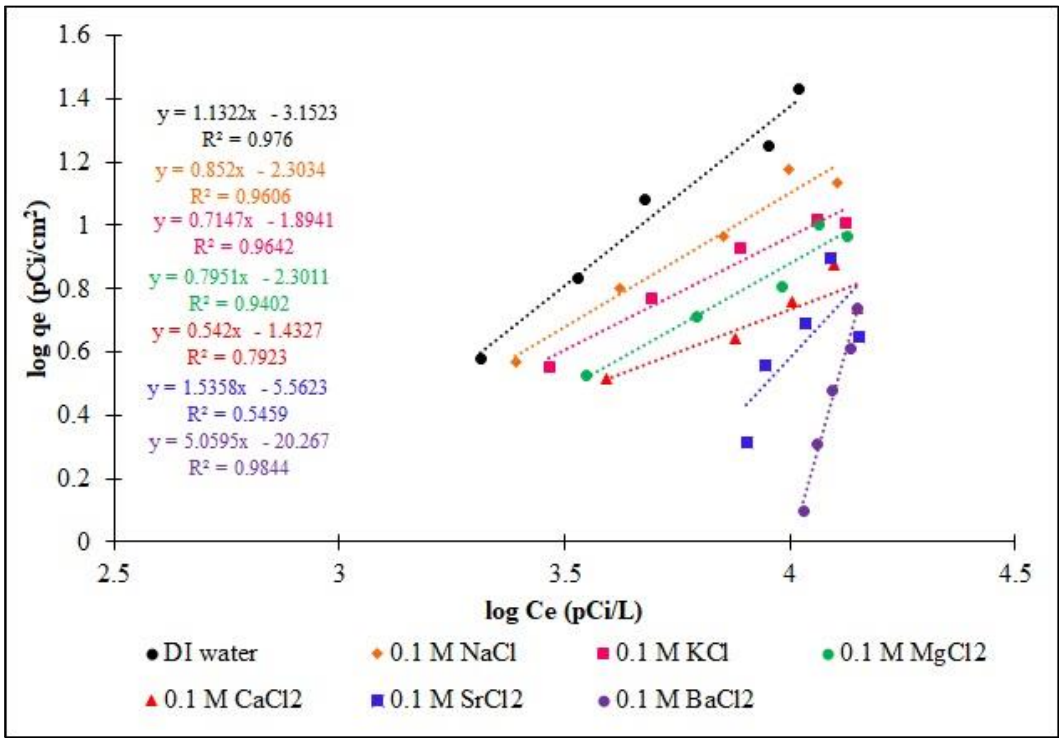


**Figure A.1.** Freundlich adsorption isotherms for Ra-226 removal by barite in 0.1 mol/L salt solutions at neutral pH and with initial Ra-226 concentration of 15,000 pCi/L.

**Kinetics of Ra-226 Removal by Barite in DI Water**

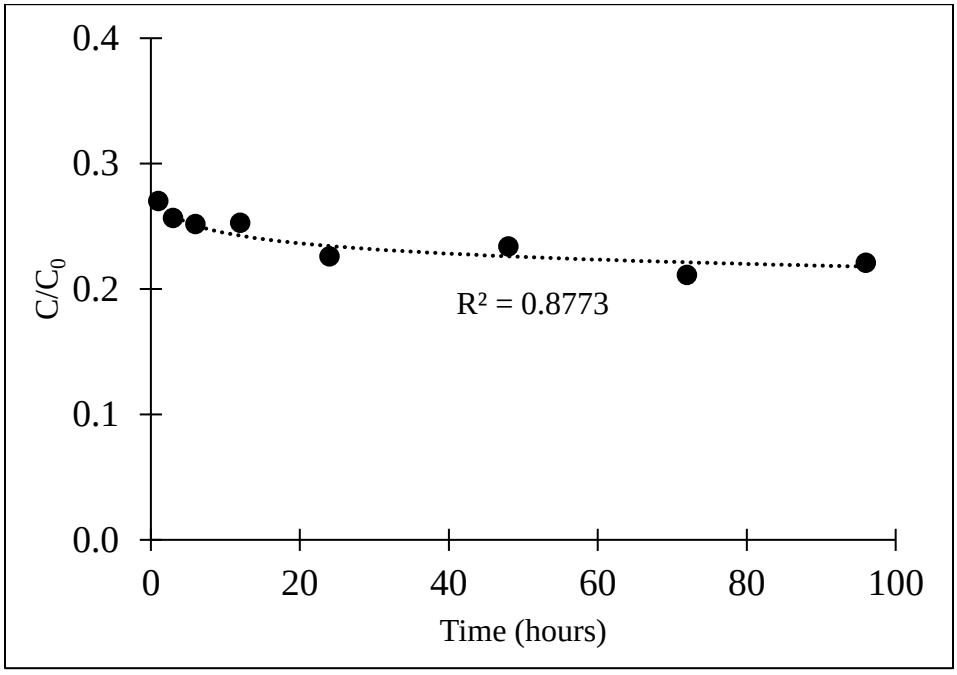


**Figure A.2.** Kinetics of Ra-226 uptake by barite at neutral pH and with initial Ra-226 concentration of 15,000 pCi/L.

**Impact of Charge and Diffusivity on Zeta Potential – Statistical Analysis**

One-way analysis of variance (ANOVA) test was conducted to determine if there is a significant effect of ion type on zeta potential of barite. Monovalent and divalent cations were separately analyzed to determine if zeta potential of barite is a function of cations diffusivity. Confidence interval was set to 95%.

**Table A.1.** ANOVA for zeta potential as a function of (a) monovalent cation type (diffusivity) and (b) divalent cation type (diffusivity)

(a)

**Factor Information**

| Factor | Levels | Values |
|---|---|---|
| Cation (diffusivity) | 2 | 1.334, 1.957 |

**Analysis of Variance**

| Source | DF | Adj SS | Adj MS | F-Value | P-Value |
|---|---|---|---|---|---|
| Cation (diffusivity) | 1 | 5.476 | 5.476 | 1.28 | 0.290 |
| Error | 8 | 34.160 | 4.270 | | |
| Total | 9 | 39.636 | | | |

(b)

**Factor Information**

| Factor | Levels | Values |
|---|---|---|
| Cation (diffusivity) | 4 | 0.706, 0.791, 0.792, 0.847 |

**Analysis of Variance**

| Source | DF | Adj SS | Adj MS | F-Value | P-Value |
|---|---|---|---|---|---|
| Cation (diffusivity) | 3 | 280.98 | 93.6605 | 102.75 | 0.000 |
| Error | 16 | 14.58 | 0.9115 | | |
| Total | 19 | 295.57 | | | |

**Debye Length $K^{-1}$** can be calculated using the following equation (Kohonen, 2000):

$$K^{-1} = \left(\frac{\varepsilon kT}{e^2 \sum_i Z_i^2 N_A C_\infty}\right)^{1/2} \quad \text{(A3)}$$

where, ε (F/m) is a water permittivity, k (J/K) is the Boltzmann constant, T (K) is the temperature, z is the charge number, e (C) is the elementary charge, $N_A$ ($mol^{-1}$) is the Avogadro number and $C_\infty$ (mol/L) is concentration of the electrolyte in bulk.

**Impact of Temperature on Ra-226 Removal – Statistical Analysis**

Two-way analysis of variance (ANOVA) test was conducted to determine if there is a significant effect of adsorbent concentration and temperature, and their interaction, on Ra-226 removal by barite. Confidence interval was set to 95%.

**Table A.2.** ANOVA for Ra-226 removal as a function of barite concentration and temperature

Analysis of Variance

| Source | DF | Adj SS | Adj MS | F-Value | P-Value |
|---|---|---|---|---|---|
| Temperature | 2 | 110.70 | 55.351 | 18.91 | 0.000 |
| Adsorbent concentration | 4 | 2863.92 | 715.979 | 244.57 | 0.000 |
| Temperature*Adsorbent concentration | 8 | 54.30 | 6.788 | 2.32 | 0.045 |
| Error | 30 | 87.82 | 2.927 | | |
| Total | 44 | 3116.74 | | | |

Since P-values for each of the variables and interaction between variables is less than 0.05 (Table A.2.), we can conclude that temperature, adsorbent concentration and interaction between two are all significant factors and that the results are statistically different. Furthermore, these analyses are presented using dotplot of Ra-226 removal.

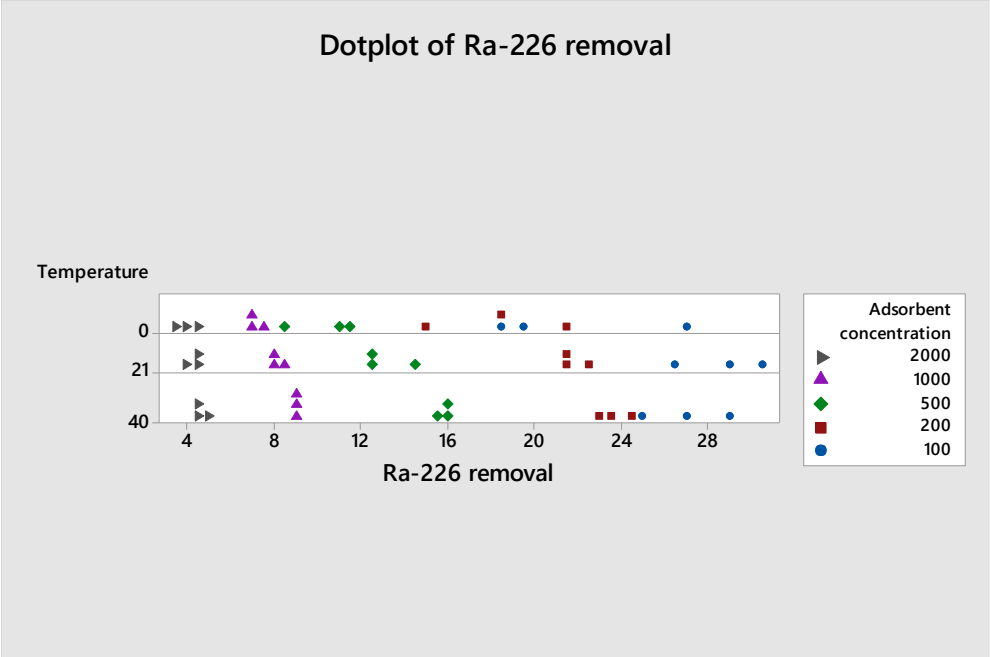


**Figure A.3.** ANOVA dotplot of Ra-226 removal

## Appendix B Supporting Information for Chapter 3

**Co-precipitation** of radium with metal-sulfate compound can be described and distribution coefficient, $K_d$, can be calculated using the following equations (Clifford, 1990; Doerner, 1925; Ganguly, 2012; Zhang, 2014):

$$Ba^{2+} + Ra^{2+} + SO_4^{2-} = Ba(Ra)SO_4 \quad \text{(B1)}$$

$$Me^{2+} + SO_4^{2-} \longrightarrow MeSO_4 \quad \text{(B2)}$$

$$Ra^{2+} + MeSO_4 \longrightarrow Me^{2+} + RaSO_4 \quad \text{(B3)}$$

$$\frac{RaSO_4}{MeSO_4} = K_d \frac{Ra^{2+}}{Me^{2+}} \quad \text{(B4)}$$

### Zeta Potential of Barite

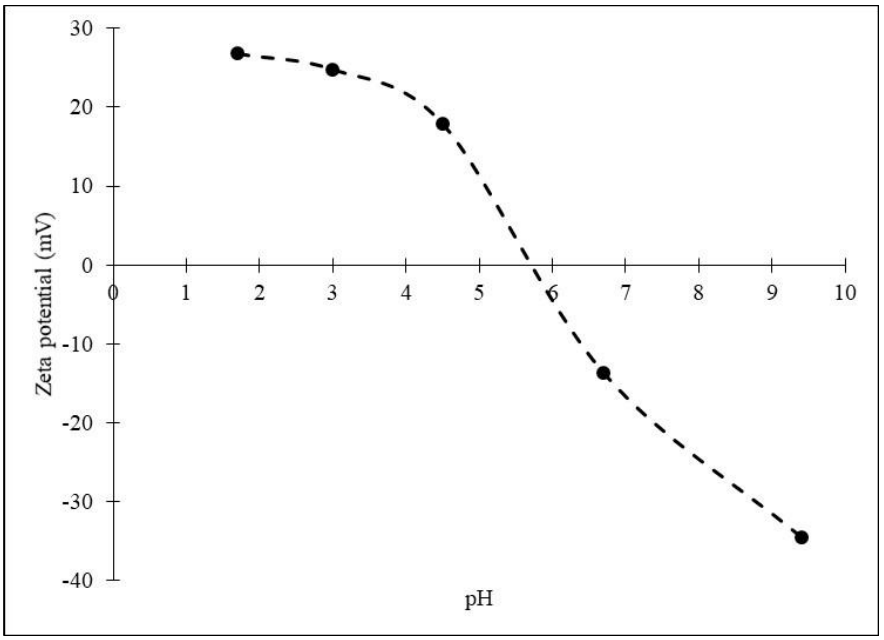


**Figure B.1.** Zeta potential of $BaSO_4$ in DI water as a fucntion of pH.

**Freundlich Isotherm** was used to model the experimental results (Kinnlburgh, 1986):

$$q_e = K_F C_e^{\frac{1}{n}} \quad \text{(B5)}$$

where, $q_e$ (pCi/cm$^2$) is adsorption capacity for Ra-226, $C_e$ (pCi/L) is the final (equilibrium) concentration of Ra-226 in the liquid phase and $K_F$ and n are Freundlich constants that are used to describe the observed adsorption trends.

**Zeta Potential of Calcite**

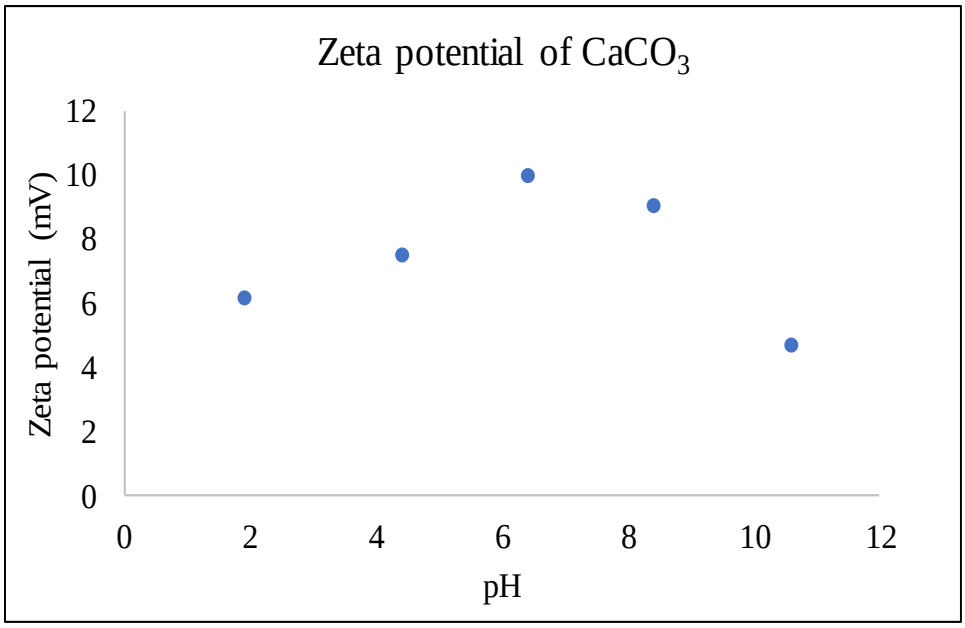


**Figure B.2.** Zeta potential of $CaCO_3$ in DI water as a function of pH.

**SEM Images** of different types of celestite and barite, and particle size distribution of celestite as a function of ionic strength are shown in figures below.

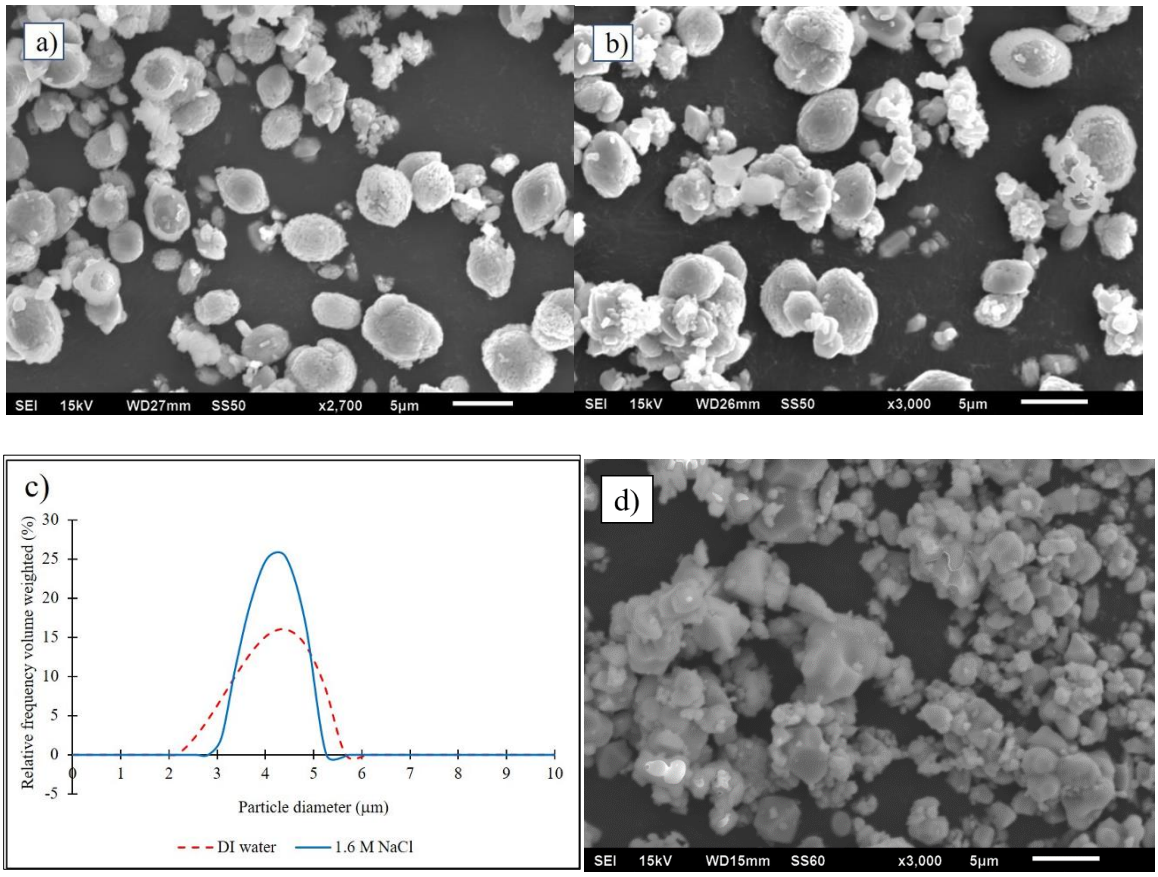


**Figure B.3.** SEM images of a) freshly precipitated and b) commercially available celestite; c) particle size distribution of commercial celestite in DI water and 1.6 M NaCl solution measured using Litesizer 500 (Anton Paar, Ashland, VA); d) commercially available barite.

## Potential Distribution and Surface Charge Calculations

Electrical potential distribution in the EDL can be described using the following equation (Hiemenz, 1986):

$$\tanh(\frac{\psi(x)}{4}) = \tanh(\frac{\psi_0}{4})e^{-Kx} \quad \text{(B6)}$$

where, x (m) is the distance from the particle surface, ψ(x) (V) is the electrical potential at the distance x, $\psi_0$ (V) is the electrical potential at the particle surface and K ($m^{-1}$) is the Debye parameter.

The assumption that the slipping plane (i.e., plane that separates immobile and mobile layers of the EDL and where zeta potential is measured) is close to EDL edge (i.e., EDL thickness or Debye length) simplifies calculations (Ding, 2015; Li, 2003):

$$x \approx K^{-1} \quad \text{(B7)}$$

Equation (B6) can be used to calculate surface potential $\psi_0$ assuming that ψ (x) is the measured zeta potential. Debye length $K^{-1}$ can be calculated using the following equation (Kohonen, 2000):

$$K^{-1} = \left(\frac{\varepsilon kT}{e^2 \sum_i Z_i^2 N_A C_\infty}\right)^{1/2} \quad \text{(B8)}$$

where, ε (F/m) is a water permittivity, k (J/K) is the Boltzmann constant, T (K) is the temperature, z is the charge number, e (C) is the elementary charge, $N_A$ ($mol^{-1}$) is the Avogadro number and $C_\infty$ (mol/L) is concentration of the electrolyte in bulk. Equation B9 can be used to calculate specific surface charge (Chapman, 1913; Gouy, 1910):

$$\sigma = \sqrt{8 N_A C_\infty \varepsilon kT} sinh\left(\frac{ze\psi_0}{2kT}\right) \quad \text{(B9)}$$

**Radium Removal by Celestite in Low and High Ionic Strength Solution**

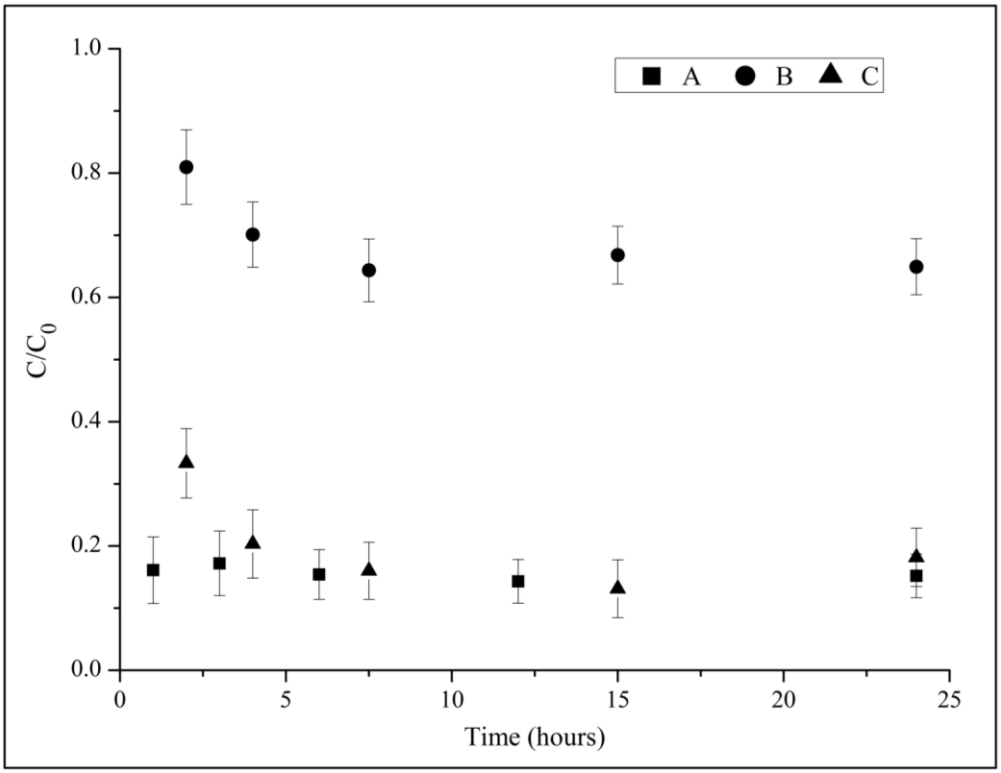


**Figure B.4.** Radium removal by celestite at pH 5.5 in low and high ionic strength solutions at initial Ra-226 activity of 5,000 pCi/L (A: 1,000 mg/L $SrSO_4$ in DI water; B: 1,000 mg/L $SrSO_4$ in 1.6 M NaCl solution; C: 2,000 mg/L of $SrSO_4$ in 1.6 M NaCl solution; experimental standard deviation calculated based on at least 3 replicates is shown using error bars).

**Ra-226 Removal by Sand and Celestite Coated Sand in Celestite Saturated Solution**

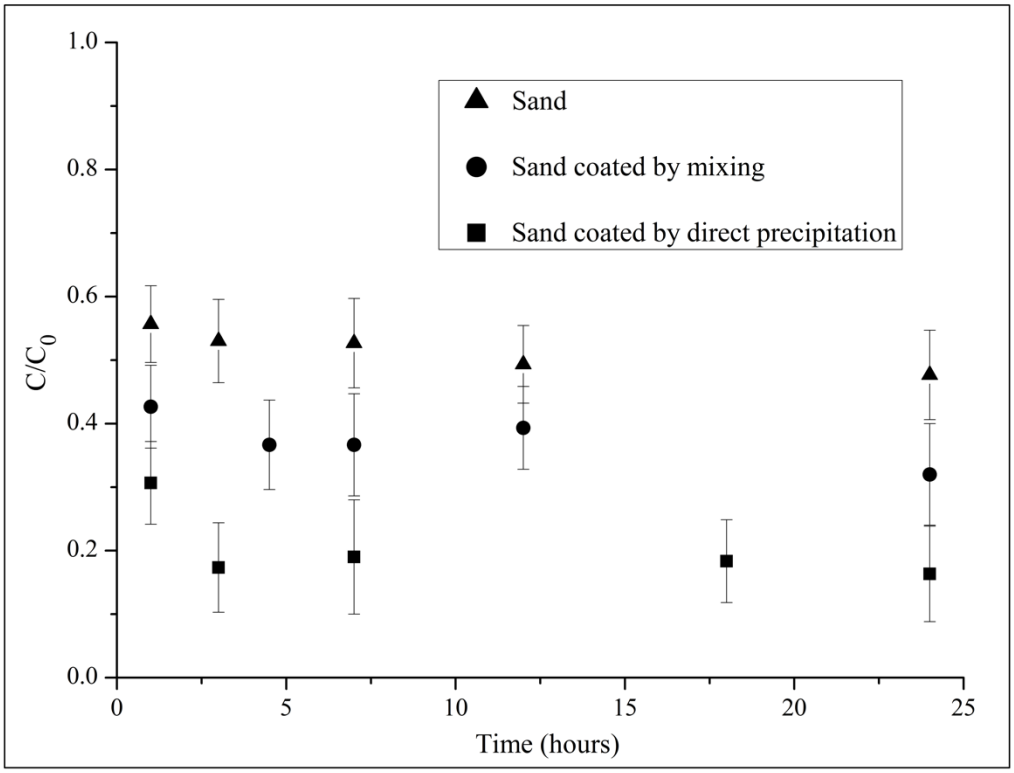


**Figure B.5.** Ra-226 removal by sand and celestite coated sand in celestite saturated solution (120 mg/L) at pH 5.5 with initial Ra-226 concentration of 5,000 pCi/L (error bars indicate experimental standard deviation calculated based on at least 3 replicates).

**SEM Images** of coated proppant after radium removal experiments under different conditions:

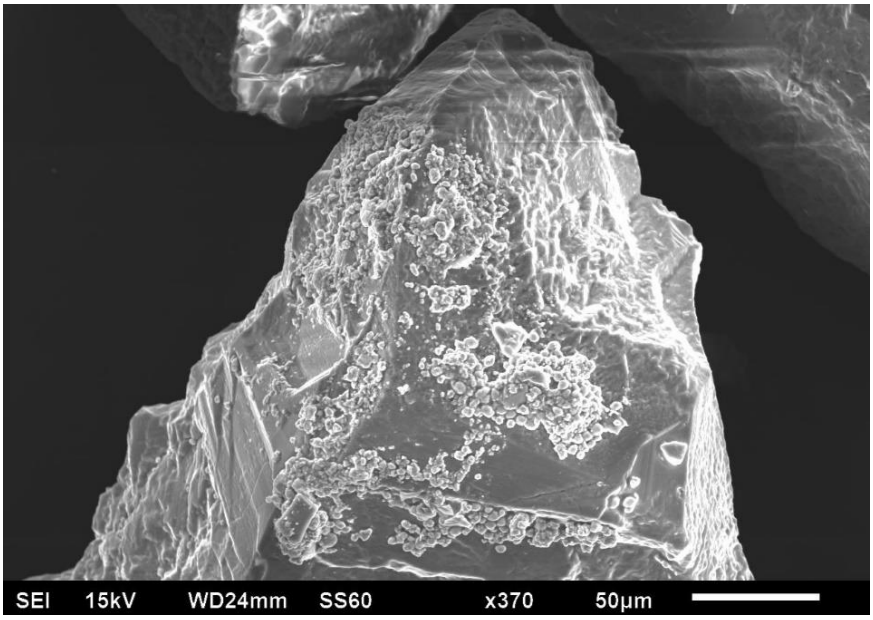


**Figure B.6.** Example of a coated sand particle after 24-hour test of radium removal in the presence of high concentration of divalent cations at 21°C and pH 5.5 with initial Ra-226 concentration of 5,000 pCi/L.

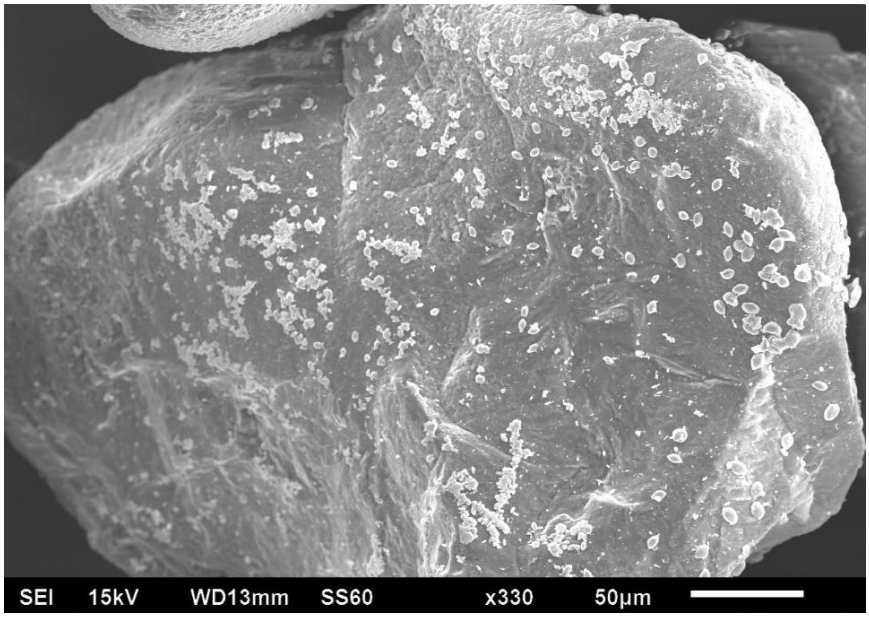


**Figure B.7.** Example of a coated sand particle after 24-hour test of radium removal in the presence of high concentration of divalent cations at 40°C and pH 5.5 with initial Ra-226 concentration of 5,000 pCi/L.

**Real Case Assessment Calculations** were done by making the following assumptions:

- Lifetime of a single well: 20 years
- Produced water flow: 1.5 $m^3$/day = 11 million L of produced water during the lifetime of a single well
- Mass of the fracking proppant for a single well: 2,000 tons = $2*10^{12}$ mg
- Ra-226 concentration in produced water: 2,500 pCi/L
- Celestite coated proppant capacity for Ra-226 uptake: 0.027 pCi/mg at 21 °C and 0.021 pCi/mg at 40 °C

Total radioactivity (from Ra-226) in produced water brought to the surface from a single well:

$$2{,}500\ \frac{\text{pCi}}{\text{L}} * 11 * 10^6\text{L} = 2.75 * 10^{10}\text{pCi}$$

Ra-226 uptake capacity of celestite coated proppant:

- at 21 °C: $2 * 10^{12} mg * 0.027 \frac{pCi}{mg} = 5.4 * 10^{10} pCi$
- at 40 °C: $2 * 10^{12} mg * 0.021 \frac{pCi}{mg} = 4.2 * 10^{10} pCi$

**Impregnation of Quartz Sand With Barite – Experimental Results**

**Table B.1.** Quartz sand impregnation with barite summary

| **Mass of quartz sand (mg)** | **Mass of $BaSO_4$ precipitated (mg)** | **Mass of coated sand (mg)** |
|---|---|---|
| 5,001 | 2,000 | 5,094 |
| 5,000 | 2,000 | 4,979 |
| 4,998 | 2,000 | 5,083 |
| 5,000 | 2,000 | 5,113 |
| 4,999 | 2,000 | 4,996 |

## Appendix C Supporting Information for Chapter 4

**Table C.1a.** Saturation indices and effluent concentrations - Figure 4.1a.

| Initial Ba (mg/L) | $SO_4^{2-}$ (mg/L) | SI | | pH | Component | Effluent (mg/L) | Removal (%) |
|---|---|---|---|---|---|---|---|
| | | $BaSO_4$ | $SrSO_4$ | | | | |
| 488 | 409 | 3.11 | 0.79 | 2 | $Mg^{2+}$ | 1,682 | 14.3 |
| | | | | | $Ca^{2+}$ | 13,944 | 23 |
| | | | | | $Sr^{2+}$ | 3,051 | 19.8 |
| | | | | | $Ba^{2+}$ | 88.78 | 81.8 |
| | | | | | $Ra^{2+}$ (pCi/L) | 687 | 86.2 |
| | | | | | $SO_4^{2-}$ | 86.14 | 79 |
| 488 | 409 | 3.12 | 0.80 | 5.4 | $Mg^{2+}$ | 1,719 | 12.4 |
| | | | | | $Ca^{2+}$ | 14,183 | 21.7 |
| | | | | | $Sr^{2+}$ | 3,110 | 18.3 |
| | | | | | $Ba^{2+}$ | 79.08 | 83.8 |
| | | | | | $Ra^{2+}$ (pCi/L) | 708 | 85.8 |
| | | | | | $SO_4^{2-}$ | 56.34 | 86.2 |
| 488 | 409 | 3.12 | 0.80 | 10 | $Mg^{2+}$ | 1,507 | 23.2 |
| | | | | | $Ca^{2+}$ | 13,492 | 25.5 |
| | | | | | $Sr^{2+}$ | 2,988 | 21.5 |
| | | | | | $Ba^{2+}$ | 80.65 | 83.5 |
| | | | | | $Ra^{2+}$ (pCi/L) | 306 | 93.8 |
| | | | | | $SO_4^{2-}$ | 44.08 | 89.2 |

**Table C.1b.** Saturation indices and effluent concentrations - Figure 4.1b.

| Initial Ba (mg/L) | $SO_4^{2-}$ (mg/L) | SI | | | Component | Effluent (mg/L) | Removal (%) |
|---|---|---|---|---|---|---|---|
| | | $BaSO_4$ | $SrSO_4$ | $CaSO_4$ | | | |
| 488 | 409 (120%) | 3.12 | 0.80 | -0.19 | $Mg^{2+}$ | 1,719 | 12.4 |
| | | | | | $Ca^{2+}$ | 14,183 | 21.7 |
| | | | | | $Sr^{2+}$ | 3,110 | 18.3 |
| | | | | | $Ba^{2+}$ | 79.08 | 83.8 |
| | | | | | $Ra^{2+}$ (pCi/L) | 708 | 85.8 |
| | | | | | $SO_4^{2-}$ | 56.34 | 86.2 |
| 488 | 682 (200%) | 3.35 | 1.02 | 0.03 | $Mg^{2+}$ | 1,691 | 13.8 |
| | | | | | $Ca^{2+}$ | 13,888 | 23.3 |
| | | | | | $Sr^{2+}$ | 3,014 | 20.8 |
| | | | | | $Ba^{2+}$ | 16.54 | 96.6 |
| | | | | | $Ra^{2+}$ (pCi/L) | 394 | 92.1 |
| | | | | | $SO_4^{2-}$ | 180.72 | 73.5 |
| 488 | 1,023 (300%) | 3.53 | 1.19 | 0.21 | $Mg^{2+}$ | 1,663 | 15.2 |
| | | | | | $Ca^{2+}$ | 13,311 | 26.5 |
| | | | | | $Sr^{2+}$ | 2,896 | 23.9 |
| | | | | | $Ba^{2+}$ | 9.62 | 98 |
| | | | | | $Ra^{2+}$ (pCi/L) | 143 | 97.1 |
| | | | | | $SO_4^{2-}$ | 415.61 | 59.4 |
| 488 | 1,705 (500%) | 3.75 | 1.41 | 0.42 | $Mg^{2+}$ | 1,652 | 15.8 |
| | | | | | $Ca^{2+}$ | 13,120 | 27.6 |
| | | | | | $Sr^{2+}$ | 2,660 | 30.1 |
| | | | | | $Ba^{2+}$ | 3.77 | 99.2 |
| | | | | | $Ra^{2+}$ (pCi/L) | 42 | 99.2 |
| | | | | | $SO_4^{2-}$ | 743.13 | 56.4 |

**Table C.2.** Saturation indices and effluent concentrations - Figure 4.2.

| Initial Ba (mg/L) | $SO_4^{2-}$ (mg/L) | SI | | | Component | Effluent (mg/L) | Removal (%) |
|---|---|---|---|---|---|---|---|
| | | $BaSO_4$ | $SrSO_4$ | $CaSO_4$ | | | |
| 488 | 409 | 3.12 | 0.80 | -0.19 | $Mg^{2+}$ | 1,719 | 12.4 |
| | | | | | $Ca^{2+}$ | 14,183 | 21.7 |
| | | | | | $Sr^{2+}$ | 3,110 | 18.3 |
| | | | | | $Ba^{2+}$ | 79.08 | 83.8 |
| | | | | | $Ra^{2+}$ (pCi/L) | 708 | 85.8 |
| | | | | | $SO_4^{2-}$ | 56.34 | 86.2 |
| 1,325 | 1,113 | 4.00 | 1.24 | 0.25 | $Mg^{2+}$ | 1,731 | 11.8 |
| | | | | | $Ca^{2+}$ | 14,289 | 21.1 |
| | | | | | $Sr^{2+}$ | 2,983 | 21.6 |
| | | | | | $Ba^{2+}$ | 58.73 | 95.6 |
| | | | | | $Ra^{2+}$ (pCi/L) | 583 | 88.3 |
| | | | | | $SO_4^{2-}$ | 68.11 | 93.9 |
| 2,710 | 2,275 | 4.64 | 1.55 | 0.56 | $Mg^{2+}$ | 1,731 | 11.8 |
| | | | | | $Ca^{2+}$ | 14,674 | 19 |
| | | | | | $Sr^{2+}$ | 2,910 | 23.5 |
| | | | | | $Ba^{2+}$ | 25.63 | 99.1 |
| | | | | | $Ra^{2+}$ (pCi/L) | 356 | 92.8 |
| | | | | | $SO_4^{2-}$ | 108.14 | 95.2 |
| 5,425 | 4,553 | 5.27 | 1.85 | 0.87 | $Mg^{2+}$ | 1,741 | 11.3 |
| | | | | | $Ca^{2+}$ | 14,698 | 18.9 |
| | | | | | $Sr^{2+}$ | 2,774 | 27.1 |
| | | | | | $Ba^{2+}$ | 8.91 | 99.8 |
| | | | | | $Ra^{2+}$ (pCi/L) | 80 | 98.4 |
| | | | | | $SO_4^{2-}$ | 125.53 | 97.2 |

**Table C.3.** Synthetic PW with varying $Sr^{2+}$, $Ba^{2+}$ and $SO_4^{2-}$ concentration - Figure 4.3.

| | Saturation index of $BaSO_4$ | | |
|---|---|---|---|
| **Component** | ***SI = 3.1*** | ***SI = 3.9*** | ***SI = 4.5*** |
| $Na^+$ (mmol/L) | 1,762 | 1,762 | 1,762 |
| $K^+$ (mmol/L) | 27.14 | 27.14 | 27.14 |
| $Mg^{2+}$ (mmol/L) | 80.71 | 80.71 | 80.71 |
| $Ca^{2+}$ (mmol/L) | 451.05 | 451.05 | 451.05 |
| $Sr^{2+}$ (mmol/L) | 3.55 – 73.48 | 9.20 – 190.44 | 18.41 – 381.09 |
| $Ba^{2+}$ (mmol/L) | 3.55 | 9.20 | 18.41 |
| $Cl^-$ (mmol/L) | 2,867 – 3,007 | 2,889 – 3,252 | 2,926 – 3,652 |
| $SO_4^{2-}$ (mmol/L) | 4.26 | 11.04 | 22.09 |

**Table C.4.** PhreeQC calculations of saturation indices for $BaSO_4$ and $SrSO_4$ in different synthetic water compositions.

| $SI_{BaSO4}$ | Sr/Ba | $SI_{SrSO4}$ | $SI_{BaSO4}/SI_{SrSO4}$ |
|---|---|---|---|
| 3.14 | 1 | -0.28 | - |
| 3.14 | 2 | 0.02 | 157.00 |
| 3.13 | 3.8 | 0.30 | 10.43 |
| 3.13 | 8 | 0.62 | 5.05 |
| 3.12 | 12.2 | 0.80 | 3.90 |
| 3.12 | 16.5 | 0.93 | 3.35 |
| 3.11 | 20.7 | 1.02 | 3.05 |
| 3.97 | 1 | 0.55 | 7.22 |
| 3.97 | 2 | 0.85 | 4.67 |
| 3.96 | 3.8 | 1.12 | 3.54 |
| 3.95 | 8 | 1.44 | 2.74 |
| 3.94 | 12.2 | 1.61 | 2.45 |
| 3.92 | 16.5 | 1.73 | 2.26 |
| 3.91 | 20.7 | 1.82 | 2.15 |
| 4.58 | 1 | 1.15 | 3.98 |
| 4.58 | 2 | 1.45 | 3.16 |
| 4.57 | 3.8 | 1.72 | 2.66 |
| 4.54 | 8 | 2.02 | 2.25 |
| 4.51 | 12.2 | 2.19 | 2.06 |
| 4.48 | 16.5 | 2.30 | 1.95 |
| 4.45 | 20.7 | 2.39 | 1.86 |

**Table C.5a.** Effluent concentrations - Figure 4.6a.

| Barite addition (g/L) | $SO_4^{2-}$ (mg/L) | Component | Effluent (mg/L) | Effluent (mmol/L) | Removal (mmol/L) | Removal (%) |
|---|---|---|---|---|---|---|
| 0 | 409 | $Mg^{2+}$ | 1,719 | 70.73 | 10.00 | 12.4 |
| | | $Ca^{2+}$ | 14,183 | 353.87 | 98.08 | 21.7 |
| | | $Sr^{2+}$ | 3,110 | 35.49 | 7.95 | 18.3 |
| | | $Ba^{2+}$ | 79.08 | 0.58 | 2.97 | 83.8 |
| | | $Ra^{2+}$ (pCi/L) | 708 | - | - | 85.8 |
| | | $SO_4^{2-}$ | 56.34 | 0.59 | 3.67 | 86.2 |
| 5 | 409 | $Mg^{2+}$ | 1,758 | 72.33 | 8.40 | 10.4 |
| | | $Ca^{2+}$ | 14,788 | 368.96 | 82.99 | 18.2 |
| | | $Sr^{2+}$ | 3,247 | 37.06 | 6.38 | 14.7 |
| | | $Ba^{2+}$ | 72.27 | 0.53 | 3.02 | 85.2 |
| | | $Ra^{2+}$ (pCi/L) | 545 | - | - | 89 |
| | | $SO_4^{2-}$ | 43.76 | 0.46 | 3.80 | 89.3 |
| 10 | 409 | $Mg^{2+}$ | 1,772 | 72.91 | 7.82 | 9.7 |
| | | $Ca^{2+}$ | 14,799 | 369.24 | 82.71 | 18.3 |
| | | $Sr^{2+}$ | 3,296 | 37.62 | 5.82 | 13.4 |
| | | $Ba^{2+}$ | 59.44 | 0.43 | 3.12 | 87.8 |
| | | $Ra^{2+}$ (pCi/L) | 488 | - | - | 90.2 |
| | | $SO_4^{2-}$ | 42.53 | 0.44 | 3.82 | 89.6 |
| 25 | 409 | $Mg^{2+}$ | 1,815 | 74.68 | 6.05 | 7.5 |
| | | $Ca^{2+}$ | 15,050 | 375.50 | 76.45 | 16.9 |
| | | $Sr^{2+}$ | 3,322 | 37.91 | 5.53 | 12.7 |
| | | $Ba^{2+}$ | 48.49 | 0.35 | 3.20 | 90.1 |
| | | $Ra^{2+}$ (pCi/L) | 344 | - | - | 93.1 |
| | | $SO_4^{2-}$ | 40.43 | 0.42 | 3.84 | 90.1 |
| 50 | 409 | $Mg^{2+}$ | 1,773 | 72.95 | 7.78 | 9.7 |
| | | $Ca^{2+}$ | 14,694 | 366.62 | 85.33 | 18.9 |
| | | $Sr^{2+}$ | 3,289 | 37.54 | 5.90 | 13.6 |
| | | $Ba^{2+}$ | 47.23 | 0.34 | 3.21 | 90.3 |
| | | $Ra^{2+}$ (pCi/L) | 162 | - | - | 96.7 |
| | | $SO_4^{2-}$ | 35.03 | 0.36 | 3.90 | 91.4 |

**Table C.5b.** Effluent concentrations - Figure 4.6b.

| Phase | Barite addition (g/L) | $SO_4^{2-}$ (mg/L) | Component | Eff. (mg/L) | Rem. (%) | Solids formation (ton/$10^6$ gallons) | Sludge* radioactivity (pCi/g) |
|---|---|---|---|---|---|---|---|
| Initial | 25 (fresh) | 409 | $Mg^{2+}$ | 1,815 | 7.5 | 19.8 | 153 |
| | | | $Ca^{2+}$ | 15,050 | 16.9 | | |
| | | | $Sr^{2+}$ | 3,322 | 12.7 | | |
| | | | $Ba^{2+}$ | 48.49 | 90.1 | | |
| | | | $Ra^{2+}$ (pCi/L) | 344 | 93.1 | | |
| | | | $SO_4^{2-}$ | 40.43 | 90.1 | | |
| Recycle 1 | 25 (recycled) | 409 | $Mg^{2+}$ | 1,805 | 8 | 20.7 | 271 |
| | | | $Ca^{2+}$ | 14,983 | 17.3 | | |
| | | | $Sr^{2+}$ | 3,349 | 12 | | |
| | | | $Ba^{2+}$ | 43 | 91.2 | | |
| | | | $Ra^{2+}$ (pCi/L) | 520 | 89.5 | | |
| | | | $SO_4^{2-}$ | 39.22 | 90.4 | | |
| Recycle 2 | 25 (recycled) | 409 | $Mg^{2+}$ | 1,888 | 3.8 | 20.6 | 367 |
| | | | $Ca^{2+}$ | 15,676 | 13.5 | | |
| | | | $Sr^{2+}$ | 3,503 | 8 | | |
| | | | $Ba^{2+}$ | 44.38 | 90.9 | | |
| | | | $Ra^{2+}$ (pCi/L) | 583 | 88.3 | | |
| | | | $SO_4^{2-}$ | 43.10 | 89.5 | | |

* Sludge is assumed to be the sum of added barite and formed solids

**Table C.6.** Effluent concentrations - Figure 4.7

| Sample ID | Initial Ba (mg/L) | $SO_4^{2-}$ (mg/L) | Sr/Ba | Component | Effluent (mg/L) | Removal (%) | Solids Formation (ton/$10^6$ gallons) | Sludge Radioactivity (pCi/g) |
|---|---|---|---|---|---|---|---|---|
| O1 | 1,325 | 1,113 | 4.5 | $Mg^{2+}$ | 1,699 | 13.4 | 25.2 | 154 |
| | | | | $Ca^{2+}$ | 16,290 | 11 | | |
| | | | | $Sr^{2+}$ | 3,254 | 14.5 | | |
| | | | | $Ba^{2+}$ | 45.05 | 96.6 | | |
| | | | | $Ra^{2+}$ (pCi/L) | 75 | 98.5 | | |
| | | | | $SO_4^{2-}$ | 16.70 | 98.5 | | |
| O2 | 1,704 | 1,430 | 3.5 | $Mg^{2+}$ | 1,726 | 12 | 26.3 | 155 |
| | | | | $Ca^{2+}$ | 16,306 | 9.8 | | |
| | | | | $Sr^{2+}$ | 3,171 | 16.7 | | |
| | | | | $Ba^{2+}$ | 37.49 | 97.8 | | |
| | | | | $Ra^{2+}$ (pCi/L) | 14 | 99.7 | | |
| | | | | $SO_4^{2-}$ | 22.88 | 98.4 | | |
| O3 | 2,983 | 2,504 | 2 | $Mg^{2+}$ | 1,707 | 13 | 31.8 | 148 |
| | | | | $Ca^{2+}$ | 15,909 | 12 | | |
| | | | | $Sr^{2+}$ | 3,172 | 16.6 | | |
| | | | | $Ba^{2+}$ | 8.94 | 99.7 | | |
| | | | | $Ra^{2+}$ (pCi/L) | 20 | 99.6 | | |
| | | | | $SO_4^{2-}$ | 50.08 | 98 | | |
| O4 | 3,977 | 3,338 | 1.5 | $Mg^{2+}$ | 1,744 | 11.1 | 44.4 | 135 |
| | | | | $Ca^{2+}$ | 16,035 | 11.3 | | |
| | | | | $Sr^{2+}$ | 3,129 | 17.8 | | |
| | | | | $Ba^{2+}$ | 7.95 | 99.8 | | |
| | | | | $Ra^{2+}$ (pCi/L) | 5 | 99.9 | | |
| | | | | $SO_4^{2-}$ | 93.46 | 97.2 | | |

## Bibliography


Akovali, Y.A., 1996. Nuclear Data Sheets for A= 226. Nuclear data sheets 77, (2), 433-470.

Akyon, B. (2017). Biological Treatment of Hydraulic Fracturing Produced Water, University of Pittsburgh.

Ali, I., Schneider, P., 2005. Crystallization of struvite from metastable region with different types of seed crystal. Journal of Non-Equilibrium Thermodynamics 30 (2), 95-111.

ALLConsulting, 2009. Modern Shale Gas Development in the United States: A Primer. Ground water protection council.

Alroudhan, A., Vinogradov, J., Jackson, M. D., 2016. Zeta potential of intact natural limestone: Impact of potential-determining ions Ca, Mg and SO4. Colloids and Surfaces A: Physicochemical and Engineering Aspects 493, (Supplement C), 83-98.

Artna-Cohen, A., 1997. Nuclear Data Sheets for A= 228. Nuclear data sheets 80, (3), 723-786.

Averyt, K.B., Paytan, A., 2003. Empirical partition coefficients for Sr and Ca in marine barite: Implications for reconstructing seawater Sr and Ca concentrations. Geochemistry, Geophysics, Geosystems 4, (5),

Bajpai, S., Chaudhuri, M., 1999. Removal of Arsenic from Ground Water by Manganese Dioxide-Coated Sand. Journal of Environmental Engineering 125, (8), 782.

Barbot, E., Vidic, N.S., Gregory, K.B., and Vidic, R.D., 2013. Spatial and Temporal Correlation of Water Quality Parameters of Produced Waters from Devonian-Age Shale following Hydraulic Fracturing. Envrionmental Science & Technology 47, 2562-2569.

Bi, Y., Zhang, H., Ellis, B. R., Hayes, K. F., 2016. Removal of radium from synthetic shale gas brines by ion exchange resin. Environmental Engineering Science 33, (10), 791-798.

Blackburn, R., Al-Masri, M. S., 1992. Determination of Radium-226 in Aqueous Samples Using Liquid Scintillation Counting. Analyst 117, 1949-1951.

Bokern, D.G., Hunter, K. A., McGrath, K. M., 2003. Charged barite− aqueous solution interface: Surface potential and atomically resolved visualization. Langmuir 19, (24), 10019-10027.

Boon, M., Jones, F., 2016. Barium Sulfate Crystallization from Synthetic Seawater. Crystal Growth & Design 16, (8), 4646-4657.

Bosbach, D.B., M., Metz, V., 2010. Experimental study on Ra2+ uptake by barite (BaSO4). Kinetics of solid solution formation via BaSO4 dissolution and RaxBa1-xSO4 (re) precipitation. Swedish Nuclear Fuel and Waste Management Co.

Bracco, J.N., Lee, S. S., Stubbs, J. E., Eng, P. J., Jindra, S., Warren, D. M., Kommu, A., Fenter, P., Kubicki, J. D., Stack, A. G., 2018. Simultaneous Adsorption and Incorporation of Sr2+ at the Barite (001)–Water Interface. The Journal of Physical Chemistry C 123, (2), 1194-1207.

Brandt, F., Curti, E., Klinkenberg, M., Rozov, K., Bosbach, D., 2015. Replacement of barite by a (Ba,Ra)SO4 solid solution at close-to-equilibrium conditions: A combined experimental and theoretical study. Geochimica et Cosmochimica Acta 155, 1-15.

Brandt, F., Klinkenberg, M., Poonoosamy, J., Weber, J., Bosbach, D., 2018. The Effect of Ionic Strength and Sraq upon the Uptake of Ra during the Recrystallization of Barite. Minerals 8, (11), 502.

Brown, M.A., Abbas, Z., Kleibert, A., Green, R. G., Goel, A., May, S., Squires, T. M., 2016a. Determination of surface potential and electrical double-layer structure at the aqueous electrolyte-nanoparticle interface. Physical Review X 6, (1), 011007.

Brown, M.A., Goel, A., Abbas, Z., 2016b. Effect of electrolyte concentration on the stern layer thickness at a charged interface. Angewandte Chemie International Edition 55, (11), 3790-3794.

Burnham, A., Han, J., Clark, C., Wang, M., Dunn, J., Palou-Rivera, I., 2011. Life-cycle greenhouse gas emissions of shale gas, natural gas, coal, and petroleum. Environmental science & technology 46, (2), 619-627.

Butkovskyi, A., Bruning, H., Kools, S. A. E., Rijnaarts, H. H. M., Van Wezel, A. P., 2017. Organic pollutants in shale gas flowback and produced waters: identification, potential ecological impact, and implications for treatment strategies. Environmental science & technology 51, (9), 4740-4754.

Case, D.A., Ben-Shalom, I. Y., Brozell, S. R., Cerutti, D. S., Cheatham, T. E. III., Cruzeiro, V. W. D., Darden, T. A., Duke, R. E., Ghoreishi, D., Gilson, M. K., 2018. AMBER 2018. University of California, San Francisco

Chapman, D.L., 1913. LI. A contribution to the theory of electrocapillarity. The London, Edinburgh, and Dublin philosophical magazine and journal of science 25, (148), 475-481.

Chapman, E.C., Capo, R.C., Stewart, B.W., Kirby, C.S., Hammack, R.W., Schroeder, K.T., Edenborn, H.M.J.E.s. and technology, 2012. Geochemical and strontium isotope characterization of produced waters from Marcellus Shale natural gas extraction. 46, (6), 3545-3553.

Chen, H., Carter, K. E., 2017. Characterization of the chemicals used in hydraulic fracturing fluids for wells located in the Marcellus Shale Play. Journal of environmental management 200, 312-324.

Chorom, M., Rengasamy, P., 1995. Dispersion and zeta potential of pure clays as related to net particle charge under varying pH, electrolyte concentration and cation type. European Journal of Soil Science 46, (4), 657-665.

Clark, C.E., Veil, J. A., 2009. Produced water volumes and management practices in the United States. Argonne National Lab.(ANL), Argonne, IL (United States).

Clifford, D.A., Cothern, C.R. and Rebers, P.A. (ed), 1990. Radon, Radium and Uranium in Drinking Water. Removal of radium from drinking water. United States: Lewis Publisher, Inc.

Collins, A.G., Davis, J. W., 1971. Solubility of barium and strontium sulfates in strong electrolyte solutions. Environmental science & technology 5, (10), 1039-1043.

Curti, E., Fujiwara, K., Iijima, K., Tits, J., Cuesta, C., Kitamura, A., Glaus, M.A., Muller, W., 2010. Radium uptake during barite recrystallization at 23 ± 2 C as a function of solution composition: An experimental $^{133}$Ba and $^{226}$Ra tracer study. Geochimica et Cosmochimica Acta 74, 3553-3570.

Dąbrowski, A., 2001. Adsorption—from theory to practice. Advances in colloid and interface science 93, (1-3), 135-224.

Ding, W., Liu, X., Song, L., Li, Q., Zhu, Q., Zhu, H., Hu, F., Luo, Y., Zhu, L., Li, H., 2015. An approach to estimate the position of the shear plane for colloidal particles in an electrophoresis experiment. Surface Science 632, 50-59.

Doerner, H.A., Hoskins, W. M., 1925. Co-precipitation of radium and barium sulfates. Journal of the American Chemical Society 47, 662-675.

Dong, X., Trembly, J., Bayless, D., 2017. Techno-economic analysis of hydraulic fracking flowback and produced water treatment in supercritical water reactor. Energy 133, 777-783.

Duzyol, S., Ozkan, A., 2014. Effect of Contact Angle, Surface Tension and Zeta Potential on Oil Agglomeration of Celestite. Minerals Engineering 65, 74-78.

Ellis, D.V., Singer, J. M., 2007. Well logging for earth scientists. Springer 692,

Ellsworth, W.L., 2013. Injection-induced earthquakes. Science 341, (6142), 1225942.

Erkey, C. (2011) Supercritical fluids and organometallic compounds: from recovery of trace metals to synthesis of nanostructured materials. Elsevier.

Fakhru'l-Razi, A., Pendashteh, A., Abdullah, L. C., Biak, D. R. A., Madaeni, S. S., Abidin, Zurina Z., 2009. Review of technologies for oil and gas produced water treatment. Journal of Hazardous Materials 170, (2-3), 530-551.

Fan, C., Kan, A. T., Zhang, P., Tomson, M. B., 2011. Barite Nucleation and Inhibition at 0 to 200* C With and Without Thermodynamic Hydrate Inhibitors. SPE Journal 16, (02), 440-450.

Fan, W., Liberati, B., Novak, M., Cooper, M., Kruse, N., Young, D., Trembly, J,, 2016. Radium-226 Removal from Simulated Produced Water Using Natural Zeolite and Ion-Exchange Resin. Industrial & Engineering Chemistry Research 55, (48), 12502-12505.

Fractracker, 2019. Pannsylvania Shale Viewer. https://www.fractracker.org/map/us/pennsylvania/pa-shale-viewer/

Freundlich, H.J.Z.P.C., 1906. Adsorption in solids. 57, 385-470.

Fröhner, K.R., Panahandeh, H., 1975. An advanced seeding process in saline water conversion. Desalination 16, (3), 261-269.

Ganguly, J., Saxena, S. K. (2012) Mixtures and mineral reactions. Springer Science & Business Media.

Germann, F.E.E., 1921. Adsorption of radium by barium sulfate. J. Am. Chem. Soc. 7, (43), 1615-1621.

Gnanapragasam, E.K., Lewis, B. G., 1995. Elastic strain energy and the distribution coefficient of radium in solid solutions with calcium salts. Geochimica et Cosmochimica Acta 59, (24), 5103-5111.

Gomez Escobar, V., Vera Tome, F., Lozano, J. C., Martin Sanchez, A., 1996. Determination of 222Rn and 226Ra in Aqueous Samples Using a Low-level Liquid Scintillation Counter. Applied Radiation and Isotopes 47, 861-867.

Gonzalez-Caballero, F., Chibowski, E., Hołysz, L., Cabrerizo, M. A., Bruque, J. M., 1989. Adsorption—desorption in celestite (SrSO4) flotation with a cationic-type collector. Colloids and surfaces 35, (1), 65-75.

Gouy, M., 1910. Sur la constitution de la charge électrique à la surface d'un électrolyte. J. Phys. Theor. Appl. 9, (1), 457-468.

Goyal, S., Raghuraman, A., Aou, K., Aguirre-Vargas, F., Medina, J. C., Tan, R., Hickman, D., 2017. Smart Proppants With Multiple Down Hole Functionalities, SPE Hydraulic Fracturing Technology Conference and Exhibition, Society of Petroleum Engineers.

Gregory, K.B., Vidic, R.D., and Dzombak, D.A., 2011. Water Management Challenges Associated with the Production of Shale Gas by Hydraulic Fracturing. Elements 7, 181-186.

Gusa, A.V., Vidic, R. D., 2018. Development of Functionalized Proppant for the Control of NORM in Marcellus Shale Produced Water. Environmental science & technology 53, (1), 373-382.

Halliburton, 2009. The Marcellus Shale - Gas/Electric Partnership, http://www.gaselectricpartnership.com/BBHalliburton%20Marcellus.pdf.

Han, R., Lu, Z., Zou, W., Daotong, W., Shi, J., Jiujun, Y., 2006a. Removal of copper(II) and lead(II) from aqueous solution by manganese oxide coated sand I. Characterization and kinetic study. Journal of Hazardous Materials B137, 384-395.

Han, R., Lu, Z., Zou, W., Daotong, W., Shi, J., Jiujun, Y., 2006b. Removal of copper(II) and lead(II) from aqueous solution by manganese oxide coated sand: II. Equilibrium study and competitive adsorption. Journal of Hazardous Materials 137, (1), 480-488.

Harvey, D., 2000. Modern Analytical Chemistry. McGraw-Hill: New York.

Hayes, T., 2009. Marcellus Shale water chemistry. POGAM Annual Conference

Haynes, W.M. (2014) CRC handbook of chemistry and physics. CRC press.

He, C., Li, M., Liu, W., Barbot, E., Vidic, R. D., 2014. Kinetics and equilibrium of barium and strontium sulfate formation in Marcellus Shale flowback water. Journal of Environmental Engineering 140, (5), B4014001.

He, C., Zhang, T., Vidic, R. D., 2016. Co-treatment of abandoned mine drainage and Marcellus Shale flowback water for use in hydraulic fracturing. Water research 104, 425-431.

He, S., Oddo, J. E., Tomson, M. B., 1995. The nucleation kinetics of barium sulfate in NaCl solutions up to 6 m and 90 C. Journal of Colloid and Interface Science 174, (2), 319-326.

Heaney, P.J., Prewitt, C. T., Gibbs, G. V., 1994. Silica Physical behavior, geochemistry and materials applications. Reviews in Mineralogy, Mineralogical Society of America 29, 1-606.

Herbowski, L., Gurgul, H., Staron, W., 2009. Experimental determination of the Stern layer thickness at the interface of the human arachnoid membrane and the cerebrospinal fluid. Zeitschrift für Medizinische Physik 19, (3), 189-192.

Hiemenz, P.C., 1986. Principles of colloid and surface chemistry. 188, 1-672.

Hill, R.J., 1977. A further refinement of the barite structure. The Canadian Mineralogist 15, (4), 522-526.

Ho, T.A., Greathouse, J. A., Lee, A. S., Criscenti, L. J., 2018. Enhanced Ion Adsorption on Mineral Nanoparticles. Langmuir 34, (20), 5926-5934.

Holditch, S., Perry, K. and Lee, K., 2007. Unconventional Gas Reservoirs - Tight Gas, Coal Seams, and Shales, Working Document of the National Petroleum Council on Global Oil and Gas Study.

Hunter, R.J. (2013) Zeta potential in colloid science: principles and applications. Academic press.

Iler, R.K., 1979. The Chemistry of Silica. Wiley-Interscience, 1-896.

Jackson, R.B., Lowry, E. R., Pickle, A., Kang, M., DiGiulio, D., Zhao, K., 2015. The depths of hydraulic fracturing and accompanying water use across the United States. Environmental science & technology 49, (15), 8969-8976.

Jackson, R.B., Vengosh, A., Carey, J. W., Davies, R. J., Darrah, T. H., O'sullivan, F., Pétron, G., 2014. The Environmental Costs and Benefits of Fracking. Annual Review of Environment and Resources 39, 327-362.

Jiang, M., Hendrickson, C. T., VanBriesen, J. M., 2014. Life cycle water consumption and wastewater generation impacts of a Marcellus shale gas well. Environmental science & technology 48, (3), 1911-1920.

Johnson, P.R., 1999. A Comparison of Streaming and Microelectrophoresis Methods for Obtaining the Zeta Potential of Granular Porous Media Surfaces. Journal of Colloid and Interface Science 209, 264-267.

Johnston, A., Martin, P., 1997. Rapid Analysis of $^{226}$Ra in waters by $\gamma$ - Ray Spectrometry Applied Radiation and Isotopes 48, (5), 631-638.

Jones, F., Oliviera, A., Parkinson, G. M.,Rohl, A. L., Stanley, A., Upson, T., 2004. The effect of calcium ions on the precipitation of barium sulphate 1: calcium ions in the absence of organic additives. Journal of Crystal Growth 262, (1-4), 572-580.

Jones, M.J., Butchins, L. J., Charnock, J. M., Pattrick, R. A. D., Small, J. S., Vaughan, D. J., Wincott, P. L., Livens, F. R., 2011. Reactions of radium and barium with the surfaces of carbonate minerals. Applied Geochemistry 26, (7), 1231-1238.

Joshi, A., Chaudhuri, M., 1996. Removal of Arsenic from Ground Water by Iron Oxide-Coated Sand. Journal of Environmental Engineering 122, (8), 769-771.

Kargbo, D.M., Wilhelm, R.G., Cambell, D.J., 2010. Natural Gas Plays in the Marcellus Shale: Challenges and Potential Opportunities. Environmental science & technology 44, 5679-5684.

Kästner, J., Carr, J. M., Keal, T. W., Thiel, W., Wander, A., Sherwood, P., 2009. DL-FIND: an open-source geometry optimizer for atomistic simulations. The Journal of Physical Chemistry A 113, (43), 11856-11865.

Katsoyiannis, I.A., Zouboulis, A. I. , 2002. Removal of arsenic from contaminated water sources by sorption onto iron-oxide-coated polymeric materials. Water research 36, 5141-5155.

Katz, L.E., Criscenti, L. J., Chen, C., Larentzos, J. P., Liljestrand, H. M., 2013. Temperature effects on alkaline earth metal ions adsorption on gibbsite: Approaches from macroscopic sorption experiments and molecular dynamics simulations. Journal of colloid interface science 399, 68-76.

Kelland, M.A., 2011. Effect of various cations on the formation of calcium carbonate and barium sulfate scale with and without scale inhibitors. Industrial Engineering Chemistry Research 50, (9), 5852-5861.

Kim, S., Omur-Ozbek, P., Dhanasekar, A., Prior, A., Carlson, K., 2016. Temporal analysis of flowback and produced water composition from shale oil and gas operations: Impact of frac fluid characteristics. Journal of Petroleum Science and Engineering 147, 202-210.

Kinnlburgh, D.G., 1986. General Purpose Adsorption Isotherms. Environmental science & technology 20, 895-904.

Klinkenberg, M., Brandt, F., Breuer, U., and Bosbach, D., 2014. Uptake of Ra during the Recrystallization of Barite: A Microscopicand Time of Flight-Secondary Ion Mass Spectrometry Study. Environmental science & technology 48, (12), 6620-6627.

Klinkenberg, M., Weber, J., Barthel, J., Vinograd, V., Poonoosamy, J., Kruth, M., Bosbach, D., Brandt, F., 2018. The solid solution–aqueous solution system (Sr, Ba, Ra) SO4+ H2O: A combined experimental and theoretical study of phase equilibria at Sr-rich compositions. Chemical Geology 497, 1-17.

Kohonen, M.M., Karaman, M. E., Pashley, R. M., 2000. Debye Length in Multivalent Electrolyte Solutions. Langmuir 16, (13), 5749-5753.

Kügler, R.T., Beißert, K., Kind, M., 2016. On heterogeneous nucleation during the precipitation of barium sulfate. Chemical Engineering Research and Design 114, 30-38.

Lancia, A., Musmarra, D., Prisciandaro, M., 1999. Measuring induction period for calcium sulfate dihydrate precipitation. AIChE Journal 45, (2), 390-397.

Langmuir, D., Riese, A. C., 1985. The thermodynamic properties of radium. Geochimica et Cosmochimica Acta 49, (7), 1593-1601.

Li, H., Wei, S., Qing, C., Yang, J., 2003. Discussion on the position of the shear plane. Journal of colloid interface science 258, (1), 40-44.

Li, Z., Shi, B., Su, Y., Wang, D. (2013) Effect of particle size on adsorption kinetics of phenanthrene in water by powered activated carbon. Huanjing Kexue Xuebao / Acta Scientiae Circumstantiae.

Liang, F., Sayed, M., Al-Muntasheri, G. A., Chang, F. F., Li, L., 2016. A comprehensive review on proppant technologies. Petroleum 2, (1), 26-39.

Litton, G.M., Olson, T. M., 1993. Colloid deposition rates on silica bed media and artifacts related to collector surface preparation methods. Environmental science & technology 27, (1), 185-193.

Lokare, O.R., Tavakkoli, S., Wadekar, S., Khanna, V., Vidic, R. D., 2017. Fouling in direct contact membrane distillation of produced water from unconventional gas extraction. Journal of Membrane Science 524, 493-501.

Lopez-Valdivieso, A., Robledo-Cabrera, A., Uribe-Salas, A., 2000. Flotation of celestite with the anionic collector sodium dodecyl sulfate. Effect of carbonate ions. International Journal of Mineral Processing 60, 79-90.

Lorne, B., Perrier, F., Avouac, J., 1999. Streaming potential measurements 1. Properties of the electrical double layer from crushed rock samples. Journal of geophysical research 104, 17,857-817,877.

Malone, M.J., Baker, P. A., Burns, S. J., 1996. Recrystallization of dolomite: An experimental study from 50-200 °C. Geochimica et Cosmochimica Acta 60, (12), 2189-2207.

Martinez-Luevanos, A., Uribe-Salas, A., Lopez-Valdivieso, A., 1999. Mechanism of adsorption of sodium dodecylsulfonate on celestite and calcite. Minerals Engineering 12, 919-936.

Martinez, A., Uribe-Salas, A., 1995. Interfacial properties of celestite and strontianite in aqueous solutions. Minerals Engineering 8, 1009-1022.

McCurdy, R., 2011. Underground Injection Wells For Produced Water Disposal. In Proceedings of the Technical Workshops for the Hydraulic Fracturing Study: Water Resources Management. U.S. EPA.

McDaniel, R.R., McCrary, A. L., 2014. Dual function proppants. Google Patents. https://patents.google.com/patent/US8763700B2/en

McGarr, A., Bekins, B., Burkardt, N., Dewey, J., Earle, P., Ellsworth, W., Ge, S., Hickman, S., Holland, A., Majer, E., 2015. Coping with earthquakes induced by fluid injection. Science 347, (6224), 830-831.

Mercer, K.L., Lin, Y., Singer, P. C., 2005. Enhancing calcium carbonate precipitation by heterogeneous nucleation during chemical softening. Journal-American Water Works Association 97, (12), 116-125.

Momma, K., Izumi, F., 2008. VESTA: a three-dimensional visualization system for electronic and structural analysis. Journal of Applied Crystallography 41, (3), 653-658.

Monnin, C.J.C.G., 1999. A thermodynamic model for the solubility of barite and celestite in electrolyte solutions and seawater to 200 C and to 1 kbar. 153, (1-4), 187-209.

Mor, S., Ravindra, K., Bishnoi, N. R., 2007. Adsorption of chromium from aqueous solution by activated alumina and activated charcoal. Bioresource Technology 98, (4), 954-957.

Mott, H.V., Singh, S., Kondapally, V. R., 1993. Factors Affecting Radium Removal Using Mixed Iron—Manganese Oxides. Journal-American Water Works Association 85, (10), 114-121.

Nasiri, M., Jafari, I., Parniankhoy, B., 2017. Oil and gas produced water management: A review of treatment technologies, challenges, and opportunities. Chemical Engineering Communications 204, (8), 990-1005.

Ng, C., Losso, J. N., Marshall, W. E., Rao, R. M., 2002. Freundlich adsorption isotherms of agricultural by-product-based powdered activated carbons in a geosmin–water system. Bioresource Technology 85, (2), 131-135.

Nicot, J., Scanlon, B. R., 2012. Water use for shale-gas production in Texas, US. Environmental science & technology 46, (6), 3580-3586.

Oetjen, K., Chan, K. E., Gulmark, K., Christensen, J. H., Blotevogel, J., Borch, T., Spear, J. R., Cath, T. Y., Higgins, C. P., 2018. Temporal characterization and statistical analysis of flowback and produced waters and their potential for reuse. Science of the Total Environment 619, 654-664.

Ouyang, B., Renock, D. J., Ajemigbitse, M. A., Van Sice, K., Warner, N. R., Landis, J. D., Feng, X., 2019. Radium in hydraulic fracturing wastewater: distribution in suspended solids and implications to its treatment by sulfate co-precipitation. Environmental Science: Processes Impacts (21), 339-351.

Palisch, T., Duenckel, R., Wilson, B., 2015. New technology yields ultrahigh-strength proppant. SPE Production & Operations 30, (01), 76-81.

Parkhurst, D.L., and Appelo, C.A.J., 2013. Description of input and examples for PHREEQC version 3-A Computer program for speciation, batch-reaction, one-dimensional transport, and inverse geochemical calculations. U.S. Geological Survey Techniques and Methods.

Prieto, M., 2009. Thermodynamics of Solid Solution-Aqueous Solution Systems. Reviews in Mineralogy & Geochemistry 70, 47-85.

Rassenfoss, S., 2011. From flowback to fracturing: water recycling grows in the Marcellus shale. Journal of Petroleum Technology 63, (07), 48-51.

Reardon, E.J., Armstrong, D.K., 1986. Celestite (SrSO4(s)) solubility in water, seawater and NaCl solution. Geochimica et Cosmochimica Acta Volume 51, 63-72.

Rezwan, K., Meier, L. P., Gauckler, L. J., 2005. Lysozyme and bovine serum albumin adsorption on uncoated silica and AlOOH-coated silica particles: the influence of positively and negatively charged oxide surface coatings. Biomaterials 26, (21), 4351-4357.

Ritcey, G.M., 1989. Tailings management: problems and solutions in the mining industry. Process Metallurgy 6, 991 p.

Rodriguez, K., Araujo, M., 2006. Temperature and pressure effects on zeta potential values of reservoir minerals. Journal of Colloid and Interface Science 300, 788-794.

Rosenberg, Y.O., Metz, V., Ganor, J., 2011a. Co-precipitation of radium in high ionic strength systems: 1. Thermodynamic properties of the Na-Ra-Cl-$SO_4$-$H_2O$ system - Estimating Pitzer parameters for $RaCl_2$. Geochimica et Cosmochimica Acta 75, 5389-5402.

Rosenberg, Y.O., Metz, V., Ganor, J., 2013. Radium removal in a large scale evaporitic system. Geochimica et Cosmochimica Acta 103, 121-137.

Rosenberg, Y.O., Metz, V., Oren, Y., Volkman, Y., Ganor, J., 2011b. Co-precipitation of radium in high ionic strength systems: 2. Kinetic and ionic strength effects. Geochimica et Cosmochimica Acta 75, 5403-5422.

Rosenberg, Y.O., Sadeh, Y., Metz, V., Pina, C. M., Ganor, J., 2014. Nucleation and growth kinetics of RaxBa1− xSO4 solid solution in NaCl aqueous solutions. Geochimica et Cosmochimica Acta 125, 290-307.

Rouquerol, J., Rouquerol, F., Llewellyn, P., Maurin, G., Sing, K. S. W. (2013) Adsorption by powders and porous solids: principles, methodology and applications. Academic press.

Rowan, E., Engle, M., Kirby, C. and Kraemer, T., 2011. Radium content of oil-and gas-field produced waters in the Northern Appalachian basin (USA)—Summary and discussion of data. Scientific Investigations Report 2011-5135. U.S. Geological Survey.

Sajih, M., Bryan, N. D., Livens, F. R., Vaughan, D. J., Descostes, M., Phrommavanh, V., Nos, J., Morris, K., 2014. Adsorption of radium and barium on goethite and ferrihydrite: A kinetic and surface complexation modelling study. Geochimica et Cosmochimica Acta 146, 150-163.

Sari, M.A., Chellam, S., 2015. Mechanisms of boron removal from hydraulic fracturing wastewater by aluminum electrocoagulation. Journal of Colloid and Interface Science 458, 103-111.

Shannon, R.D., 1976. Revised effective ionic radii and systematic studies of interatomic distances in halides and chalcogenides. Acta crystallographica section A: crystal physics, diffraction, theoretical general crystallography 32, (5), 751-767.

Shih, J., Saiers, J. E., Anisfeld, S. C., Chu, Z., Muehlenbachs, L. A., Olmstead, S. M., 2015. Characterization and analysis of liquid waste from Marcellus Shale gas development. Environmental science & technology 49, (16), 9557-9565.

Shukla, J., Mohandas, V. P., Kumar, A., 2008. Effect of pH on the Solubility of CaSO4· 2H2O in Aqueous NaCl solutions and Physicochemical Solution Properties at 35 C. Journal of Chemical Engineering Data 53, (12), 2797-2800.

Silva, J.M., Matis, H., Kostedt, W. L., Watkins, V., 2012. Produced water pretreatment for water recovery and salt production. Research partnership for secure energy for America, final report 08122-08136.

Smith, K., 1992. An overview of naturally occurring radioactive materials (NORM) in the petroleum industry. Argonne National Lab., IL (United States).

Smith, K.P., Blunt, D. L., Williams, G. P., Arnish, J. J., Pfingston, M., Herbert, J., Haffenden, R. A., 1999. An assessment of the disposal of petroleum industry NORM in nonhazardous landfills. Argonne National Laboratory.

Söhnel, O., Mullin, J. W., 1988. Interpretation of crystallization induction periods. Journal of Colloid and Interface Science 123, (1), 43-50.

Sovacool, B.K., 2014. Cornucopia or curse? Reviewing the costs and benefits of shale gas hydraulic fracturing (fracking). Renewable and Sustainable Energy Reviews 37, 249-264.

Subramonian, S., Clifford, D., Vijjeswarapu, W., 1990. Evaluating ion exchange for removing radium from groundwater. Journal-American Water Works Association 82, (5), 61-70.

Tasker, T.L., Burgos, W.D., Ajemigbitse, M.A., Lauer, N.E., Gusa, A.V., Kuatbek, M., May, D., Landis, J.D., Alessi, D.S., Johnsen, A.M., 2019. Accuracy of methods for reporting inorganic element concentrations and radioactivity in oil and gas wastewaters from the

Appalachian Basin, US based on an inter-laboratory comparison. Environmental Science: Processes & Impacts 21, (2), 224-241.

Thiel, G.P., 2014. Treating produced water from hydraulic fracturing: composition effects on scale formation and desalination system selection. Desalination 346, 54-69.

Thiel, G.P., Tow, E. W., Banchik, L. D., Chung, H. W., 2015. Energy consumption in desalinating produced water from shale oil and gas extraction. Desalination 366, 94-112.

Torrie, G.M., Valleau, J. P., 1977. Nonphysical sampling distributions in Monte Carlo free-energy estimation: Umbrella sampling. Journal of computational physics 23, (2), 187-199.

U.S.E.I.A., 2015. World Shale Resources Assessment. U.S. Department of Energy. https://www.eia.gov/analysis/studies/worldshalegas/

U.S.E.I.A., 2018. Annual Energy Outlook 2018. U.S. Department of Energy https://www.eia.gov/outlooks/archive/aeo18/pdf/AEO2018.pdf

U.S.E.I.A., 2019. Annual Energy Outlook 2019. U.S. Department of Energy. https://www.eia.gov/dnav/ng/hist/n9050us2a.htm

U.S.EPA, 1976. National Interim Primary Drinking Water Regulations.

Vaishya, R.C., Gupta, S. K., 2002. Modeling arsenic(III) adsorption from water by sulfate-modified iron oxide-coated sand (SMIOCS). Journal of Chemical Technology and Biotechnology 78, 73-80.

Vaishya, R.C., Gupta, S. K., 2006. Arsenic(V) Removal by Sulfate Modified Iron Oxide-Coated Sand (SMIOCS) in a Fixed Bed Column. Water Quality Research Journal of Canada 41, (2), 157-163.

Valentine, R.L., Spangler, K. M., Meyer, J., 1990. Removing radium by adding preformed hydrous manganese oxides. Journal-American Water Works Association 82, (2), 66-71.

Vdovic, N., 2001. Electrokinetic behaviour of calcite - the relationship with other calcite properties. Chemical Geology 177, 241-248.

Vdovic, N., Biscan, J., 1998. Electrokinetics of natural and synthetic calcite suspensions. Colloids and Surfaces A: Physicochemical and Engineering Aspects 137, 7-14.

Veil, J., Clark, C., 2011. Produced water volume estimates and management practices. SPE Production & Operations 26, (03), 234-239.

Veil, J.A., Smith, K. P., Tomasko, D., Elcock, D., Blunt, D., Williams, G. P., 1998. Disposal of NORM-contaminated oil field wastes in Salt Caverns. Argonne National Lab., IL (US).

Vengosh, A., Jackson, R. B., Warner, N., Darrah, T. H., Kondash, A., 2014. A critical review of the risks to water resources from unconventional shale gas development and hydraulic fracturing in the United States. Environmental science & technology 48, (15), 8334-8348.

Vidic, R.D., Brantley, S. L., Vandenbossche, J. M., Yoxtheimer, D. and Abad, J. D., 2013. Impact of Shale Gas Development on Regional Water Quality. Science 340(6413)

Vinograd, J.R., McBain, J. W., 1941. Diffusion of Electrolytes and of the Ions in their Mixtures. Journal of the American Chemical Society 63, (7), 2008-2015.

Vinograd, V.L., Brandt, F., Rozov, K., Klinkenberg, M., Refson, K., Winkler, B., Bosbach, D., 2013. Solid–aqueous equilibrium in the BaSO4–RaSO4–H2O system: first-principles calculations and a thermodynamic assessment. Geochimica et Cosmochimica Acta 122, 398-417.

Vinograd, V.L., Kulik, D. A., Brandt, F., Klinkenberg, M., Weber, J., Winkler, B., Bosbach, D., 2018. Thermodynamics of the solid solution-Aqueous solution system (Ba, Sr, Ra) SO4+ H2O: II. Radium retention in barite-type minerals at elevated temperatures. Applied Geochemistry 93, 190-208.

Wadekar, S.S., Vidic, R. D., 2017. Influence of active layer on separation potentials of nanofiltration membranes for inorganic ions. Environmental science & technology 51, (10), 5658-5665.

Wang, J., Burken, J. G., Zhang, X. J., 2006. Effect of seeding materials and mixing strength on struvite precipitation. Water Environment Research 78, (2), 125-132.

Wang, R., Chen, J., Liu, Z., 1987. The adsorption behaviour of microamounts of radium on inorganic ion exchangers. Journal of radioanalytical and nuclear chemistry 111, (2), 289-295.

Weber, J., Barthel, J., Brandt, F., Klinkenberg, M., Breuer, U., Kruth, M., Bosbach, D., 2016. Nano-structural features of barite crystals observed by electron microscopy and atom probe tomography. Chemical Geology 424, 51-59.

Weber, J., Barthel, J., Klinkenberg, M., Bosbach, D., Kruth, M., Brandt, F., 2017. Retention of 226Ra by barite: The role of internal porosity. Chemical Geology 466, 722-732.

Werner, A.K., Vink, S., Watt, K., Jagals, P., 2015. Environmental health impacts of unconventional natural gas development: A review of the current strength of evidence. Science of the Total Environment 505, 1127-1141.

Yukselen-Aksoy, Y., Kaya, A., 2011. A study of factors affecting on the zeta potential of kaolinite and quartz powder. Environ Earth Sco 62, 697-705.

Zhang, N., Lin, L., Gang, D., 2008. Adsorptive selenite removal from water using iron-coated GAC adsorbents. Water research 42, (14), 3809-3816.

Zhang, T. (2015a). Origin and fate of radium in flowback and produced water from Marcellus Shale gas exploration, University of Pittsburgh, Pittsburgh.

Zhang, T., Gregory, K., Hammack, R.W. and Vidic, R.D., 2014. Co-precipitation of radium with barium and strontium sulfate and its impact on the fate of radium during treatment of produced water from unconventional gas extraction. Environmental science & technology 48, (8), 4596-4603.

Zhang, T., Hammack, R.W., Vidic, R.D., 2015b. Fate of Radium in Marcellus Shale Flowback Water Impoundments and Assessment of Associated Health Risks. Environmental science & technology 49, 9347-9354.